

**Columbia University
in the City of New York**

**DEPARTMENT OF CIVIL ENGINEERING
AND ENGINEERING MECHANICS**



ANALYSIS OF DAMAGED CONCRETE FRAME BUILDINGS

by

Magdy S.L. Roufaiel

and

Christian Meyer

May 1983

Technical Report No. NSF-CEE-81-21359-1

Prepared for the National Science Foundation

Under Grant No.-CEE-81-21359

Reproduction in whole or in part is permitted for any purpose
of the United States Government.



ABSTRACT

This report presents a general analysis procedure for simulating the earthquake response of reinforced concrete frame buildings, which may or may not have been damaged during previous exposures to strong ground motions. The establishment of this analysis procedure requires the completion of the following tasks: 1) The accurate modeling of the behavior of general reinforced concrete frame members subjected to strong cyclic loads; 2) The definition of a damage parameter, which correlates well with the structure's residual strength and stiffness, and which is suitable for subsequent reliability analyses; 3) The establishment of a procedure for the dynamic analysis of damaged concrete frames.

A theory for a new mathematical model of frame members is developed and its accuracy is verified by simulating various experiments for which data were available in the literature. New local and global damage parameters are defined, and a procedure for analyzing damaged frames is outlined. Herein it is assumed that the building's fundamental frequency is known or can be determined in post-earthquake field measurements. The analysis procedure is verified by reproducing some shaking table tests that had been carried out at the University of Illinois. Some interesting albeit preliminary conclusions could be drawn from these limited studies: 1) The accuracy of the new frame member model is excellent for practical purposes; 2) The

proposed definitions of damage parameters are useful and reliable indicators for damage states; 3) The agreement between experimental measurements and theoretical response predictions for damaged concrete frame is remarkable.

ACKNOWLEDGMENTS

This report was written in partial fulfillment of the requirements of the degree of Doctor of Philosophy by Magdy S.L. Roufaiel under the supervision of Professor Christian Meyer.

This study is a part of an ongoing research project on the reliability of damaged concrete buildings, which is supported by the National Science Foundation under grant number CEE-81-21359.

Numerical studies were carried out on the HP-21MX minicomputer of the Department of Civil Engineering and Engineering Mechanics, and on the IBM/370 computer of the Columbia University Center for Computing Activities.

Experimental data for the shaking table tests were provided by Professor M.A. Sozen of the University of Illinois, and Professor R.W. Clough of the University of California, Berkeley.

We appreciate the care and patience of Mrs. Reva Goldkopf in typing the manuscript.

TABLE OF CONTENTS

	PAGE
ABSTRACT	i
ACKNOWLEDGMENTS	iii
TABLE OF CONTENTS	iv
CHAPTER 1 INTRODUCTION	1
1.1 General	1
1.2 Previous Work on Models for Concrete Frame Analysis	4
1.3 Previous Work on Damage Definition	7
1.4 Scope and Objective	8
CHAPTER 2 A MATHEMATICAL MODEL FOR R/C FRAME MEMBERS	11
2.1 Introduction	11
2.2 Material Constitutive Laws	12
2.2.1 Reinforcing Steel	12
2.2.2 Concrete	12
2.3 Primary Moment-Curvature Relationships	17
2.4 Hysteretic Behavior of Reinforced Concrete	18
2.5 Shear Effect on Hysteretic Behavior	21
2.6 Unloading and Reloading Flexural Stiffnesses	25
2.7 Tangent Stiffness Matrix	26
2.8 Axial Load Effect	30
2.9 Strength Degradation During Cyclic Loading	32
2.10 Damage Indicator and Failure Definition	36

	PAGE
CHAPTER 3	
NONLINEAR ANALYSIS OF R/C MEMBERS	
AND FRAMES	53
3.1 Introduction	53
3.2 Analysis of Reinforced Concrete	
Cantilever Beams	54
3.2.1 Experiment by Ma, Bertero and Popov	54
3.2.2 Experiment by Atalay and Penzien	57
3.2.3 Experiment by Popov, Bertero	
and Krawinkler	59
3.3 Analysis of Frame Subassemblies	60
3.3.1 Experiment by Scribner and Wight	60
3.3.2 Experiment by Healey and Sozen	63
3.3.3 Experiment by Clough and Gidwani	66
3.4 Summary and Conclusions	67
CHAPTER 4	
DYNAMIC ANALYSIS OF DAMAGED CONCRETE	
FRAMES	107
4.1 Introduction	107
4.2 Global Damage Parameter	109
4.3 Damaged Frame Analysis Procedure	114
4.4 Analytical Study of a Damaged Frame	116
4.4.1 Accuracy of Damaged Frame Response	
Analysis	116
4.4.2 Global and Local Damage	118
4.4.3 Sensitivity of Analysis Results	120
4.4.4 Effect of Damage on Subsequent	
Response	121

	PAGE
CHAPTER 5 SUMMARY AND CONCLUSIONS	133
5.1 Summary	133
5.2 Conclusions	137
5.3 Recommendations for Further Studies	139
REFERENCES	142
APPENDIX A	148



CHAPTER 1
INTRODUCTION

1.1 General

The design of buildings against earthquake loadings has received a considerable amount of attention in the last few decades. This task is particularly difficult when the load-carrying structural system is a reinforced concrete frame. A few highly publicized buildings which had behaved less than satisfactorily during the recent San Fernando and Imperial Valley earthquakes have demonstrated that the strict adherence to building code requirements alone is not a guarantee of satisfactory performance.

The response of concrete buildings to strong seismic ground motions is complicated by its strong nonlinear nature. Current design philosophy is based on the principle that a building will withstand strong ground motions most effectively and economically, if a large amount of the earthquake energy input into the structure is dissipated through inelastic action in plastic hinges. Such plastic hinges will naturally occur in the regions of maximum moment, i.e., at the ends of the most highly stressed beams and columns. Plastic hinges are in general not desirable in columns, because of the increased likelihood of the formation of a mechanism and the concomitant danger of instability. But also, high axial forces drastically reduce the energy absorption capacity of a column, therefore

decreasing the effectiveness of plastic hinges therein. For this reason it has been generally accepted that the strong column-weak beam design philosophy is preferable.

The mathematical simulation of the response of reinforced concrete members to strong cyclic loads is extraordinarily difficult. We are dealing here with members made up of two different materials, steel and concrete, both of which have nonlinear stress-strain laws. In addition, concrete cracks at low tensile stresses and experiences microcracking at relatively low compression, which leads to progressive material softening under increasing load. Even though improved reinforcement details can offer very effective confinement of the concrete, thereby raising both its strength and ductility, concrete experiences a progressive deterioration under repeated load excursions into the inelastic range. This has been observed in numerous laboratory experiments, in which the diminishing member stiffness causes a gradual decrease of the areas enclosed within the hysteresis loops of the load-deflection curves. After exceeding a certain critical strain or displacement level, tests also exhibit a gradual weakening of maximum strength or load-carrying capacity.

This steady decrease both in stiffness and possibly strength can have serious practical consequences. A building which has been subjected to a strong earthquake and seems to have performed satisfactorily may have experienced a critical decrease in stiffness and strength which may make

it much more vulnerable to the numerous aftershocks. It is conceivable that certain levels of damage could also be the result of other accidental overloads as well as multiple exposure to strong winds.

In contrast to the study of seismic behavior of theoretically undamaged concrete buildings, the study of damaged concrete buildings is still in its infancy. It requires the solution of the following three tasks:

1. The adequately accurate modeling of the response of general reinforced concrete frame members to strong cyclic loads;
2. The definition of a damage parameter which correlates well with the structure's residual strength or stiffness or both, and which can be determined relatively easily in a post-earthquake field inspection;
3. The establishment of a procedure for the dynamic analysis of damaged concrete frames, which will permit subsequent studies to determine the reliability of buildings in a seismic environment.

The first task has received the most attention of researchers in the past. Several important experiments have been conducted which were extremely instructive with respect to the understanding of inelastic cyclic response of reinforced concrete members. Most of these tests will be referred to in detail in subsequent chapters.

Some work has been done previously in regard to damage definition, but the proposed parameters are not well-suited for the analysis procedure presented herein.

Previous research on the response analysis of damaged concrete frames is virtually nonexistent.

1.2 Previous Work on Models for Concrete Frame Analysis

The mathematical models proposed for the simulation of concrete members can be subdivided into three categories, according to their complexity and associated cost⁽¹⁾.

The most complex and expensive models have been devised for finite element analysis⁽²⁾. A wide variety of tests have been simulated successfully with such models. Because of the large number of degrees of freedom and the resulting computational expenses typically associated with such studies, finite element analysis will be used for only unusual design tasks such as those related to safety-class nuclear power plant structures. The majority of finite element studies will be restricted to research in order to study the behavior of concrete members and to derive from these studies simplified models applicable to more common design situations.

On the next lower level of complexity, the moment-curvature relationships of sections are determined by subdividing the cross-sections into a finite number of layers so that these may be called "semi-finite element" models^(3,4). The computational effort required to establish

complete moment-curvature curves for each member makes the use of also such models rather infeasible for the nonlinear dynamic analysis of large structures.

In order to reduce the computation expense, another step of simplification has to be taken, which leads to the direct determination of moment-curvature relationships for an entire member. Such models, which may be termed "member-size" models, are often accurate enough for practical purposes. A number of such models have been proposed in the literature.

Probably the first one proposed, the Clough⁽⁵⁾ model employs a simple bilinear relationship between moment and curvature. A member is assumed to consist of two imaginary parallel beam elements - an elastoplastic one to represent the yielding characteristics and a fully elastic one to represent strain hardening. Plastic deformations are assumed to be limited to the ends of the members in hinges of zero length. This model proved to be adequate for the analysis of structures made of materials with simple bilinear stress-strain laws, such as steel. For the analysis of concrete structures with degrading material properties it is inadequate.

Hidalgo and Clough⁽⁶⁾ have improved the above model by introducing a stiffness degradation parameter, which is a function of the maximum displacement amplitude experienced by the structure during previous earthquake exposures. The results of analysis employing this model were found to be

rather sensitive to small variations of this degradation parameter.

Giberson⁽⁷⁾ has proposed a model consisting of a linear elastic beam element and two nonlinear springs at the ends to simulate concentrated plastic hinges. To determine the moment-curvature relationship of the springs, the member was divided into two cantilever beams by assuming an inflection point at midspan. Litton⁽⁸⁾ has developed a similar model, but in order to obtain the member stiffness matrix, the stiffness of the member excluding the plastic end regions was inverted; to this flexibility matrix the current flexibility values of the nonlinear springs were added, and the combined flexibility matrix was then inverted to compute the combined stiffness matrix. Suko and Adams⁽⁹⁾ have refined Giberson's model by computing the spring stiffnesses with the point of contraflexure determined by an initial elastic analysis. Otani⁽¹⁰⁾ has extended these models by adjusting the plastic hinges at the beam ends to account for bond deterioration in the joint regions.

None of the above member models consider either the effect of the finite size of the plastic regions or the phenomenon of strength degradation. In addition, some models employ parameters which need to be determined from experiments.

Herein, a member-size model will be presented which takes the finite size of the plastic regions into account. It is felt that the straightforward theory of the model and

the elimination of some inconsistencies inherent in the simpler models⁽¹¹⁾ warrant the slightly increased computational effort required. The most important aspect of the model is the fact that there is no need for a priori test data with which the free parameters of other models have to be adjusted to fit the load-deflection curves to given experimental results.

1.3 Previous Work on Damage Definition

Turning to the second task to be solved for dynamic analysis of damaged frames, a definition of damage is needed which can be used directly in a structural response analysis. In past studies, damage has generally been treated rather subjectively. For example, building inspectors were trained to fill out certain forms designed to assess building damage by relying strongly on their past experience and subjective judgement. Alternatively, damage can be looked at from a strictly economical viewpoint, using a scale from zero for no damage to a maximum of one, representing total replacement cost.

Wiggins and Moran⁽¹²⁾ have proposed one such empirical procedure for grading existing buildings on a scale from 0 to 180 points. The building is given points in several different categories and the sum of all points is taken as a measure of its structural reliability. Similarly, Culver et al⁽¹³⁾ have proposed another field evaluation method, easy to use, but again of limited use in a general

methodology because of the subjective judgment required on the part of the investigators.

A more suitable approach has been taken by Bertero et al⁽¹⁴⁾ which introduces the concept of damageability limit states. A more general approach which involves structural damage considerations has been outlined by Ting et al⁽¹⁵⁾ and Liu and Yao⁽¹⁶⁾. Shibata and Sozen⁽¹⁷⁾ have introduced a damage parameter as the ratio between the initial stiffness and the reduced secant stiffness at maximum deformation.

None of the studies mentioned has proposed a definition of a damage parameter suitable for the dynamic analysis of a damaged reinforced concrete frame. Such a parameter should 1) be as free from subjective judgment as possible; 2) be relatively easy to determine on the basis of field measurements; and 3) be indicative of the amount of stiffness and strength degradation. Herein, such a damage parameter will be presented which is based either on the post-earthquake fundamental period of the building or the maximum roof displacement experienced in previous earthquakes.

1.4 Scope and Objective

This study will develop the tools necessary to perform nonlinear dynamic analyses of reinforced concrete frames which may or may not have been damaged during prior exposure to earthquake ground motions. As outlined earlier, this objective requires the solution of three different

tasks, namely the development of an appropriate model for a general reinforced concrete frame member; the establishment of a suitable damage parameter; and the actual response analysis procedure for damaged concrete frames.

In Chapter 2, a new mathematical model for frame members will be described, which is different from others presented in the literature in that the finite size of plastic regions is taken into account, and which requires for a complete definition the specification of only a few elementary material properties of steel and concrete and the geometric section properties. It is capable of simulating the complete behavior of such members under strong cyclic loads up to advanced states of deterioration, even under the presence of high shear and axial forces.

The accuracy of the model developed in Chapter 2 will be evaluated in Chapter 3 by simulating a large number of experimental tests reported in the literature and by comparing the analytical and experimental results. This comparison extends to individual cantilever beams, beam-column subassemblies and entire building frames, of which scale models have been tested on the shaking tables of the Universities of California and Illinois.

A general analytical procedure for damaged concrete frames will be presented in Chapter 4. Since the shaking table tests consisted of a series of ground motions for the same frames which resulted in increasing levels of damage, they serve as appropriate examples to evaluate the accuracy

of the proposed analytical procedure.

Chapter 5 contains a brief summary and the conclusions to be drawn from this study. Also, a list of problems suggested for future study is given.

CHAPTER 2

A MATHEMATICAL MODEL FOR R/C FRAME MEMBERS

2.1 Introduction

A mathematical model for reinforced concrete frame members is presented in this chapter, which is different from others presented in the literature in that the finite size of plastic regions is taken into account. Moreover the model requires the specification of only a few elementary material properties of steel and concrete to simulate the complete behavior under strong cyclic loads, even under the presence of high shear and axial forces.

This model is an extension of an earlier model developed in the course of an ongoing research project on the reliability of damaged concrete frames (18-23) carried out at Columbia University. In contrast to the earlier version, the new model takes into account the effect of axial and shear forces, as well as the strength degradation which accompanies strong cyclic response. In addition, new definitions of damage and failure parameters are introduced which will be useful for subsequent reliability studies.

The accuracy of the proposed model will be demonstrated in Chapter 3 by analyzing numerous members and structures for which experimental test results are available in the literature. The comparison between all experimental and analytical results shows excellent agreement, leading to the conclusion that the model is very effective in predicting

the nonlinear behavior of reinforced concrete frame members.

2.2 Material Constitutive Laws

2.2.1 Reinforcing Steel

A typical stress-strain curve for steel is shown in Fig. (2.1). For the purpose of the present analysis, the actual curve is idealized by a bilinear curve, consisting of an elastic part characterized by the initial modulus of elasticity

$$E_s = \frac{f_{sy}}{\epsilon_{sy}} \quad (2.1)$$

and an inelastic part with strain hardening ratio

$$p_s = \frac{f_{su} - f_{sy}}{\epsilon_{su} - \epsilon_{sy}} \frac{1}{E_s} \quad (2.2)$$

where f_{sy} and ϵ_{sy} are the yield stress and strain respectively, f_{su} is the ultimate stress, and ϵ_{su} is the strain at ultimate stress.

2.2.2 Concrete

Unlike steel, concrete exhibits different behavior in tension and compression. The tensile strength can be safely ignored because under strong cyclic loading the concrete will crack after a few cycles and lose most of its tensile strength. Confinement of concrete has an effect on the stress-strain relationship which is most significant in the

unloading range. Figure (2.2) shows experimental stress-strain curves for square prisms confined with various contents of square ties (24).

In the past, various expressions have been proposed to idealize the stress-strain curve of confined concrete, Fig. (2.3). Chan (25) proposed a trilinear curve, Fig. (2.3a). The first two lines approximate the curve for unconfined concrete up to stress f_p , while the slope of the third line is a function of the lateral confinement. The curve by Soliman and Yu (26), Fig. (2.3b), consists of a parabola and two straight line segments. Roy and Sozen (27) proposed a bilinear curve, Fig. (2.3c), a loading branch up to the maximum stress f'_c and an unloading branch with a slope determined from test results. Kent and Park's curve (28), Fig. (2.3d) consists of a second order parabola up to the maximum stress f'_c , a linear unloading branch, and a horizontal linear portion with a residual constant stress of $.2 f'_c$. The slope of the unloading branch is a function of the uniaxial cylinder strength, f'_c , the ratio of width of confined concrete to spacing of hoops, and the ratio of volume of hoop steel to volume of concrete core.

Most of the above models have neglected the effect of confinement on concrete strength. Also, the models incorporating parabolic loading branches require iterative procedures to compute moment-curvature relationships. Below, a new model is proposed to represent the stress-strain behavior of concrete, Fig. (2.4), which accounts for

the confinement effect both on the concrete strength and the slope of the unloading branch, yet avoids the complications associated with parabolic functions. Also it will permit the definition of concrete failure.

The proposed curve consists of three linear branches, the first two of which approximate the loading part of the curve, while the third one represents the unloading part. The slope of the falling branch depends only on the ratio of the volume of hoop steel to volume of confined concrete. The proposed trilinear curve has the following characteristics:

- 1) The ultimate strength of the concrete, f_{cu} , is a function of the uniaxial cylinder strength, f'_c , and the degree of confinement, ρ .
- 2) The loading part is a bilinear curve such that the area under the bilinear curve is the same as the area of the parabola proposed by Kent and Park. The slope of the first line is equal to the initial slope of the parabola.
- 3) Coordinates of the cut-off point of the unloading branch, $0.2 f_{cu}$ and ϵ_m , are chosen empirically. Experimental evidence suggests that when the extreme concrete compression fibre is strained to the value ϵ_m or beyond, the strength of the concrete member starts to degrade, when subjected to subsequent load cycles. Atalay and Penzien (29) have noticed that this occurs at about the same time when the concrete cover spalls off. This point will be termed as the "onset of failure" because the

member can sustain only a few load cycles of decreasing amplitude after reaching such a critical strain ϵ_m .

The proposed curve is completely determined by specifying the following three values, Fig. (2.4):

- 1) uniaxial strength of plain concrete, f'_c ;
- 2) strain at maximum stress, ϵ_o ;
- 3) volumetric ratio of confinement steel given by

$$\rho_s = \frac{2(b'' + d'') A_s''}{b'' d'' s} \quad (2.3)$$

where b'' and d'' are the width and depth of the confined core, A_s'' is the hoop cross-sectional area, and s is the hoop spacing.

Referring to Fig. (2.4), the following variables are defined:

$$\begin{aligned} f_{cu} &= \alpha_c f'_c \\ \epsilon_{cu} &= \alpha_c \epsilon_o \\ f_{cy} &= \frac{2}{3} f_{cu} \\ \epsilon_{cy} &= \frac{1}{3} \epsilon_{cu} \\ \epsilon_m &= \beta_c \epsilon_{cu} \end{aligned} \quad (2.4)$$

where α_c and β_c are factors which account for the confinement effect on concrete strength and ultimate strain, respectively. These factors are determined from the following empirical expressions,

$$\alpha_c = 1 + 10 \rho'' \quad (2.5)$$

$$\beta_c = 2 + 600 \rho'' \quad (2.6)$$

The first, "elastic," branch of the trilinear curve has a slope equal to the modulus of elasticity

$$E_c = \frac{2f_{cu}}{\epsilon_{cu}} \quad (2.7)$$

The second, "inelastic," branch is characterized by the strain hardening ratio

$$p_c = 0.25 \quad (2.8)$$

The third line, the "unloading" branch has the negative slope

$$- \bar{p}_c E_c = \frac{.8f_{cu}}{\epsilon_{cu} - \epsilon_m} \quad (2.9)$$

Figure (2.5) compares for different confinement ratios some test results (24) with Kent and Park's idealization (28) and the trilinear model proposed herein. The most

noticeable difference between the two analytical models is the lack of strength enhancement in the Kent and Park model. Also the proposed model requires less computational effort than the one by Kent and Park.

2.3 Primary Moment-Curvature Relationship

It is assumed that plane sections remain plane in an average sense even after cracking of concrete, and that steel and concrete material laws can be approximated as described in the previous section. Then the primary moment-curvature relationship (i.e., for monotonically increasing moment) of a beam section can be derived using conventional reinforced concrete theory only. Details are given in Appendix A.

A typical primary moment-curvature curve is shown in Fig. (2.6). The curve is linear almost up to the yield point (M_y, ϕ_y) , defined as the point at which the tension steel starts to yield. For moments greater than M_y the moment-curvature relationship becomes nonlinear, but the deviation from a bilinear curve is small and can safely be ignored, Fig. (2.6), as long as the axial force is small, as will be discussed later. The procedure described in Appendix A allows the determination of the bending moment M_m associated with the curvature ϕ_m at which the concrete strain reaches the failure value ϵ_m , Fig. (2.4). The slopes of the two branches of the $M - \phi$ curve are then given by

$$(EI)_e = \frac{M_y}{\phi_y} \quad (2.10)$$

and

$$p(EI)_e = \frac{M_m - M_y}{\phi_m - \phi_y} \quad (2.11)$$

Thus, the primary moment-curvature relationship is determined and valid up to the failure of the concrete cover, which is assumed to occur when the concrete at the extreme fiber is strained to a value of ϵ_m .

2.4 Hysteretic Behavior of Reinforced Concrete

Under load reversals, the stiffness of a reinforced concrete member changes due to the cracking of concrete and debonding effects at the steel-concrete interface. A number of empirical models have been proposed in the past to represent the hysteretic behavior of reinforced concrete members:

- 1) Simple bilinear formulations were the first ones employed by researchers (30,31), Fig. (2.7a). A simple bilinear model cannot reproduce the stiffness degradation of actual concrete members and is, therefore, only very approximate.
- 2) The concept of degrading bilinear model has been introduced by Clough (5) and represents a clear improvement over the simple bilinear formulations, Fig. (2.7b).

- 3) A general trilinear model has been proposed by Takeda et al (32) with an elaborate set of rules to reproduce the hysteresis behavior under load reversals, Fig. (2.7c). This model is sufficiently accurate for many applications and, for this reason, has been adopted by a number of other investigators (33,34).
- 4) Iwan (35) has decomposed the general hysteretic response into three basic behavior components - perfectly plastic, elasto-plastic or simple Coulomb slip, and irreversible or directional slip behavior. With this decomposition it is possible to identify basic behavior parameters and calibrate them against test results.
- 5) Baber and Wen (36) have combined four different functions to obtain closed hysteresis loops with a sufficient number of free parameters to model both softening and hardening materials. The deterioration parameter was chosen to be a function of the total energy dissipated by hysteretic action, although according to some tests (37,38) rather stable hysteresis loops can be obtained, i.e., energy can be dissipated without significant stiffness degradation.
- 6) Other models have been proposed, for example, by Atalay and Penzien (29), and Tani et al (39).

For the purpose of this study, a modified Takeda-type model is used to represent hysteretic moment-curvature relationships, Fig. (2.8). The model has, basically, five different types of branches. These are identified in

Fig. (2.8) by corresponding numbers with circles.

1) Elastic loading and unloading: as long as the maximum moment does not exceed the yield moment, M_y , the load-deformation relationship

$$\Delta M = (EI)_1 \Delta \phi \quad (2.12)$$

holds, where

$$(EI)_1 = (EI)_e \quad (2.13)$$

is given by Eq. (2.10).

2) Inelastic loading: if the moment exceeds the yield moment as well as the maximum inelastic moment reached in any previous cycle, and if the moment is still increasing, then the moment-curvature relationship is given by

$$\Delta M = (EI)_2 \Delta \phi \quad (2.14)$$

where

$$(EI)_2 = p(EI)_e \quad (2.15)$$

is given by Eq. (2.11).

3) Inelastic unloading: if the yield limit has been exceeded in a previous cycle, and if the absolute value of the moment is decreasing without a change in sign (branch 3 in Fig.(2.8)), then the moment-curvature relationship is given by

$$\Delta M = (EI)_3 \Delta \phi \quad (2.16)$$

The computation of $(EI)_3$ will be presented in Section 2.6.

4) Inelastic reloading during closing of cracks: In a reversed loading cycle, previously opened cracks tend to close, leading to an increase in stiffness and the characteristic "pinched" shape of the moment-curvature curve. This phenomenon is particularly pronounced in the presence of high shear forces. If the absolute value of the moment is increasing and its value is still less than a certain "pinching moment" for the current cycle (to be defined in the next section), then

$$\Delta M = (EI)_4 \Delta \phi \quad (2.17)$$

where $(EI)_4$ will be discussed in Section 2.6.

5) Inelastic reloading after closing of cracks: if in a reversed loading cycle, the absolute value of the moment is increasing, and its value exceeds the pinching moment, then

$$\Delta M = (EI)_5 \Delta \phi \quad (2.18)$$

where $(EI)_5$ will be given in Section 2.6.

2.5 Shear Effect on Hysteretic Behavior

Figure (2.9) shows two different types of moment-curvature behavior. The first one is characterized by stable hysteresis loops, Fig. (2.9a), which exhibit gradually decreasing stiffnesses for loading cycles of

increasing amplitudes. The second type, illustrated in Fig. (2.9b) is markedly different. Within an individual reloading cycle, the initial stiffness is somewhat low and increases with increasing load up to a certain level, giving the hysteresis loop the characteristic pinched shape.

As reported by Ma et al (4) the main reason for the difference between the two types of hysteresis loops is the presence of high shear stresses. They noticed that stable hysteresis loops are obtained when the maximum nominal shear stress, v_{\max} , is less than $3.5 \sqrt{f'_c}$. In this case the Bauschinger effect on steel and bond deterioration can be considered the main source of stiffness degradation. When v_{\max} is greater than $3.5 \sqrt{f'_c}$, stiffness degradation will be accentuated, resulting in pinched load-deformation curves. In other words, when load reversal occurs within the inelastic range with high shear stresses, the open shear cracks will initially permit the transfer of shear forces mostly through dowel action only, leading to a rather low stiffness. After the closing of such cracks, aggregate interlock and shear friction cause a significant increase of the member stiffness.

In order to include the shear effect in the present mathematical model, the stiffness of a section during reloading is assumed to be nonlinear and will be represented by two straight-line segments, Fig. (2.10). The first line connects the "point of reloading" $(0, \phi_r)$ and the "pinching point" (M_p, ϕ_p) . The second line connects the latter point

with the point of resumed inelastic loading (M_x, ϕ_x) . The first line represents reloading before the closing of shear cracks and is identified in Figs. (2.8) and (2.10) by number 4. The second line segment approximates reloading after the closing of shear cracks and is labelled in Figs. (2.8) and (2.10) by the number 5.

The pinching moment (M_p, ϕ_p) is determined as follows. If shear stresses are negligible and the hysteresis loops are stable during reloading, no pinching is likely to occur, and branches 4 and 5 will form a single straight line. In this case the pinching point (M_p, ϕ_p) will degenerate to a "point of no pinching" (M_n, ϕ_n) , Fig. (2.10), with the coordinates

$$\phi_n = \phi_r \frac{(\overline{EI})}{(EI)_e - (EI)_e} \quad (2.19)$$

and

$$M_n = (EI)_e \phi_n \quad (2.20)$$

where

$$(\overline{EI}) = \frac{M_x}{\phi_x - \phi_r} \quad (2.21)$$

Introducing a pinching factor, α_p , which represents the effect of shear stress on the hysteresis behavior, that $\alpha_p = 1$, if the shear effect is negligible, and $\alpha_p = 0$ if the shear effect completely controls the load-deformation behavior, then it is possible to define the coordinates of the pinching point as

$$M_p = \alpha_p M_n \quad (2.22)$$

$$\phi_p = \alpha_p \phi_n \quad (2.23)$$

In order to relate the pinching factor to the relative shear of a section, it appears advantageous to introduce the nondimensional ratio of the shear span, a , to the effective depth of the beam, d . In a cantilever beam subjected to an end load, the shear span is equal to the beam length, ℓ , and therefore the ratio ℓ/d can be used to represent the degree of pinching of the moment curvature loops. In a typical building frame, inflection points are located approximately at midspan, so that $a = \ell/2$. The empirical equation

$$\alpha_p = 0.4 \frac{a}{d} - 0.6 \quad (2.24)$$

where

$$\alpha_p = 0 \quad \text{if} \quad \frac{a}{d} < 1.5$$

$$\alpha_p = 1 \quad \text{if} \quad \frac{a}{d} > 4$$

adequately describes the relationship between the pinching factor, α_p , and the shear span ratio, $\frac{a}{d}$.

In summary, during reloading, the point of pinching (M_p, ϕ_p) can be determined as follows:

1. Given the shear span ratio, $\frac{a}{d}$, compute the pinching factor, α_p , using Eq. (2.24).
2. Locate the point of no pinching (M_n, ϕ_n) , using Eqs. (2.19) and (2.20).
3. Locate the pinching point (M_p, ϕ_p) , using Eqs. (2.22) and (2.23).

2.6 Unloading and Reloading Flexural Stiffnesses

The stiffnesses $(EI)_3$, $(EI)_4$, and $(EI)_5$ associated with branches 3, 4 and 5 in Fig. (2.8) are determined as follows. Upon unloading in the inelastic range, an auxiliary point with the following coordinates is introduced, Fig. (2.11),

$$M_o = \frac{P}{1-p} (\phi_1^+ (EI)_1 - M_1^+) \quad (2.25)$$

$$\phi_o = \frac{1}{1-p} (\phi_1^+ - \frac{M_1^+}{(EI)_1}) \quad (2.26)$$

where M_1^+ and ϕ_1^+ are, respectively, the maximum moment and curvature reached in the positive direction during the current load cycle. The inelastic unloading stiffness follows as

$$(EI)_3^+ = \frac{M_1^+}{\phi_1^+ - \phi_r^+} \quad (2.27)$$

where

$$\phi_r^+ = \phi_o - \frac{M_o}{(EI)} \quad (2.28)$$

is the residual curvature at zero moment, in the positive direction, and

$$(\overline{EI}) = \frac{M_x^- - M_o}{\phi_x^- - \phi_o} \quad (2.29)$$

is the stiffness of the reversed loading branch, without pinching. M_x^- and ϕ_x^- are the maximum moment and curvature reached during any of the previous load cycles in the negative direction. With the values of ϕ_r^+ , M_x^- , and ϕ_x^- known, the pinching point (M_p^-, ϕ_p^-) can be determined as described in the previous section. The stiffnesses for the two reversed loading branches follow as

$$(EI)_4^- = \frac{M_p^-}{\phi_r^+ - \phi_p^-} \quad (2.30)$$

and

$$(EI)_5^- = \frac{M_x^- - M_p^-}{\phi_x^- - \phi_p^-} \quad (2.31)$$

as illustrated in Fig. (2.11).

2.7 Tangent Stiffness Matrix

To compute the tangent stiffness matrix of a general frame member, the element is subdivided into three regions, Fig. (2.12):

1. an inelastic region of length x_i at node i , having the average stiffness $(\overline{EI})_i$,

2. an inelastic region of length x_j at node j , having the average stiffness $(\overline{EI})_j$, and
3. a central region of length $(l - x_i - x_j)$, having the initial elastic stiffness $(EI)_e$.

For the six planar degrees of freedom identified in Fig. (2.12), the tangent stiffness of this frame element can be written as

$$[K_e] = \begin{bmatrix} k_{11} & 0 & 0 & k_{14} & 0 & 0 \\ & k_{22} & k_{23} & 0 & k_{25} & k_{26} \\ & & k_{33} & 0 & k_{35} & k_{36} \\ \text{symm} & & & k_{44} & 0 & 0 \\ & & & & k_{55} & k_{56} \\ & & & & & k_{66} \end{bmatrix} \quad (2.32)$$

The coefficients

$$k_{11} = k_{44} = -k_{14} = \frac{EA}{l} \quad (2.33)$$

are assumed to remain constant. k_{33} , k_{36} , and k_{66} are obtained from their flexibility counterparts, which in turn can be computed by integrating the moment-curvature expressions over the entire length of the member.

Denoting by

$$\begin{aligned} Q_i &= \frac{(EI)_e}{(EI)_i} \\ Q_j &= \frac{(EI)_e}{(EI)_j} \end{aligned} \quad (2.34)$$

the stiffness ratios for the end regions i and j, the flexibility coefficients are given by

$$f_{ii} = \frac{1}{3(EI)_e \ell^2} [(Q_j - 1)x_j^3 - (Q_i - 1)(\ell - x_i)^3 + Q_i \ell^3] \quad (2.35a)$$

$$f_{jj} = \frac{1}{3(EI)_e \ell^2} [(Q_i - 1)x_i^3 - (Q_j - 1)(\ell - x_j)^3 + Q_j \ell^3] \quad (2.35b)$$

$$f_{ij} = \frac{1}{3(EI)_e \ell^2} [(Q_j - 1)x_j^2(1.5\ell - x_j) + (Q_i - 1)x_i^2(1.5\ell - x_i) + \frac{\ell^3}{2}] \quad (2.35c)$$

The corresponding stiffness coefficients follow as

$$\begin{aligned} K_{33} &= f_{jj} / (f_{ii}f_{jj} - f_{ij}^2) \\ K_{66} &= f_{ii} / (f_{ii}f_{jj} - f_{ij}^2) \\ K_{36} &= -f_{ij} / (f_{ii}f_{jj} - f_{ij}^2) \end{aligned} \quad (2.36)$$

and the remaining coefficients follow from statics

$$\begin{aligned} K_{23} &= -K_{35} = (K_{33} + K_{36})/\ell \\ K_{26} &= -K_{56} = (K_{36} + K_{66})/\ell \\ K_{22} &= K_{55} = -K_{25} = (K_{33} + 2K_{36} + K_{66})/\ell^2 \end{aligned} \quad (2.37)$$

The length x_i and stiffness ratio Q_i of the plastic region at node i depend on the current branch of the $M - \phi$ diagram. For elastic loading or unloading, we have

$$\begin{aligned}x_i &= 0 \\ Q_i^1 &= 0\end{aligned}\tag{2.38}$$

For inelastic loading (see branch 2 in Figure (2-8)), the length of the plastic region is determined by

$$x_i = \frac{M_i - M_y}{M_i + M_j} l\tag{2.39a}$$

because bending moments can be assumed to vary linearly along the beam length. The stiffness ratio within the plastic region is constant over the length x_i and equal to the value at node i , i.e.

$$Q_i^2 = \frac{(EI)_e}{(EI)_2}\tag{2.39b}$$

Upon inelastic unloading, x_i remains the maximum plastic region length reached in any previous inelastic loading cycle. But now the stiffness varies over the length of the plastic region, and for an accurate analysis, it would be necessary to compute the stiffnesses at all sections. This would be a time-consuming task and require considerable computer storage. In order to simplify this task, an empirical averaging process is used (22,23). Directly at node i the stiffness has to be equal to $(EI)_3$, while at the border line between plastic and elastic regions it is $(EI)_e$. We approximate the variable stiffness by an average value, assumed to be constant over the length of the

plastic region and given by

$$(\overline{EI})_3 = \frac{(EI)_3 (EI)_e}{c(EI)_e + (1 - c) (EI)_3} \quad (2.40)$$

where c is an empirical constant, for which values between 0.5 and 0.75 have been found to give most accurate results. In the present analysis a value of 0.5 is used.

The stiffness ratio for the plastic region at node i during inelastic unloading follows as

$$Q_i^3 = \frac{(EI)_e}{(\overline{EI})_3} = c \left(\frac{(EI)_e}{(EI)_3} - 1 \right) + 1 \quad (2.41)$$

Similarly, the stiffness ratios during inelastic reloading (branches 4 and 5 in Fig. (2.8)) are

$$Q_i^4 = \frac{(EI)_e}{(\overline{EI})_4} = c \left(\frac{(EI)_e}{(EI)_4} - 1 \right) + 1 \quad (2.42)$$

$$Q_i^5 = \frac{(EI)_e}{(\overline{EI})_5} = c \left(\frac{(EI)_e}{(EI)_5} - 1 \right) + 1 \quad (2.43)$$

2.8 Axial Load Effect

The presence of an axial force in a member modifies the primary moment-curvature relationship as shown in Fig. (2.13). It can be noticed in this figure that the axial force affects primarily the values of the yield moment and curvature at failure. A high axial force increases the yield moment because of the precompression of the steel, but

it also limits the capacity of a member to sustain high strains. Figure (2.13) also shows that the assumption of linearity of the inelastic loading branch is reasonable as long as the axial load, P , remains moderate, i.e., as long as it stays approximately below 50% of the balanced load, P_b .

Based on the behavior illustrated in Fig. (2.13), we will consider the moment-curvature relationship to be bilinear if the computed slope of the inelastic loading branch is positive. If the axial load exceeds approximately $0.5 P_b$, the second slope is likely to become negative. In this case, the member has very little energy dissipation capacity, so that it appears to be reasonable to consider the yield point as the failure point.

When a building is subjected to an earthquake, axial forces in the columns change as a function of time, because of the overturning moment as well as due to vertical accelerations. The accurate computation of member responses considering variable axial forces is very difficult and time-consuming in general. In order to simplify the response analysis, we assume here that the axial load remains constant and equal to the gravity load effect, present at the beginning of the cyclic load history.

Another effect of axial forces is the phenomenon known as the $P-\Delta$ effect, which cannot be ignored when a member undergoes large inelastic displacements. Numerous procedures have been proposed (40-45) for computing these

second-order effects. For most practical purposes it appears to be sufficient to approximate the P-Δ effect by using a consistent geometric stiffness matrix for each member as proposed by Bolotin⁽⁴⁵⁾:

$$[K_g] = \frac{P}{30} \begin{bmatrix} 0 & 0 & 0 & 0 & 0 & 0 \\ & \frac{36}{\lambda} & 3 & 0 & -\frac{36}{\lambda} & 3 \\ & & 4\lambda & 0 & -3 & -\lambda \\ \text{symm} & & & 0 & 0 & 0 \\ & & & & \frac{36}{\lambda} & -3 \\ & & & & & 4\lambda \end{bmatrix} \quad (2.44)$$

where P is the axial force, and λ is the member length.

2.9 Strength Degradation During Cyclic Loading

Under load reversals, not only the stiffness of a reinforced concrete member decreases, but also its strength deteriorates, provided the member is strained beyond a certain critical load level. This means that in subsequent cycles, the maximum load required to deform the member to a given level of deformation decreases, once this certain critical load level has been exceeded. To the writers' knowledge, this strength degradation has not been included in any of the mathematical models proposed previously.

Strength degradation and the corresponding critical load are functions of several variables, such as the degree of confinement and the value of axial force. Atalay and

Penzien⁽²⁹⁾ have noticed during their experiments that the strength degradation commences with the spalling off of the concrete cover. In Section 2.2, this point had been associated with a concrete failure strain ϵ_m , Fig. (2.4), which was empirically related to the confinement steel according to Equation (2.6). Also the terminal point (M_m, ϕ_m) of the primary moment-curvature curve, Fig. (2.6), had been defined as the point associated with the curvature at which the concrete strain reaches the value ϵ_m . According to Fig. (2.13), this point is strongly influenced by the axial force.

Our theory here is based on the assumption that the member strength does not degrade as long as the curvature of the most highly stressed section is less than ϕ_m . Beyond this level of deformation (i.e., for $\phi > \phi_m$), the member strength at a section decreases during each cycle of loading following the cycle during which the curvature exceeded ϕ_m . The reduction in strength appears to be proportional to the amount of deformation beyond the critical curvature ϕ_m . Spalling off of concrete on one side of the member reduces the moment capacity mainly when this side is under compression. However, the strength for loading in the opposite direction is also affected, presumably because the loss of concrete cover on the now tension side exposes the main reinforcement and leads to some bond slip.

One method of computing the reduced strength would be to use the dimensions of the diminished section, i.e.

without the spalled-off concrete, and to modify the primary moment-curvature curve accordingly. A preferable method, considered herein, is to consider the original undiminished section, but to assume a fictitious increased maximum level of deformation.

Let (M_x^+, ϕ_x^+) and (M_x^-, ϕ_x^-) designate respectively the maximum moment and curvature reached during all previous cycles, in the positive and negative direction, Fig. (2.14). If the maximum curvature during any previous cycle has exceeded the critical curvature ϕ_m^+ in the positive direction, and if unloading occurs in the current cycle, starting at some point (M, ϕ) in the positive region, then the points of maximum deformation, (M_x^+, ϕ_x^+) and (M_x^-, ϕ_x^-) , are modified to the higher values, $(\bar{M}_x^+, \bar{\phi}_x^+)$ and $(\bar{M}_x^-, \bar{\phi}_x^-)$ such that:

$$\bar{\phi}_x^+ = (1 + \gamma^+) \phi_x^+ \quad (2.45)$$

$$\bar{M}_x^+ = M_x^+ + (\bar{\phi}_x^+ - \phi_x^+) (EI)_2^+ \quad (2.46)$$

$$\bar{\phi}_x^- = (1 + \gamma^-) \phi_x^- \quad (2.47)$$

$$\bar{M}_x^- = M_x^- + (\bar{\phi}_x^- - \phi_x^-) (EI)_2^- \quad (2.48)$$

in which γ^+ and γ^- represent the fictitious increases in the maximum curvatures in the positive and negative direction, respectively. They are given by

$$\gamma^+ = \gamma_c \left(1 - 1.84 \frac{P}{P_b}\right) \frac{\phi_x^+ - \phi_m^+}{\phi_x^+} \quad (2.49)$$

$$\gamma^- = \gamma \gamma^+ \quad (2.50)$$

where $\frac{P}{P_b} < 0.5$ is the ratio of the axial force to the balanced load. γ represents the degradation effect in the negative direction, taken as a fraction of the effect in the positive direction. The experimental data seem to indicate a value of $\gamma = 0.2$, which will be used here. γ_c is a factor selected to reflect the workmanship or quality control during construction.

All test specimens analyzed herein have been constructed in laboratories, presumably under near-ideal conditions with regard to workmanship and quality control. In such cases, a value of $\gamma_c = 1$ is used. For structures erected under more realistic construction conditions, somewhat lower standards can be expected in many cases, with the possible consequences of reduced strengths and accelerated strength degradation of critical members. It is beyond the scope of this dissertation to propose numerical values for γ_c which reflect realistic construction conditions, but there exists information in the literature on workmanship in concrete construction which could be utilized for such a study (46). It will be the subject of subsequent studies to investigate the effect of workmanship on the reliability of concrete buildings.

The suggested method of simulating strength degradation is empirical and approximate. However, it is based on the observation that in laboratory experiments, members usually fail after very few cycles, once the concrete strain ϵ_m has been exceeded. The actual number of cycles to failure depends on the confinement degree, and the magnitudes of axial and shear forces. For practical purposes, it is appropriate to define the curvature associated with ϵ_m as a point of incipient failure because subsequently, the member will be able to dissipate only a small amount of energy until either the steel buckles or ruptures, or the member loses its torsional stiffness.

2.10 Damage Indicator and Failure Definition

The reliability of a building to withstand future earthquakes depends greatly on the strength and stiffness degradation, which its major structural components may have experienced in an earlier earthquake. Therefore it is logical to adopt a damage definition related to residual strength and stiffness. Shibata and Sozen⁽¹⁷⁾ have introduced the damage ratio

$$DR = \frac{K_0}{K_r} \quad (2.51)$$

as an indicator of damage, where K_0 is the initial stiffness, and K_r the minimum reduced secant stiffness. For individual sections of reinforced concrete members, this

damage ratio can readily be computed when the moment-curvature relationship is determined. It is called the flexural damage ratio and is given by

$$\text{FDR} = \max \left[\frac{\phi_x^+}{M_x^+}; \frac{\phi_x^-}{M_x^-} \right] (EI)_e \quad (2.52)$$

A value of $\text{FDR} = 1$ means that the member has not undergone any inelastic deformations, while values $\text{FDR} > 1$ can be considered to be proportional to the degree of damage. But as damage indicator, FDR is of only limited usefulness, and it cannot be used to define failure at all. A value of $\text{FDR} = 3$, for example, might signify failure for one member and only moderate damage for another member, or for the same member with a smaller axial force.

For the present analysis we introduce a modified flexural damage ratio defined as

$$\text{MFDR} = \max [\text{MFDR}^+; \text{MFDR}^-] \quad (2.53)$$

where

$$\text{MFDR}^+ = \frac{M_m^+}{M_x^+} \frac{\phi_x^+}{\phi_m^+} \quad \text{and} \quad \text{MFDR}^- = \frac{M_m^-}{M_x^-} \frac{\phi_x^-}{\phi_m^-} \quad (2.54)$$

This damage ratio represents the ratio between the secant stiffness at the onset of failure, (M_m, ϕ_m) , and the minimum secant stiffness, Fig. (2.15). It is a more useful indicator of damage. The value of $\text{MFDR} = 0$ indicates that

deformations have remained elastic and there is no damage. The value of MFDR = 1 means that the member has been loaded to the point where the concrete starts to fail, thus indicating initiation of the strength degradation process which may lead to eventual total failure. The value of MFDR = 1 can therefore be considered to correspond with a state called the "onset of failure." For practical purposes this onset of failure is actually tantamount to failure so that MFDR values between 0 and 1 may serve as a measure of damage. For example, MFDR values from 0 to 0.25 can be regarded to indicate low damage, values from 0.25 to 0.5 represent moderate damage, from 0.5 to 0.75 high damage, and values between 0.75 and 1.0 can be interpreted to indicate severe damage.

In actual response analyses, the computations can be continued after reaching the value MFDR = 1; therefore values of MFDR > 1 will not be uncommon. In such cases the MFDR values increase with the number of cycles following the onset of failure, indicating a progressive degradation of strength. For example, for one of the test beams analyzed in Chapter 3, a value of MFDR = 7.1 has been computed. Such a high value corresponds to such a small residual strength and stiffness that for all practical purposes the member has failed. The actual numerical value for MFDR is rather irrelevant in such situations, whereas the fact that a member has reached a value of MFDR > 1 is much more significant.

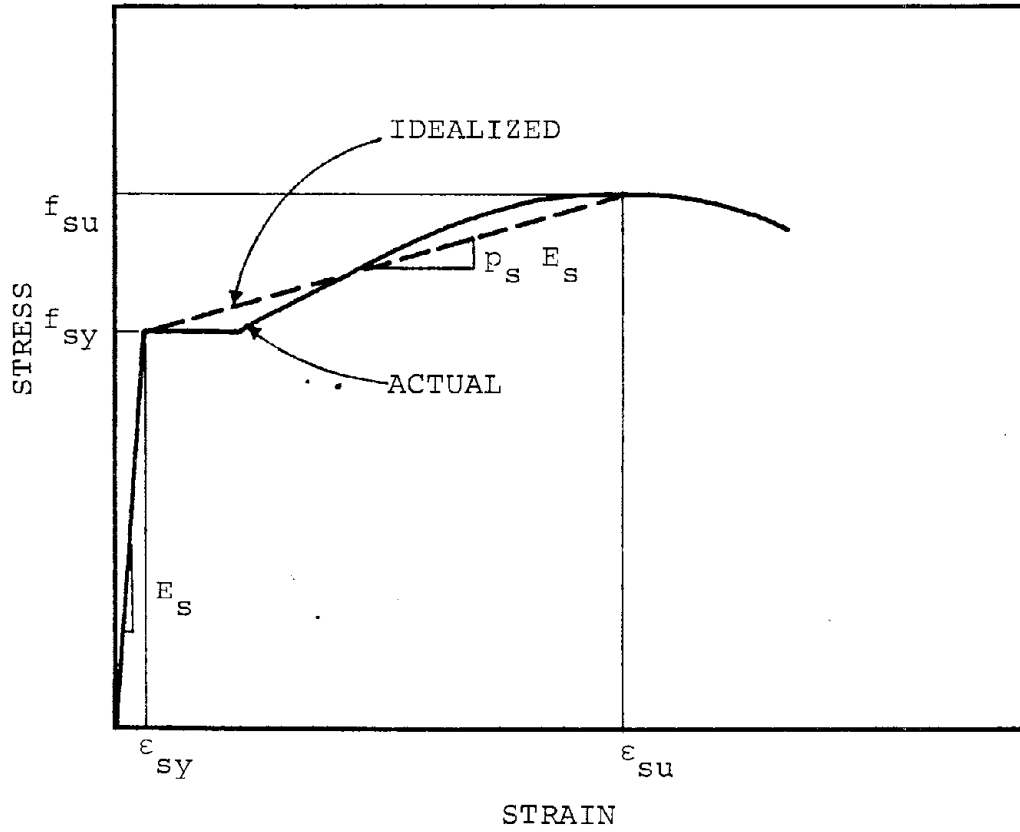


Fig.(2.1). Steel stress-strain curve

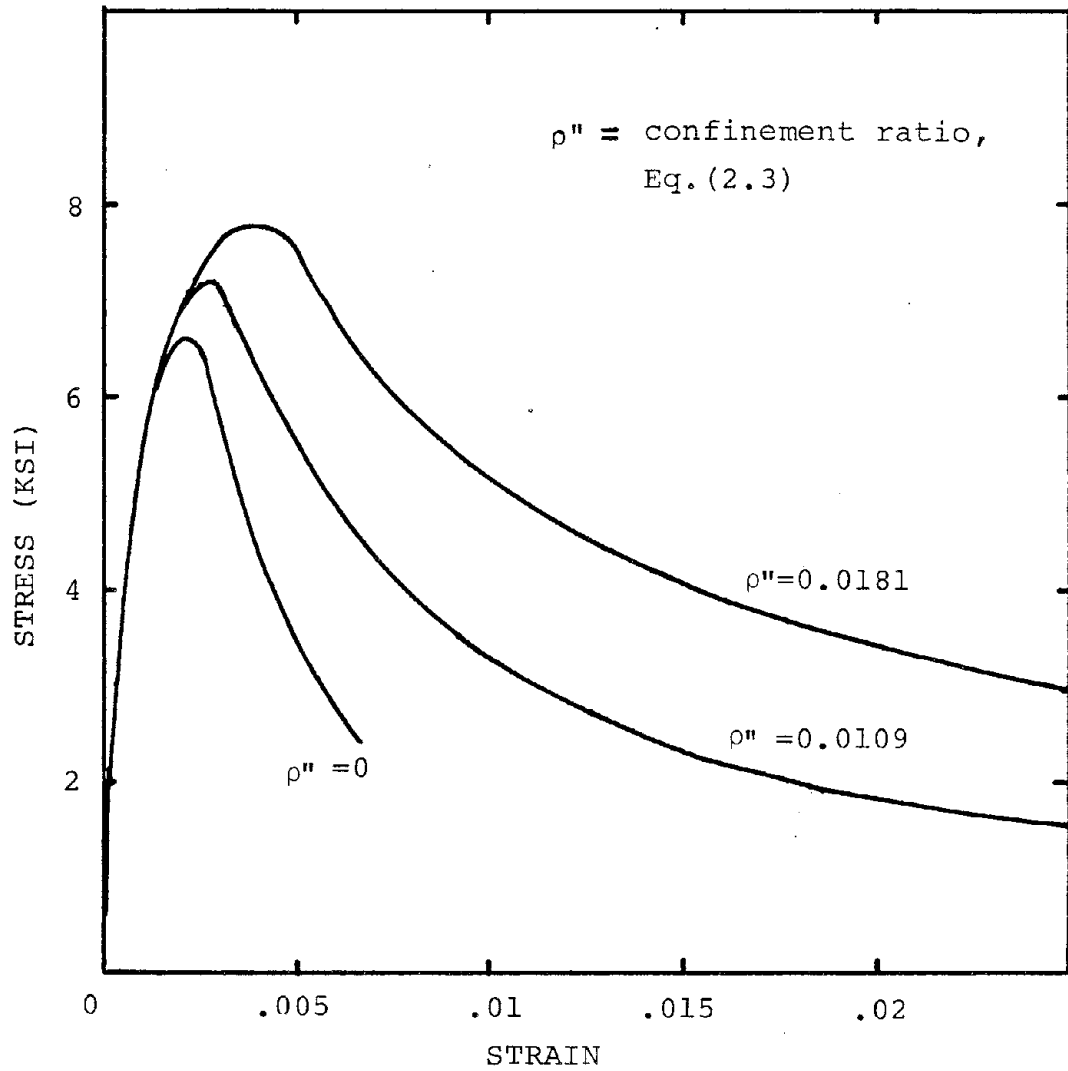
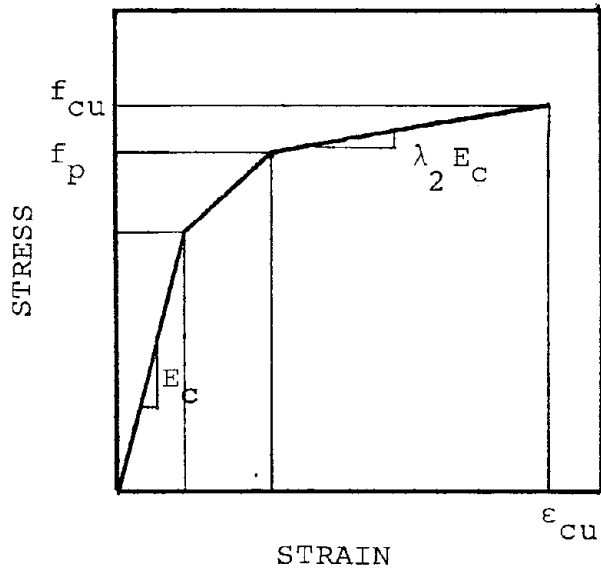
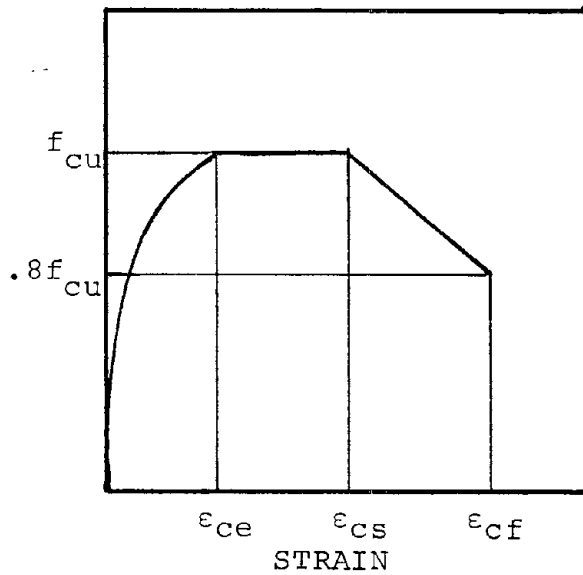


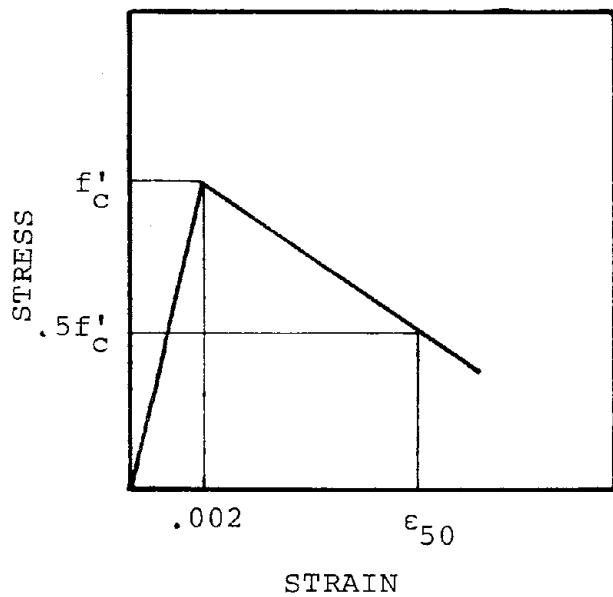
Fig.(2.2). Concrete stress-strain curves for square prisms confined with various contents of square ties⁽²⁴⁾



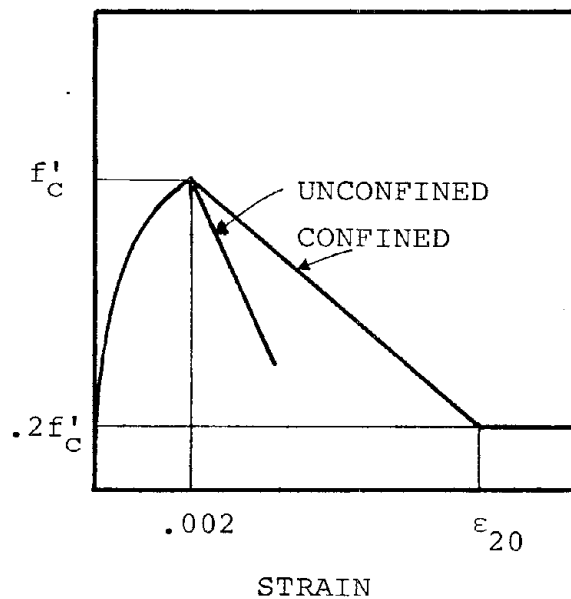
a) Chan curve⁽²⁵⁾



b) Soliman & Yu curve⁽²⁶⁾



c) Roy & Sozen curve⁽²⁷⁾



d) Kent & Park curve⁽²⁸⁾

Fig.(2.3). Some proposed stress-strain curves for concrete confined by rectangular hoops

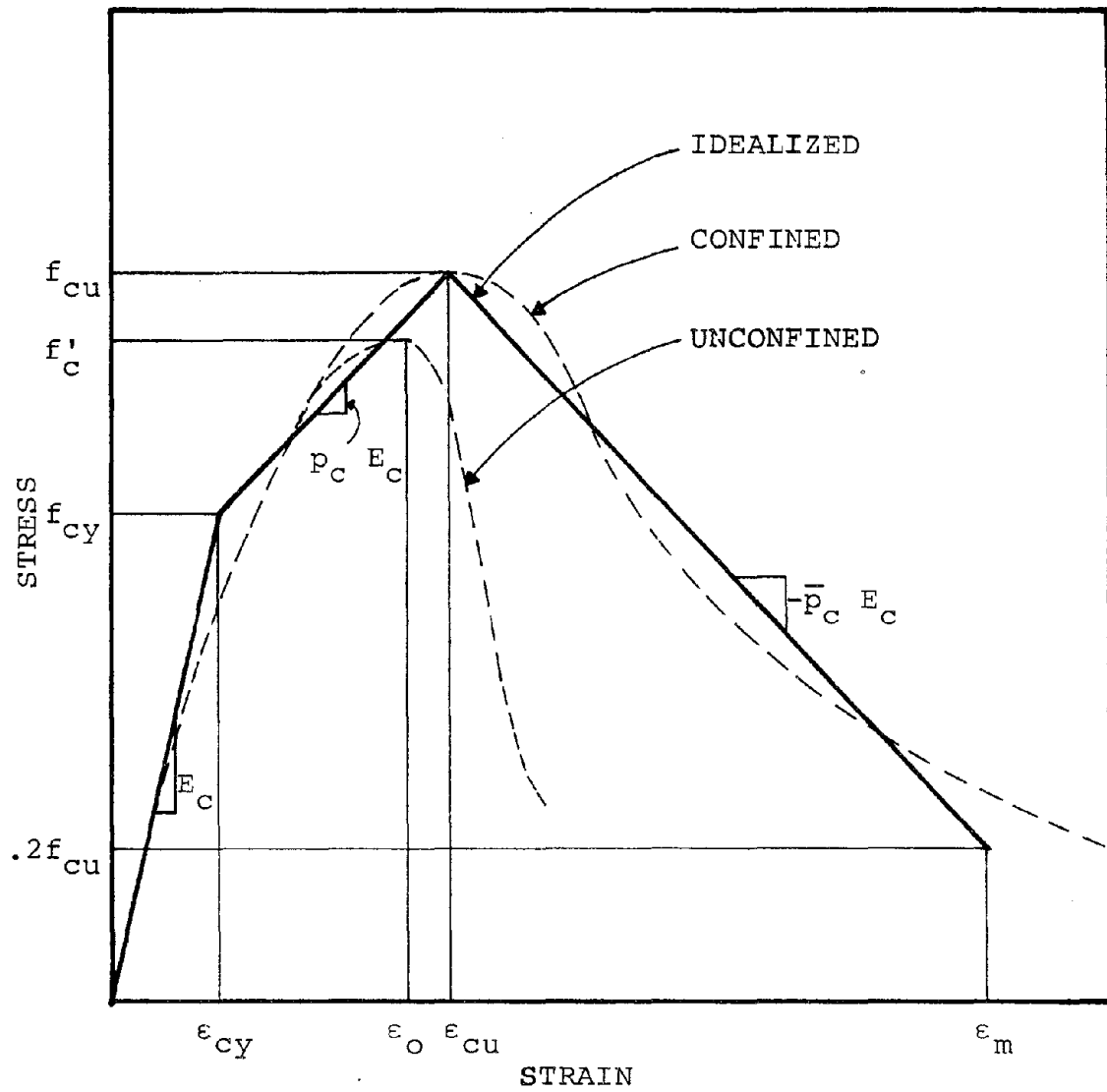


Fig.(2.4). Adopted stress-strain curve for concrete

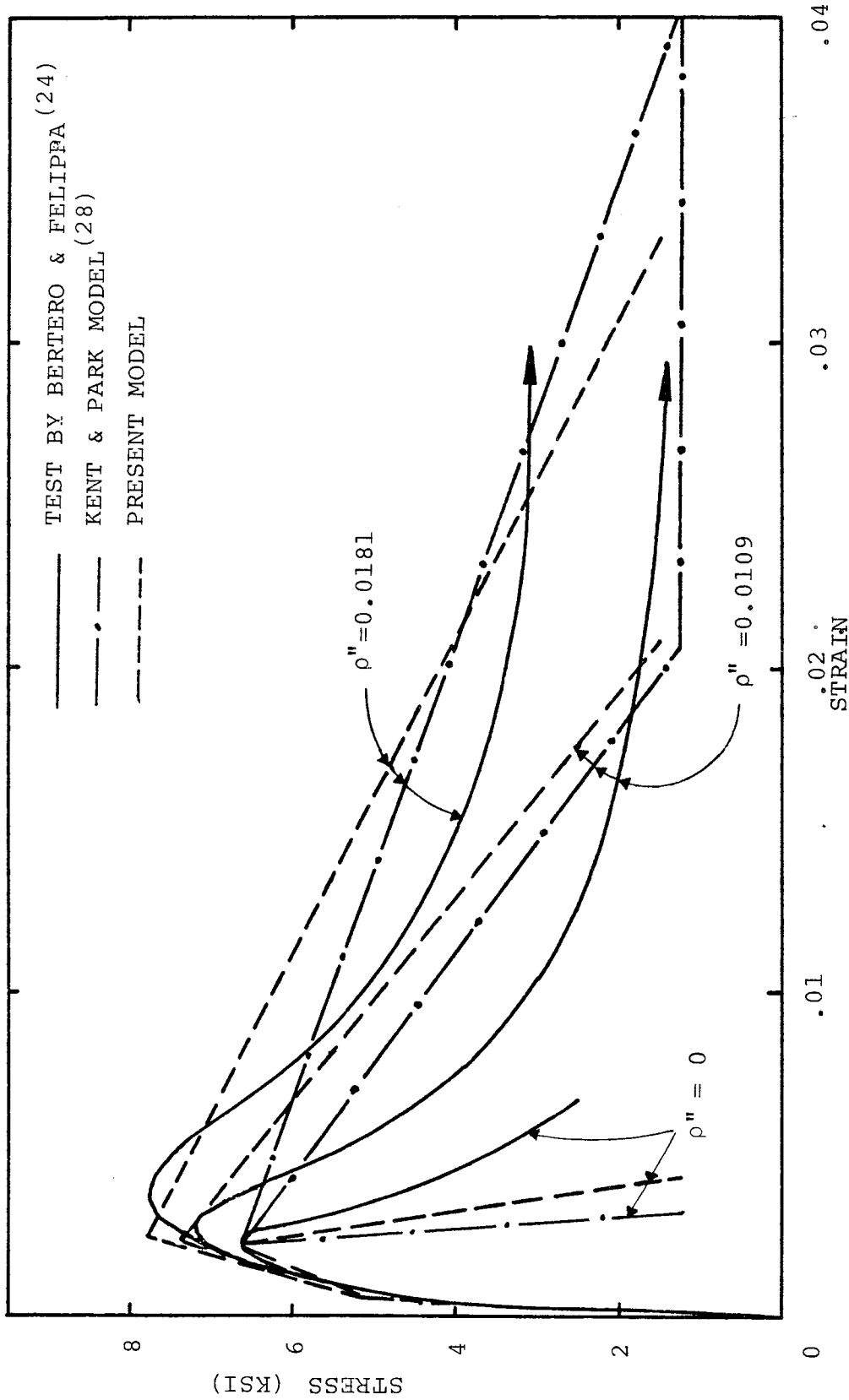


Fig. (2.5). Experimental and analytical stress-strain relationship for confined concrete

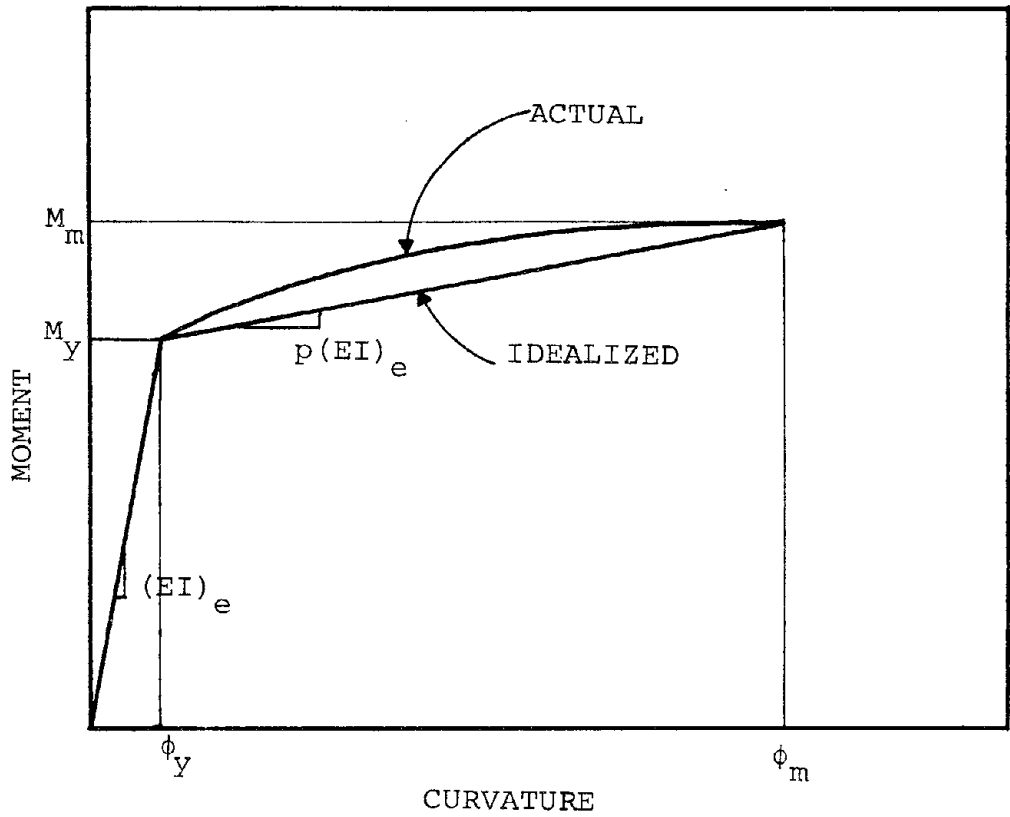
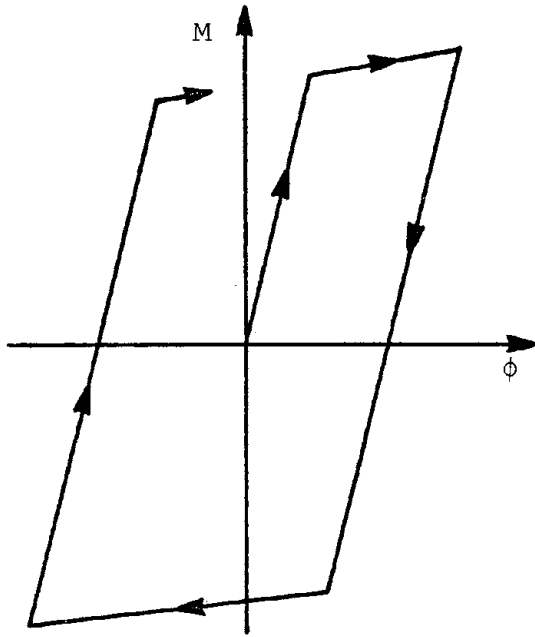
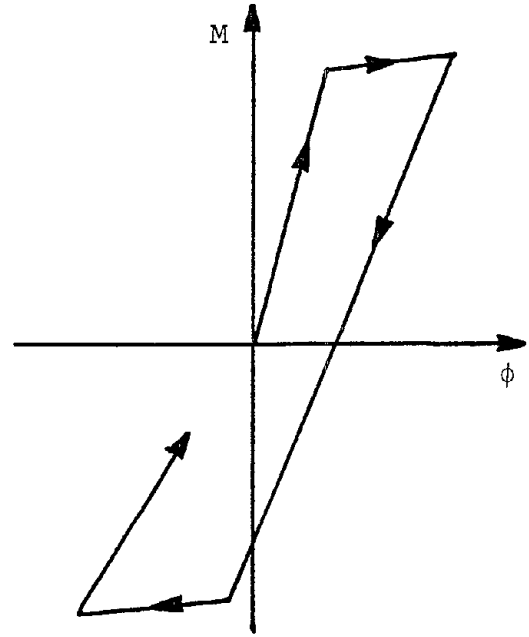


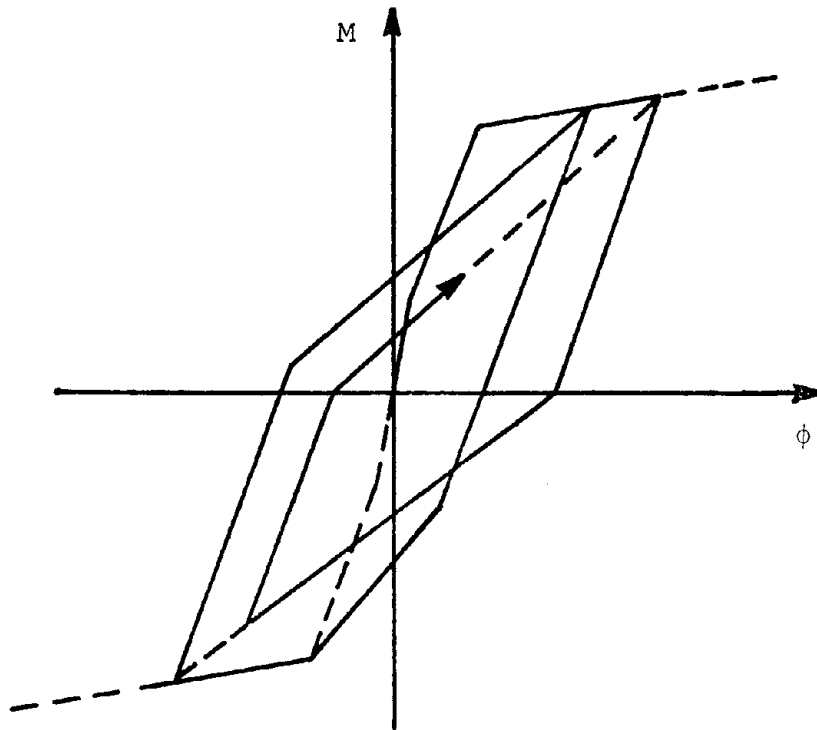
Fig.(2.6). Primary moment-curvature relationship for a beam section



a) BILINEAR



b) BILINEAR DEGRADING



c) TRILINEAR TAKEDA TYPE

Fig.(2.7). Hysteretic models

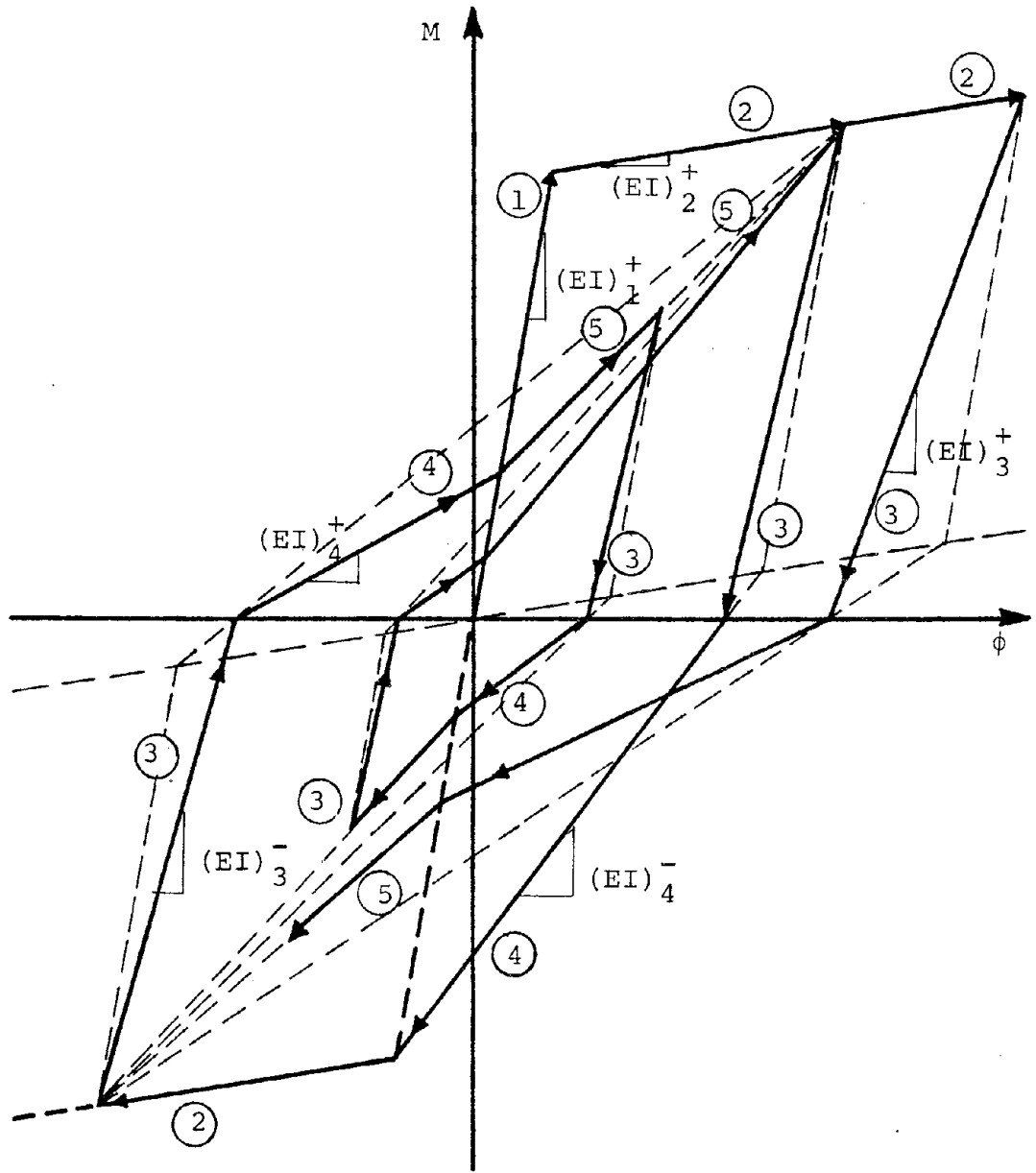
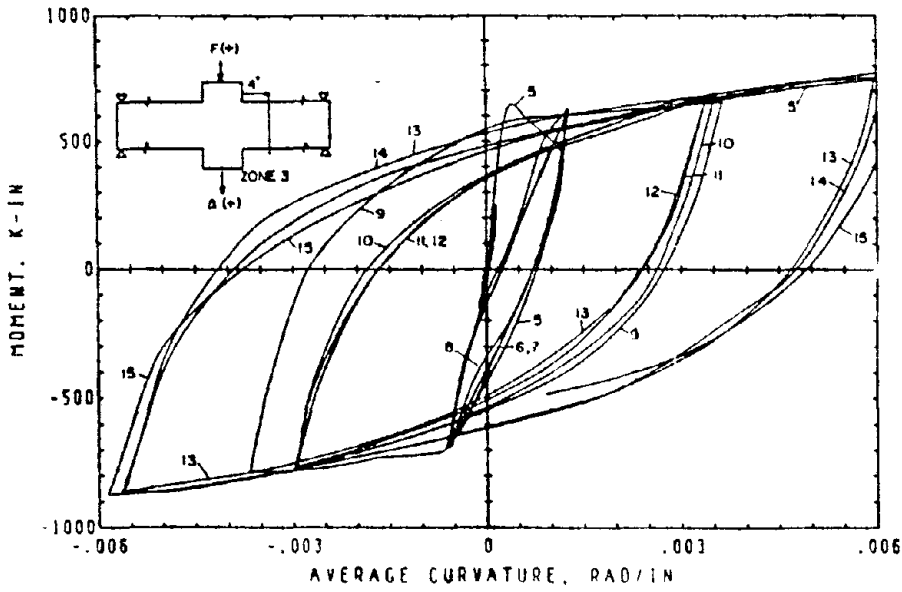
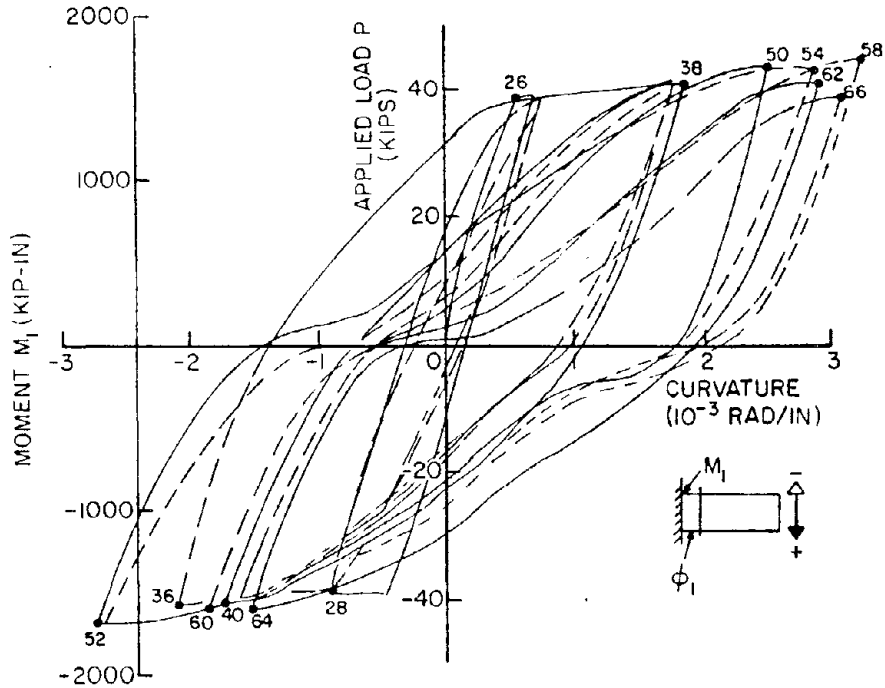


Fig.(2.8). Hysteretic moment-curvature idealization



a) Stable moment-curvature behaviour⁽³⁷⁾



b) Pinched moment-curvature behaviour⁽⁴⁾

Fig.(2.9). Types of hysteretic loops

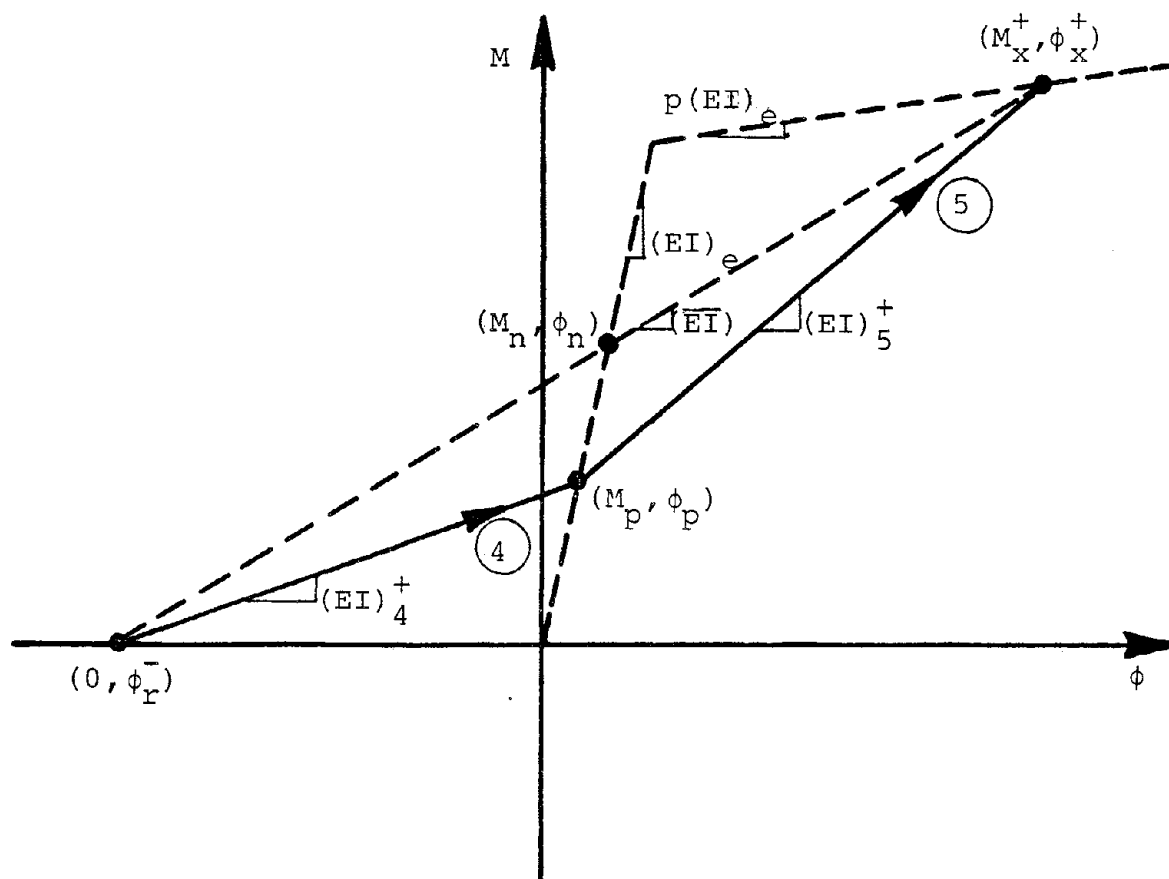


Fig.(2.10). Pinched reloading curve

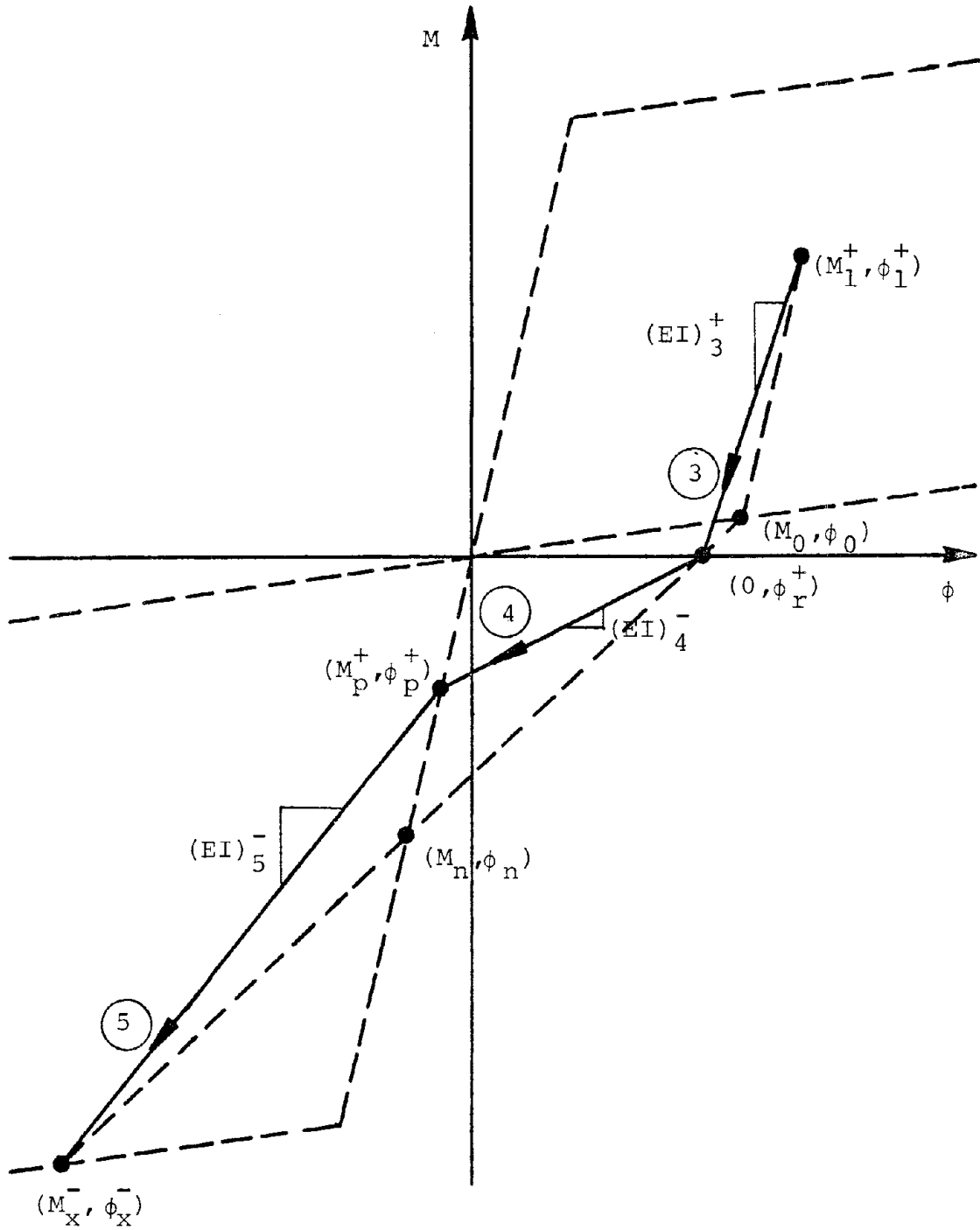


Fig.(2.11). Unloading and reloading stiffnesses

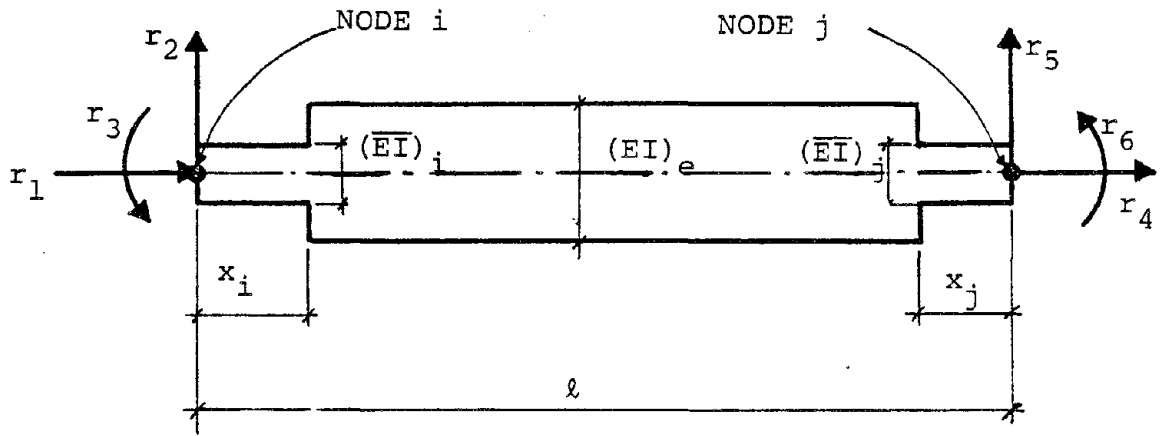


Fig.(2.12). Frame member model

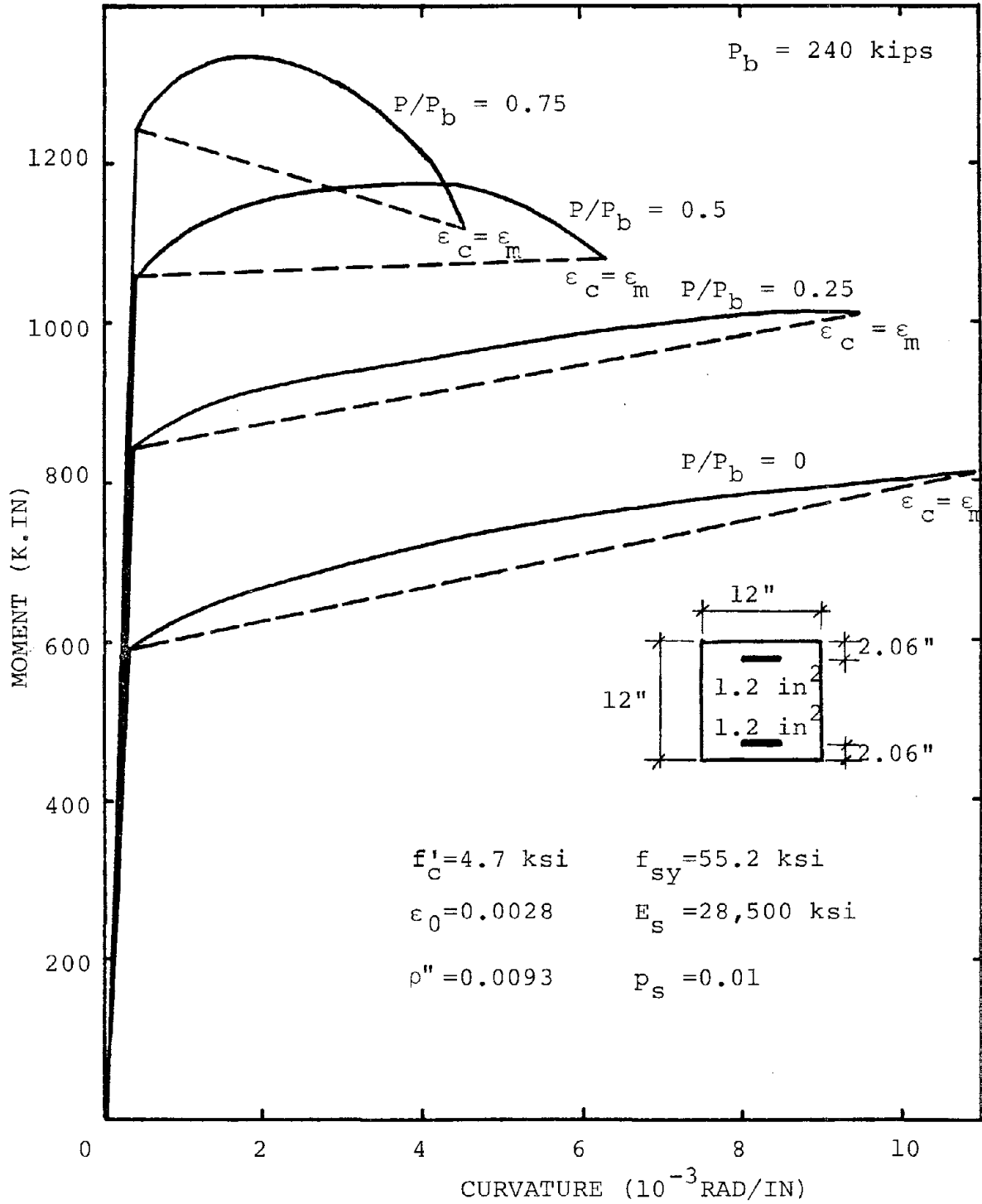


Fig.(2.13). Effect of axial force on the primary moment-curvature relationship

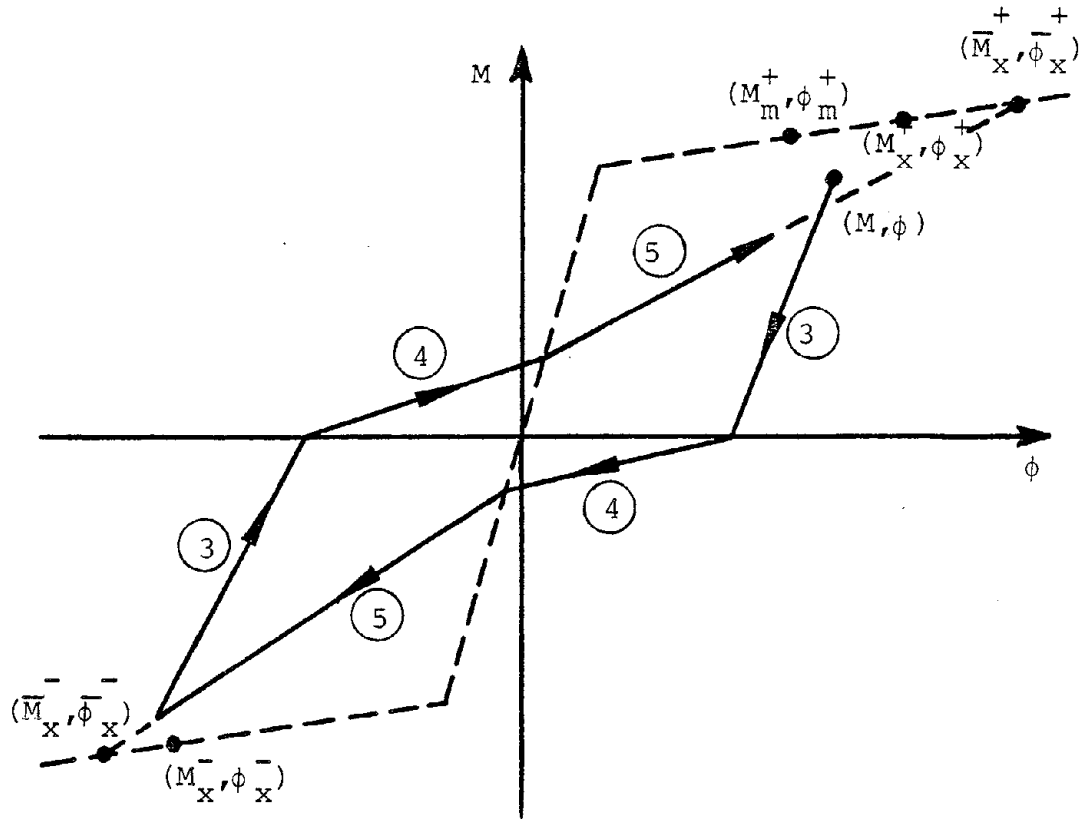


Fig.(2.14). Strength degradation during cyclic loading

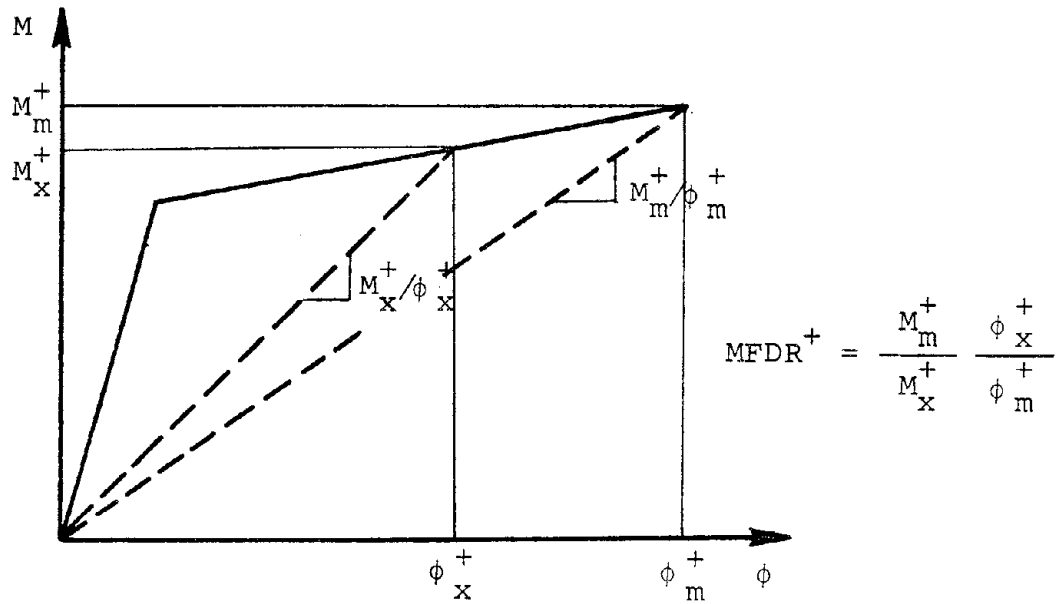


Fig.(2.15). Modified flexural damage ratio

CHAPTER 3

NONLINEAR ANALYSIS OF R/C MEMBERS AND FRAMES

3.1 Introduction

It is the objective of this chapter to evaluate the accuracy of the model proposed in Chapter 2 in predicting the nonlinear behavior and the degree of damage of reinforced concrete members, subassemblies, or entire frames subjected to strong cyclic loading. This has been accomplished in two stages.

First, a computer program has been written to analyze the response of simple reinforced concrete cantilever beams. This program was used to analyze the responses of twenty beams which had been tested in three different experimental investigations. Section 3.2 summarizes both the analytical and experimental results obtained for the twenty cantilever beams.

In the second stage of validation, the proposed model has been incorporated into DRAIN-2D⁽⁴⁷⁾, a general-purpose nonlinear analysis computer program. This program was then used to analyze three different types of structures, for which experimental results were available in the literature. The analytical and experimental results for these test structures are presented in Section 3.3.

An overall evaluation of the mathematical model is given in Section 3.4, with the basic conclusion that the proposed model is very effective in predicting the nonlinear

behavior of reinforced concrete frames.

3.2 Analysis of Reinforced Concrete Cantilever Beams

The mathematical model described in Chapter 2 has been programmed for an HP-21MX minicomputer system located at the Civil Engineering and Engineering Mechanics Department of Columbia University. The program can analyze the response of a reinforced concrete cantilever beam for a prescribed displacement history at the free end. The input data consist of the properties of the reinforcing steel and concrete, geometric dimensions, longitudinal and confinement reinforcement, the axial force, and the displacement history. The output consists of the load-deflection curve, values of the modified flexural damage ratio (see section 2.10) and the dissipated energy given by the areas enclosed in the load-deflection loops.

The responses of twenty beams, which had been tested in three different experimental investigations, will be presented in the following three subsections.

3.2.1 Experiment by Ma, Bertero and Popov⁽⁴⁾

The first group of beams to be analyzed was tested by Ma, Bertero and Popov at the University of California, Berkeley. This group consisted of six beams with rectangular sections (R1 - R6), and three with T-section (T1-T3). Three pairs of beams (R1 and R2, R3 and R4, T1 and T2) were built identically to study the effect of different

loading conditions on the inelastic behavior of the specimens. All beams had the same span length of 62.5 inches, except for specimen R5 which had a span length of 38.5 inches. All specimens had a confinement steel ratio of $\rho = 1\%$, except for beams R1 and R2, for which $\rho = .53\%$. The concrete strength, f'_c , ranged from 4.19 ksi to 5.07 ksi for the various beams. The data required to analyze these nine beams are summarized in Tables (3.1) and (3.2). Except for beams R4 and T2, all specimens were subjected to several load cycles with increasing displacement amplitudes until a sudden drop in strength occurred, which was interpreted as constituting failure. Load-deformation data were continuously recorded until the beams had failed completely, or until the measured deformations had reached a magnitude at which continued recording might have impaired the functioning of the gages. In contrast, test beams R4 and T2 were loaded directly to the largest deformation permitted by the stroke of the actuator (about 4 inches). The load was then reversed, up to the same displacement in the opposite direction, and this process was repeated until failure occurred.

The first test, Fig. (3.1), is that of a specimen with a relatively stable hysteresis behavior, up to a tip deflection of approximately 2.6 inches, at which time the concrete is strained beyond ϵ_m , i.e., subsequently a rapid deterioration of the specimen can be observed, which for all intents and purposes constitutes failure. The absence of

pinching in the individual hysteresis loops indicates that this test beam failed primarily in bending.

Test specimen R4, Fig. (3.2), was subjected to two severe load cycles, both of which far exceeded the point defined earlier as the onset of failure. Actual failure occurred by rupturing of the longitudinal reinforcement. Had this failure mode not occurred, a rapid deterioration of the member could have been expected.

The third test, illustrated in Fig. (3.3), exhibits pronounced pinching of hysteresis loops, indicating the presence of high shear. In fact, the final failure can be called a typical shear failure.

It is noteworthy that in all three cases the agreement between theory and test is excellent. The results for the other six beams are not reproduced here because they display a similar level of agreement.

The experimental and analytical values of the dissipated energy both at the onset of failure, and at the termination of each test are listed in Table (3.3). The agreement between the computed and measured values is excellent, and an important indication of the accuracy with which the analytical model can be expected to predict the nonlinear behavior of reinforced concrete members under strong cyclic load. Also displayed in Table (3.3) are the computed values of the modified flexural damage ratio, MFDR, at the observed onset of failure and at the termination of each experiment. With the exception of beam R4, the value

of $MFDR=1$ correlates strongly with the onset of failure which was defined as the point where the maximum concrete strain reached the value of the crushing strain ϵ_m . The reason why beam R4 had the comparatively high value of 3.91 can be found in the unusual loading history consisting of only two cycles as shown in Fig. (3.2). In fact, the first load cycle, which resulted in the damage ratio $MFDR=2.83$, can be considered as having already initiated the failure.

3.2.2 Experiment by Atalay and Penzien⁽²⁹⁾

The second group of members selected to evaluate the proposed model were tested by Atalay and Penzien, also at the University of California, Berkeley. This group of members consisted of twelve specimens with axial forces varying from 25% of the balanced force, P_b , to $.75 P_b$, and having two different steel confinement ratios (.93% and 1.53%). Only the first eight specimens (S1-S8) are considered here, because the remaining four members (S9-S12) were subjected to high axial forces, which reduced the ductility of the members so much as to make their energy absorption capacities insignificant, as explained in Section (2.8). Specimen S9, for example, was loaded with an axial force of $.75P_b$. It experienced a drop in strength at a tip deflection of 1 inch and failed at 2 inches. Specimen S1, on the other hand, which was loaded with an axial force of only $.25P_b$, did not experience a reduction in strength until reaching a tip deflection of 3.2 inches. The test was

terminated at a tip displacement of 4 inches without failing the specimen.

The data used to analyze this group of members are summarized in Tables (3.4) and (3.5). The test specimens were simply supported at both ends and subjected to concentrated midspan loads. The reinforcing bars were welded to rigid steel plates at midspan in order to prevent slip in this region. Therefore, each member can be idealized by two identical cantilevers, with half the load applied at the free end of each, Fig. (3.4). Each test specimen was subjected to displacement-controlled cyclic loads. The displacement amplitudes were held constant for several cycles before being increased to the next higher value, until the specimen failed or the test had to be terminated for other reasons.

The experimental and analytical load-deflection curves for specimens S1, S4 and S5 are reproduced in Figs. (3.4-6). The good agreement is representative for that of all other examples not shown here.

During the experiments, the displacement amplitudes at which the concrete cover started to spall off were recorded. These were defined earlier to constitute the onset of failure. The modified flexural damage ratios associated with these displacement amplitudes are given in Table (3.6). These values correlate reasonably well with the definition for the onset of failure (MFDR=1). For members S5 to S8, the values are somewhat higher than 1,

indicating small differences between the observed and computed points of incipient failure. For example, the failure for specimen S5 was observed to commence at a displacement amplitude of 2 inches, while the corresponding computed value was 1.8 inches.

Table (3.6) also lists the modified flexural damage ratios and the measured and computed dissipated energies at the time each test was terminated. The first three specimens survived the test, but the concrete in the critical regions experienced extensive damage in all three cases. This result is in agreement with the MFDR values, which are close to 1, except for specimen S2. The reason for the high value of MFDR for specimen S2 is that the analytical model had predicted a more severe degradation of strength than the test. The other five specimens failed due to buckling or rupturing of reinforcing bars after spalling of concrete. These results correlate well with the high MFDR values, which ranged from 2.02 to 7.10.

3.2.3 Experiment by Popov, Bertero and Krawinkler⁽⁴⁸⁾

The third group of beams analyzed herein was tested by Popov, Bertero and Krawinkler. This group consisted of three cantilever beams (B35, B46, B43) with different confinement ratios and material properties. The data needed to analyze these three beams are presented in Tables (3.7) and (3.8).

The experimental and analytical load-deflection curves

reproduced in Figs. (3.7-9) show the usual good agreement. The modified flexural damage ratios for the three beams were computed to be 2.45, 1.21 and .93, i.e., the mathematical model predicted failure by the time of test termination.

3.3 Analysis of Frame Subassemblies

The mathematical model described in Chapter 2 has been incorporated into DRAIN-2D, a general-purpose nonlinear dynamic analysis program.⁽⁴⁷⁾ Developed originally to analyze the response of structures to earthquake excitations, it was modified for the purpose of the present study to analyze frames or frame subassemblies, both for static and dynamic cyclic loads. Below, the results for three example structures are presented, for which experimental test data were available.

3.3.1 Experiment by Scribner and Wight⁽⁴⁹⁾

A group of beam-column subassemblies, representing an exterior beam-column joint in a building, was tested statically by Scribner and Wight at the University of Michigan. This group consisted of eight half-size (Group I) and four full-size (Group II) T-shaped reinforced concrete beam-column subassemblies. A schematic representation of the test setup is shown in Fig. (3.10).

The purpose of this experiment was to investigate the effect of intermediate longitudinal shear reinforcement on the hysteretic behavior of flexural members subjected to

large repeated reversal loadings. Therefore, specimens 2, 4, 6, 8, 10 and 12 were built identically to specimens 1, 3, 5, 7, 9 and 11, respectively, except that intermediate longitudinal reinforcement was added to the even-numbered specimens. Because modelling of members with intermediate reinforcement is beyond the scope of the present investigation, only the odd-numbered specimens were considered here. (A small modification of the model would permit the inclusion of such reinforcement.)

The data used to analyze this group of subassemblies are given in Tables (3.9-13). The loading procedure was similar for all specimens. First, an axial force (40 kips for Group I and 100 kips for Group II) was applied at the two ends of the column and kept constant during the test. Then, a prescribed displacement history was applied at the tip of the beam. This history consisted of six cycles of displacement ductility four in the positive direction and ductility three in the negative direction. If a specimen survived all six cycles, then additional cycles of higher ductilities were applied. As can be noticed from the test setup, Fig. (3.10), the axial force applied to the column does not affect the inelastic behavior of the beams, but only affects the yield characteristics of the column itself.

Experimental and analytical load-deflection curves for the tip of the beam are reproduced in Figs. (3.11-16). Except for specimen 1, the first set of six load cycles initiated failure of all test specimens, indicated by a more

or less pronounced drop in strength. This behavior was predicted by the analytical model, indicating the validity of incipient failure definition. The experimental and analytical load-deflection curves compare reasonably well, except that during unloading some test specimens appeared to be stiffer than the corresponding analytical model. This difference caused some discrepancies between the recorded and computed values of the dissipated energies, listed in Table (3.14). These discrepancies ranged from -24% to +4%, with an average of -13%. Considering the severity of the loading applied in this test series, wherein most initial load cycles exceeded the load of failure initiation, the agreement between test and theory appears to be very reasonable.

With the exception of specimen 5, the behavior of all specimens was controlled mainly by flexural deformations. Only specimen 5 was subjected to relatively high shear stresses which caused the characteristic pinched hysteresis loops, Fig. (3.13). It is an indication of the reliability of the analytical model that its accuracy is independent of the relative amount of shear.

Specimen 1 was the only one which survived the test without buckling or rupture of steel, but with some damage to the concrete in the critical region of the beam. All other specimens had failed completely at the termination of the test. This result correlates well with the modified flexural damage ratios computed for the end of the test and

listed in Table (3.14). The value of MFDR=.918 for specimen 1 indicates approximate onset of failure. For the other specimens, the computed values ranged from 2.185 to 4.496, indicating severe strength degradation and high probability of complete failure. None of the columns suffered any damage, and the computed MFDR values were zero for all specimens.

3.3.2 Experiment by Healey and Sozen (50)

This was a dynamic test carried out on the shaking table of the University of Illinois by Healey and Sozen. The primary objective of the experiment was to study the nonlinear dynamic behavior of a small-scale ten-story, three-bay reinforced concrete frame, Fig. (3.17). The three bays of the structure had equal span lengths of 305 mm. The center-to-center story heights were 229 mm for the second through ninth level, and 279 mm for the first and tenth level. Before the dynamic tests a total mass of 2770 kg was distributed equally to each level. Detailed information regarding member dimensions, material properties and reinforcement is summarized in Fig. (3.17).

The test structure was subjected to three consecutive ground acceleration histories. Each one of these was the El Centro earthquake, scaled to different peak accelerations, namely .4g, .93g and 1.25g. These three tests were referred to as "Run One," "Run Two" and "Run Three." In this chapter, only Run One is considered because the analysis is

based on the assumption of no damage prior to loading. Test Runs Two and Three will be considered in Chapter 4.

Numerous measurements of the natural frequencies had been made before and after various testing phases, during which the difficulties of obtaining reliable data were demonstrated. The computed frequencies, reported elsewhere, (22,23) compared well with the recorded values, especially in light of the uncertainties exhibited by the different experimental techniques. The model used for the studies reported in Refs. 22 and 23 was not as comprehensive as the one presented herein, but the computed frequencies were almost identical.

The base acceleration input for Run One is plotted in Fig. (3.18), together with the measured and computed roof displacement histories. The frame response was governed primarily by the first mode, therefore all floor responses looked very much alike, except for the amplitudes, and the comparison between theory and experiment displayed in Fig. (3.18) is representative for the entire frame response. The good agreement indicates the adequacy of the analytical model, especially in view of damage estimates, for which this model is intended in subsequent studies.

After having subjected the test model to the acceleration of Run One, the specimen was coated to permit the marking and recording of new cracks. The structure incurred little cracking during Run One; all observed crack widths were less than or equal to 0.1 mm. Fig. (3.19) shows

the crack pattern after the test. Also indicated on Fig. (3.19) are the computed values of the modified flexural damage ratios, MFDR, for all members. A study of these results leads to the following conclusions:

1. The MFDR values correlate quite well with the observed crack pattern.
2. The MFDR values for the columns are considerably lower than those computed for the beams. This result seems to indicate that the frame was designed according to the common strong column-weak beam concept, so that most energy is dissipated in the beams, not the columns.
3. The observed crack pattern displayed in Fig. (3.19) does not show cracks at the base of the frame, even though the computed MFDR values indicate that there should be some. As reported in Ref. 50, the second test, Run Two, with a peak acceleration of .93g, had caused spalling of concrete at the base of one column. Therefore it is not likely that Run One, with a peak acceleration of .4g caused no cracking at the base at all.
4. The most important conclusion is that the values of the modified flexural damage ratios computed for the various members were rather low. Even the maximum value of .338, for the exterior beams of the sixth floor, indicates rather low damage. This observation agrees with the experimental evidence.

3.3.3 Experiment by Clough and Gidwani (51)

A scale model of a two-story, one-bay frame building, Fig. (3.20), has been tested on the shaking table of the University of California by Clough and Gidwani. The original structure was designed to satisfy the code requirements. Heavy concrete blocks were placed on both floors (Fig. (3.20)) for similitude reasons, in order to maintain the frequencies of the prototype frame. The idealization of the frame as well as the data required for analysis are given in Fig. (3.21).

The frame was subjected to three consecutive ground acceleration histories. Each one of these was the N69W Taft earthquake, scaled to different peak accelerations, namely .10g, .57g and .65g.

The first test, designated as W1, consisted of a ground motion which stressed the frame only within the working stress range. This loading caused some limited cracking of concrete, but reinforcing steel stresses remained well below yield. This is also indicated by the modified flexural damage ratios, which were computed to be zero for all members. The experimental and analytical top-story displacement histories are reproduced in Fig. (3.22), together with the ground acceleration motion.

The purpose of the second test, W2, was to subject the slightly cracked frame to severe ground accelerations, which would stress the reinforcing steel well into the inelastic range. The good agreement between experimental and

analytical roof displacements, displayed in Fig. (3.23), represents the level of accuracy of the present model in predicting the nonlinear behavior of frame members. The observed damage during the test and the computed values of the modified flexural damage ratios, MFDR, for various members are indicated in Fig. (3.24). It can be seen from that figure that the values of MFDR correlate well with the observed degree of damage. The floor beams had minor cracks and the computed maximum MFDR value was .036. The columns had significant flexural cracks and the computed maximum MFDR value was .522. This value indicates a high damage according to the scale proposed in Section 2.10.

The third test, W3, will be considered in Chapter 4 because the frame had been damaged during test W2, and our analysis, up to this point, considers only undamaged frames.

3.4 Summary and Conclusions

In this chapter the mathematical model for reinforced concrete frame members has been evaluated by simulating four different kinds of experimental tests: 1) three different series of simple cantilever beams; 2) a series of beam-column subassemblies; 3) a scale model of a ten-story frame; 4) a scale model of a two-story frame. In all cases, the nonlinear behavior as characterized by load-deflection hysteresis curves for static loading or displacement histories for dynamic ground motion was predicted very well by the model. Also, the energy

dissipation characteristics were accurately reproduced in all cases.

For subsequent reliability analyses of damaged concrete buildings it is important to introduce useful definitions of damage and failure. The modified flexural damage ratio, MFDR, defined in Section 2.10 is believed to satisfy all requirements. In Table (3.15) MFDR values for all twenty test beams analyzed in Section 3.2 are summarized, together with two different damage parameters. The first one was used by Banon et al.⁽⁵²⁾ to develop a stochastic model for damage in reinforced concrete members. It is based on the single-component mechanical model, which considers concentrated plastic hinges at the beam ends. This damage parameter is called flexural damage ratio, FDR, and defined as

$$FDR = \frac{K_f}{K_r} \quad (3.1)$$

where K_f is the initial elastic flexural stiffness of the member,

$$K_f = \frac{3EI}{\lambda^3} \quad (3.2)$$

and K_r is the reduced secant stiffness;

$$K_r = \frac{P_{\max}}{\delta_{\max}} \quad (3.3)$$

where λ is the cantilever length, δ_{\max} the maximum tip displacement reached in any loading cycle, and P_{\max} is the load corresponding to δ_{\max} . The FDR values listed in Table (3.15) were given in Ref. 52.

The second column of Table (3.15) contains the flexural damage ratios computed according to Eq. (2.52). The differences between the two damage parameters are due to the fact that the first one is a measure of the stiffness degradation for the entire member, while the second one reflects the degradation of the stiffness of the most highly stressed section.

Both damage parameters can serve as measures of overall degradation of similar members, but neither one contains an inherent measure of damage severity or failure.

The modified flexural damage ratios, MFDR, summarized in the third column of Table (3.15) have been shown earlier to closely correlate with the onset of failure (MFDR=1), defined to coincide with the spalling of concrete; therefore it can serve as a reliable prediction of failure. Excepting the special case of beam R4 discussed earlier, the MFDR values range from .92 to 2.42, with an average of 1.35 and a variance of .29. Therefore, it can be concluded that this damage parameter can be used with confidence in Chapter 4 for reliability analysis involving damaged frames.

The last column of Table (3.15), which lists the MFDR values for the termination of each test, corroborates this finding in that it clearly indicates a high probability of complete failure of each test specimen, which in fact did experience failure by most standards. Thus it can be said that the higher the computed MFDR value, the more severe will be the expected damage, and the residual strength and stiffness will be correspondingly small.

Table (3.1) Material properties of the beams
tested by Ma, Bertero and Popov (4)

Beam	E_s (ksi)	p_s	f_{sy} (ksi)	ϵ_{su}	f'_c (ksi)	ϵ_o $\times 10^5$
R1	28,700	.01	66	.18	5.07	225
R2	28,700	.01	66	.18	4.19	210
R3	28,700	.01	66	.18	4.58	225
R4	28,700	.01	66	.18	4.38	245
R5	29,111	.01	65.5	.18	4.58	222
R6	29,111	.01	65.5	.18	4.34	225
T1	28,700	.01	66	.18	4.79	226
T2	28,700	.01	66	.18	4.61	226
T3	29,111	.01	65.5	.18	4.47	205

E_s : steel modulus of elasticity

p_s : steel strain hardening ratio

f_{sy} : steel yield stress

ϵ_{su} : steel strain at maximum stress

f'_c : concrete strength

ϵ_o : concrete strain at maximum stress

Table (3.2) Dimensions and reinforcement data of the beams tested by Ma, Bertero and Popov (4)

Beam	L (in)	P (k)	H (in)	B _b (in)	D _{cb} (in)	A _{sb} (in ²)	B _t (in)	D _{ct} (in)	A _{st} (in ²)	ρ ["] %
R1	62.5	0	16	9	2	1.764	9	2	0.932	0.53
R2	62.5	0	16	9	2	1.764	9	2	0.932	0.53
R3	62.5	0	16	9	2	1.764	9	2	0.932	1.
R4	62.5	0	16	9	2	1.764	9	2	0.932	1.
R5	38.5	0	16	9	2	1.764	9	2	1.764	1.
R6	62.5	0	16	9	2	1.764	9	2	1.764	1.
T1	62.5	0	16	9	2	2.00	36	2	0.932	1.
T2	62.5	0	16	9	2	2.00	36	2	0.932	1.
T3	62.5	0	16	9	2	2.00	36	2	1.764	1.

L : Beam length

P : Axial force

ρ["] : Confinement ratio; equation (2.3)

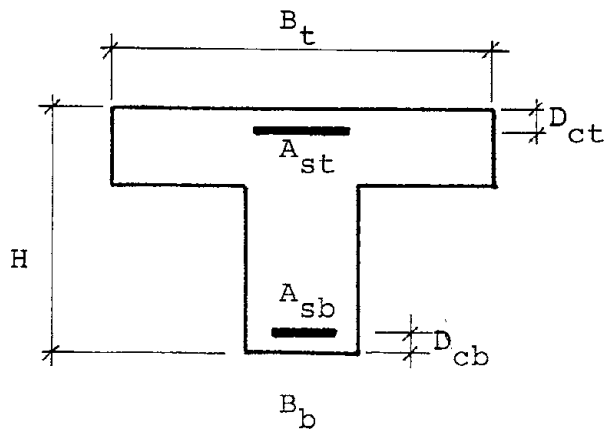


Table (3.3) Analytical and experimental results of the beams tested by Ma, Bertero and Popov (4)

Beam	Onset of Failure			Termination of Test		
	Modified Flexural Damage Ratio	Dissipated Energy (k-in)		Modified Flexural Damage Ratio	Dissipated Energy (k-in)	
		Test	Analysis		Test	Analysis
R1	1.43	335	313	4.63	460	474
R2	1.28	267	316	2.37	364	440
R3	1.21	583	526	1.66	710	699
R4	3.91	289*	224	3.91	289	224
R5	1.02	349	343	1.98	550	555
R6	0.98	738	761	0.98	738	761
T1	0.92	519	544	0.92	519	544
T2	0.99	234	180	0.99	234	180
T3	1.00	803	877	1.00	902	982

*The value given in Ref. (4) was 336, but the actual area computed from the corresponding experimental load-deflection curve is 289.

Table (3.4) Material properties of the beams tested by Atalay and Penzien (29)

Beam	E_s (ksi)	p_s	f_{sy} (ksi)	ϵ_{su}	f'_c (ksi)	ϵ_o $\times 10^5$
S1	28,500	.01	55.2	.2	4.22	280
S2	28,500	.01	55.2	.2	4.45	280
S3	28,500	.01	55.2	.2	4.235	280
S4	28,500	.01	55.2	.2	4.005	280
S5	28,500	.01	55.2	.2	4.26	280
S6	28,500	.01	55.2	.2	4.61	280
S7	28,500	.01	55.2	.2	4.615	280
S8	28,500	.01	55.2	.2	4.44	280

E_s : steel modulus of elasticity

p_s : steel strain hardening ratio

f_{sy} : steel yield stress

ϵ_{su} : steel strain at maximum stress

f'_c : concrete strength

ϵ_o : concrete strain at maximum stress

Table (3.5) Dimensions and reinforcement data of the beams tested by Atalay and Penzien (29)

Beam	L (in)	P (k)	H (in)	B _b (in)	D _{cb} (in)	A _{sb} (in ²)	B _t (in)	D _{ct} (in)	A _{st} (in ²)	ρ" %
S1	60	60	12	12	2.06	1.2	12	2.06	1.2	1.53
S2	60	60	12	12	2.06	1.2	12	2.06	1.2	.93
S3	60	60	12	12	2.06	1.2	12	2.06	1.2	1.53
S4	60	60	12	12	2.06	1.2	12	2.06	1.2	.93
S5	60	120	12	12	2.06	1.2	12	2.06	1.2	1.53
S6	60	120	12	12	2.06	1.2	12	2.06	1.2	.93
S7	60	120	12	12	2.06	1.2	12	2.06	1.2	1.53
S8	60	120	12	12	2.06	1.2	12	2.06	1.2	.93

L : Beam length

P : Axial force

ρ" : Confinement ratio; equation (2.3)

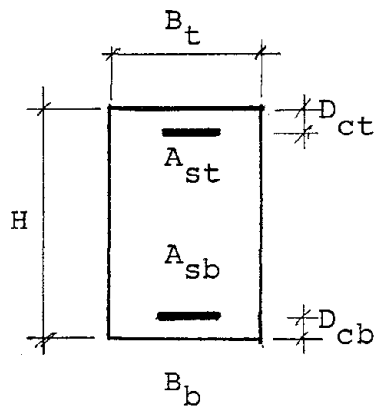


Table (3.6) Analytical and experimental results of the beams tested by Atalay and Penzien (29)

Beam	Modified Flexural Damage Ratio at Onset of Failure	Termination of Test		
		Modified Flexural Damage Ratio	Dissipated Energy (k-in)	
			Test	Analysis
S1	1.11	1.11	1253	1236
S2	0.97	4.96	1066	839
S3	0.90	1.00	1074	1056
S4	0.96	3.35	1201	1097
S5	1.53	3.93	1237	1593
S6	2.62	6.71	990	1072
S7	2.02	2.02	1051	1214
S8	2.20	7.10	730	872

Table (3.7) Material properties of the beams tested by Popov, Bertero and Krawinkler (48)

Beam	E_s (ksi)	ρ_s	f_{sy} (ksi)	ϵ_{su}	f'_c (ksi)	ϵ_o $\times 10^5$
B35	29,000	.005	67	.18	3.86	250
B46	29,000	.005	67	.18	3.99	250
B43	29,000	.005	60	.18	5.03	250

Table (3.8) Dimensions and reinforcement data of the beams tested by Popov, Bertero and Krawinkler (48)

Beam	L (in)	P (k)	H (in)	B_b (in)	D_{cb} (in)	A_{sb} (in ²)	B_t (in)	D_{ct} (in)	A_{st} (in ²)	ρ " %
B35	78	0	29	15	3.75	6	15	3.75	6	.61
B46	78	0	29	15	3.75	6	15	3.75	6	.82
B43	78	0	29	15	3.75	6	15	3.75	6	1.64

Table (3.9) Steel properties for the specimens
tested by Scribner and Wight (49)

Member	E_s (ksi)	ρ_s	f_{sy} (ksi)	ϵ_{su}
Beams : Sp. 1-8	27,200	.007	54.4	.168
Columns: Sp. 1-8	28,200	.006	56.4	.16
Beams : Sp. 9-12	29,900	.008	55.0	.18
Columns: Sp. 9-12	30,000	.01	69.5	.20

Table (3.10) Concrete properties for the specimens
tested by Scribner and Wight (49)

Specimen	f'_c (ksi)	ϵ_o $\times 10^5$	ρ'' (beams) %	ρ'' (columns) %
1	4.95	325	1.2	2.4
3	4.94	358	0.88	2.4
5	4.08	397	1.2	2.4
7	3.84	466	0.97	2.4
9	5.13	315	1.34	0.009
11	4.73	300	1.34	0.009

Table (3.11) Dimensions of the specimens tested by Scribner and Wight (49)

Specimen	l_1 (in)	e (in)	l_2 (in)
1	47.5	6	30
3	47.5	6	30
5	37	6	30
7	47.5	6	30
9	69	9	48
11	57	9	48

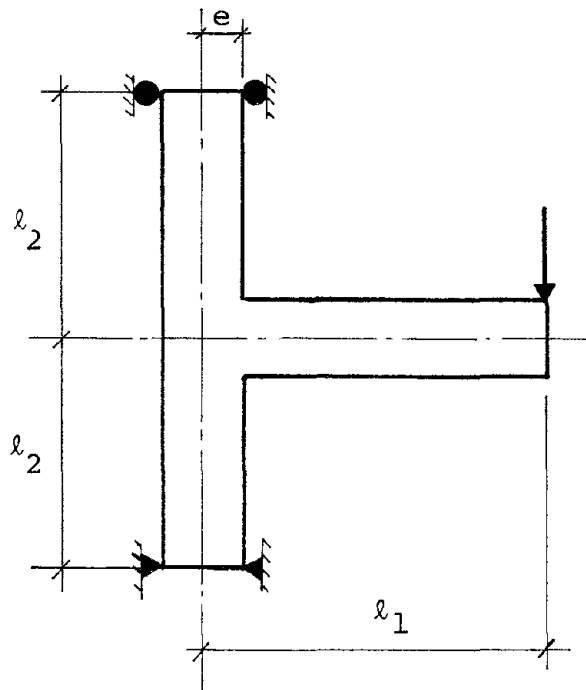
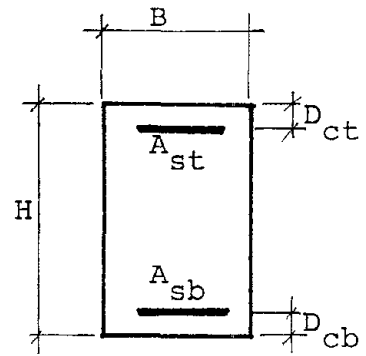
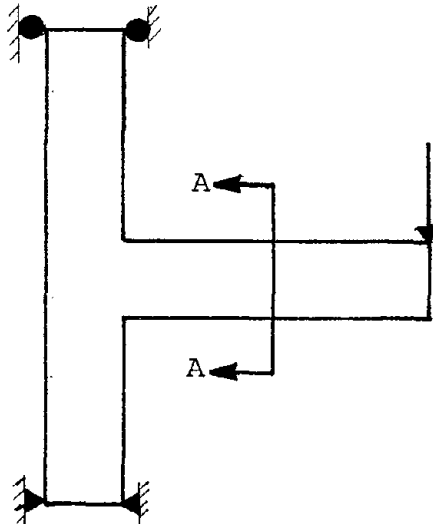


Table (3.12) Dimensions and reinforcement of the beams in the test by Scribner and Wight (49)

Specimen	H (in)	B (in)	D_{cb} (in)	A_{sb} (in ²)	D_{ct} (in)	A_{st} (in ²)
1	10	8	1.3	0.613	1.4	0.884
3	12	8	1.8	0.92	1.9	1.326
5	10	8	1.3	0.613	1.4	0.884
7	12	8	1.8	0.92	1.9	1.326
9	14	10	1.8	2.404	1.9	3.14
11	14	10	1.8	2.404	1.9	3.14



CROSS SECTION A-A

Table (3.13) Dimensions and reinforcement of the columns in the test by Scribner and Wight (49)

Specimen	H (in)	B (in)	D _c (in)	A _s (in ²)
1 - 8	12	8	1.5	0.884
9 - 12	18	12	2.	2.982

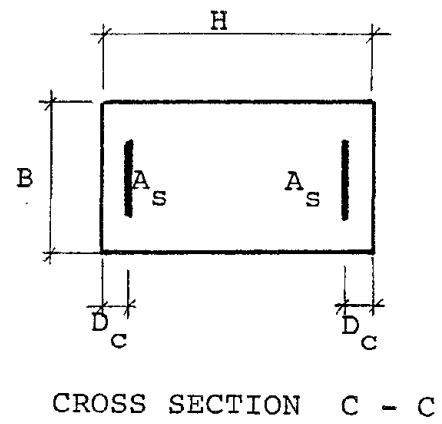
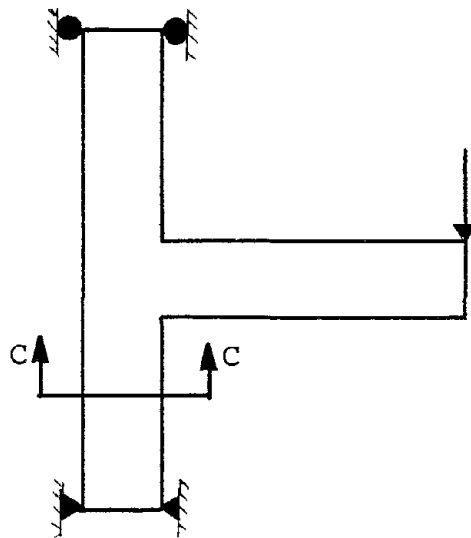


Table (3.14) Analytical and experimental results
for the test by Scribner and Wight (49)

Specimen	Modified Flexural Damage Ratio	Dissipated Energy (k-in)	
		Analytical	Experimental
1	0.918	287	366
3	2.534	323	311
5	2.185	255	315
7	3.411	399	407
9	2.412	975	1269
11	4.496	552	723

Table (3.15) Damage parameters

Specimen	Member FDR ⁽¹⁾	Local FDR ⁽²⁾	MFDR ⁽³⁾	MFDR ⁽⁴⁾
R1	6.8	17.0	1.43	4.63
R2	7.8	32.0	1.28	2.37
R3	8.5	18.7	1.21	1.66
R4	10.6	41.9	3.91	3.91
R5	11.0	25.3	1.02	1.98
R6	7.4	23.8	0.98	0.98
T1	9.0	21.7	0.92	0.92
T2	11.4	23.2	0.99	0.99
T3	8.5	26.6	1.00	1.00
S1	--	33.8	1.11	1.11
S2	--	22.2	0.97	4.96
S3	10.4	27.8	0.90	1.00
S4	13.1	20.3	0.96	3.35
S5	14.6	33.6	1.53	3.93
S6	14.1	40.8	2.62	6.71
S7	13.1	47.5	2.02	2.02
S8	12.2	33.1	2.20	7.10
B35	--	45.9	2.45	2.45
B46	--	38.3	1.21	1.21
B43	11.0	30.2	0.93	0.93

(1) Ref. (52)

(2) Eq. (2.47)

(3) modified flexural damage ratio at onset of failure

(4) modified flexural damage ratio at termination of test

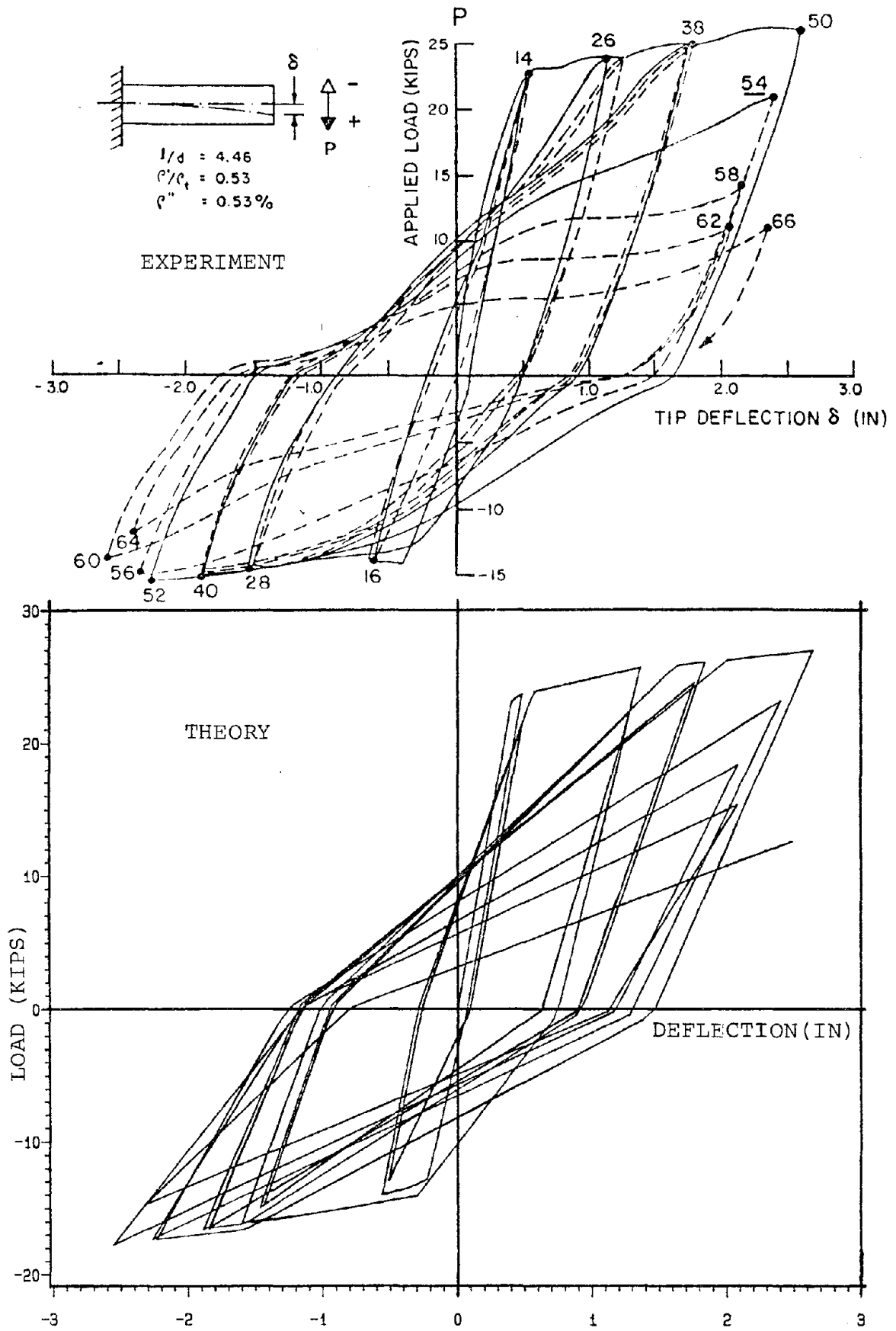


Fig. (3.1). Load-deflection curves for specimen R1 in the experiment by Ma, Bertero and Popov(4)

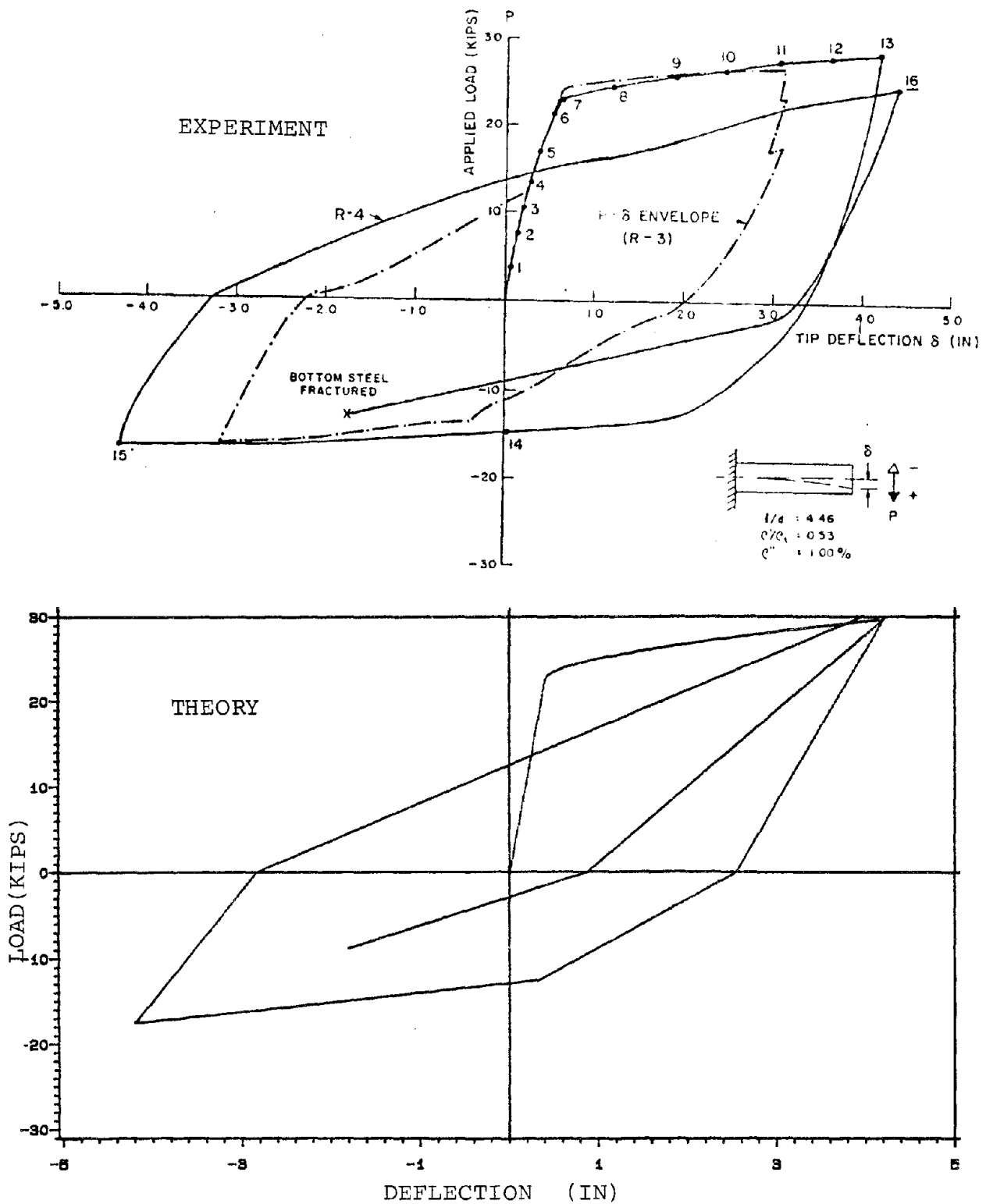


Fig.(3.2). Load-deflection curves for specimen R4 in the experiment by Ma, Bertero and Popov⁽⁴⁾

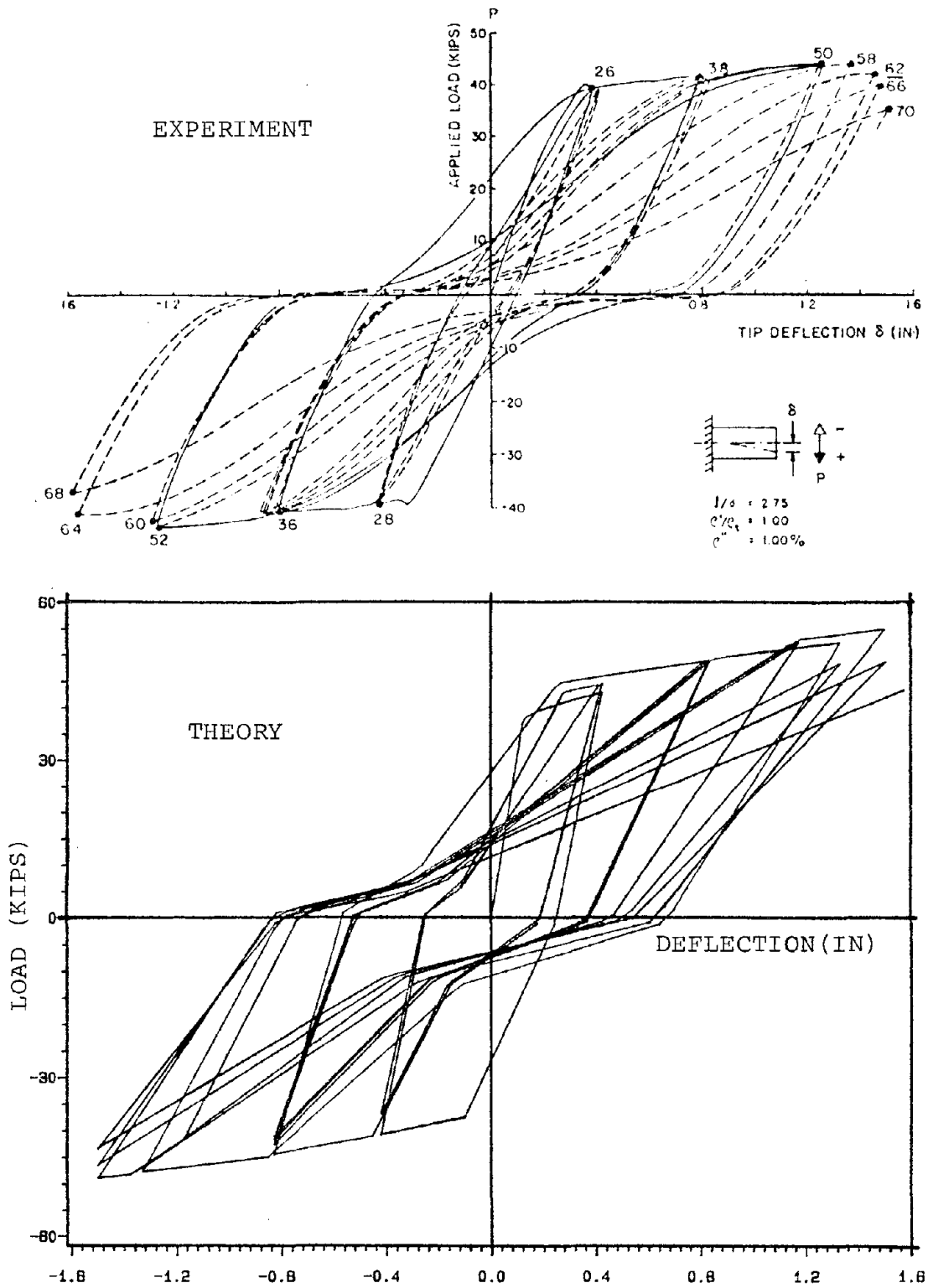


Fig.(3.3). Load-deflection curves for specimen R5 in the experiment by Ma, Bertero and Popov⁽⁴⁾

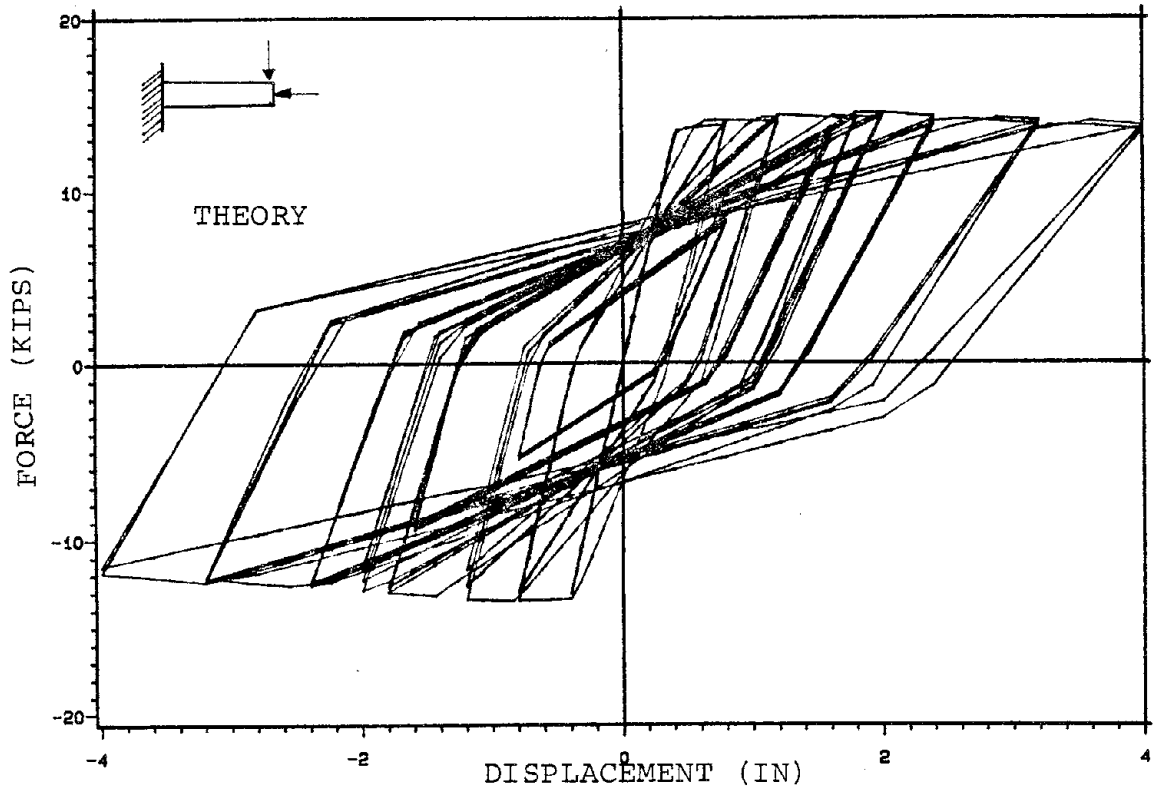
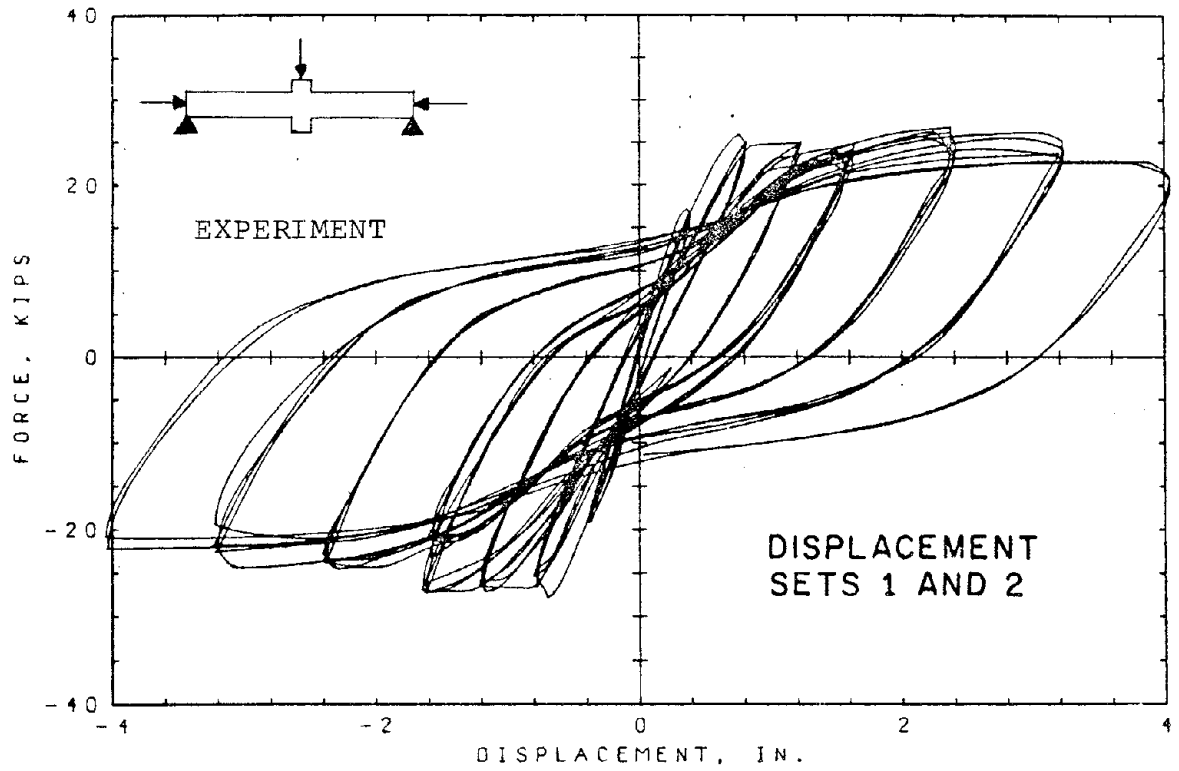


Fig.(3.4). Load-deflection curves for specimen S1 in the experiment by Atalay and Penzien⁽²⁹⁾

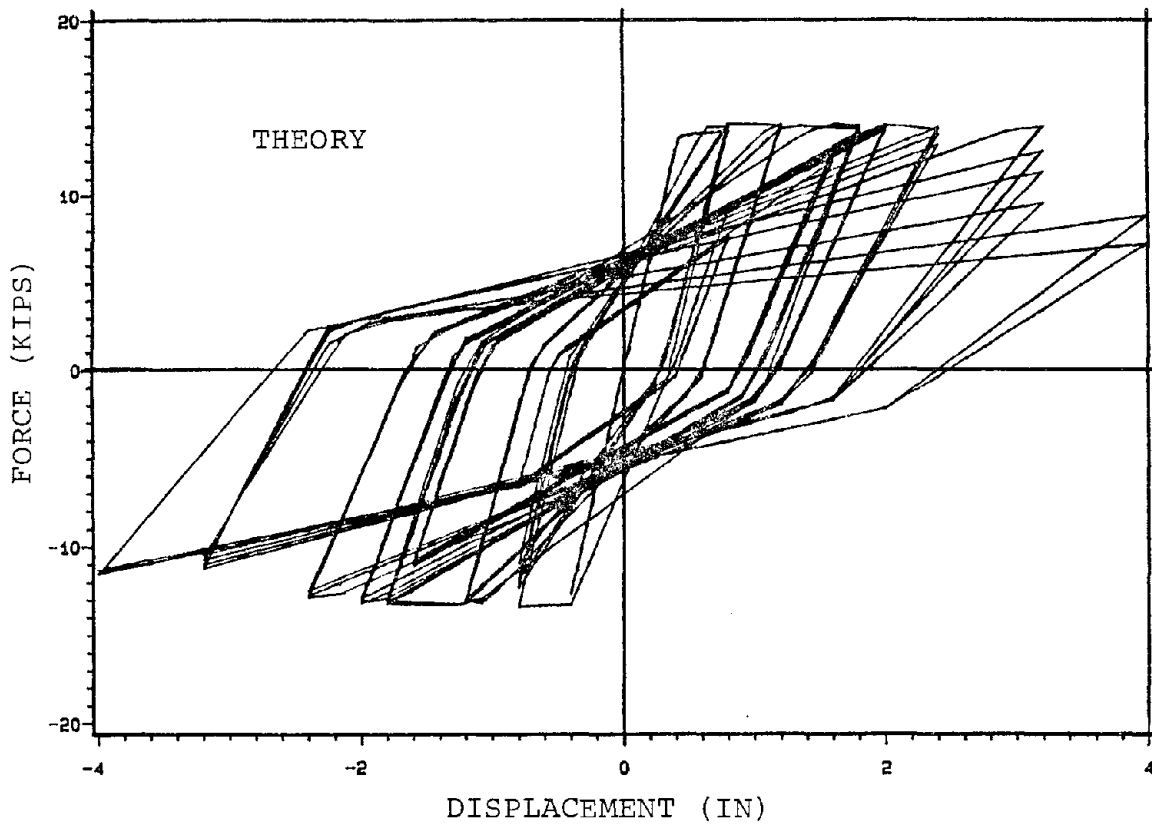
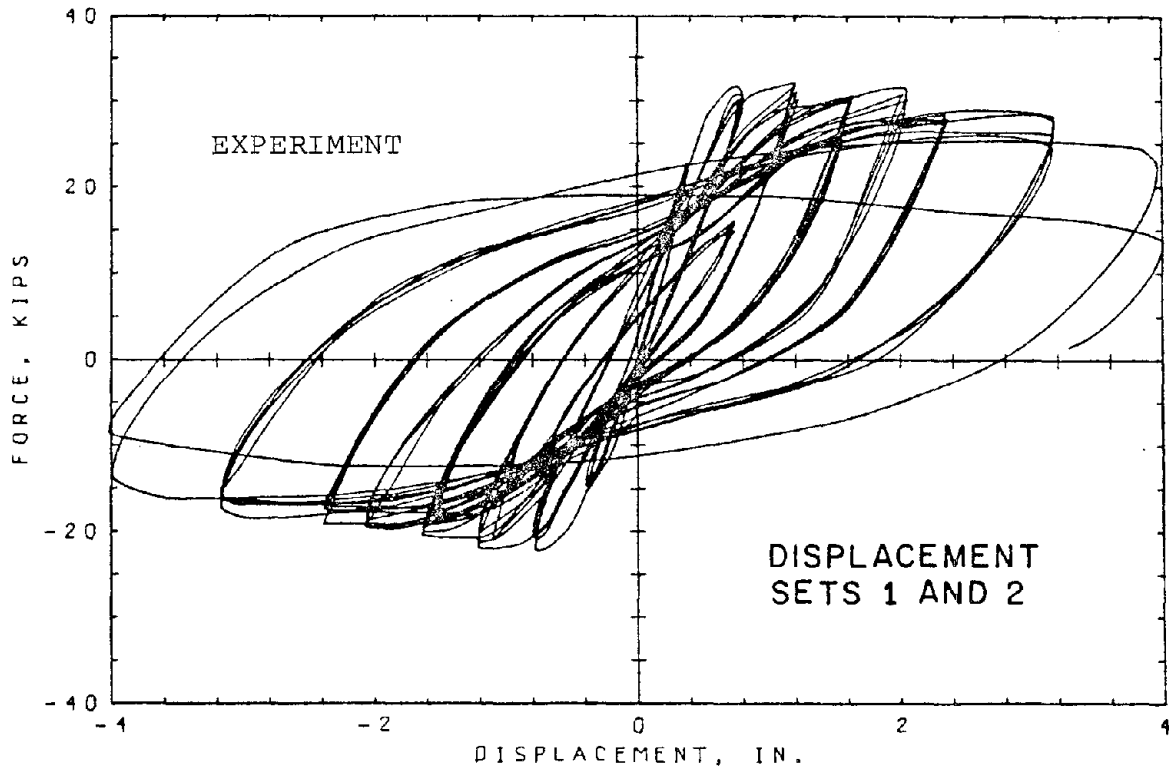


Fig.(3.5). Load-deflection curves for specimen S4 in the experiment by Atalay and Penzien⁽²⁹⁾

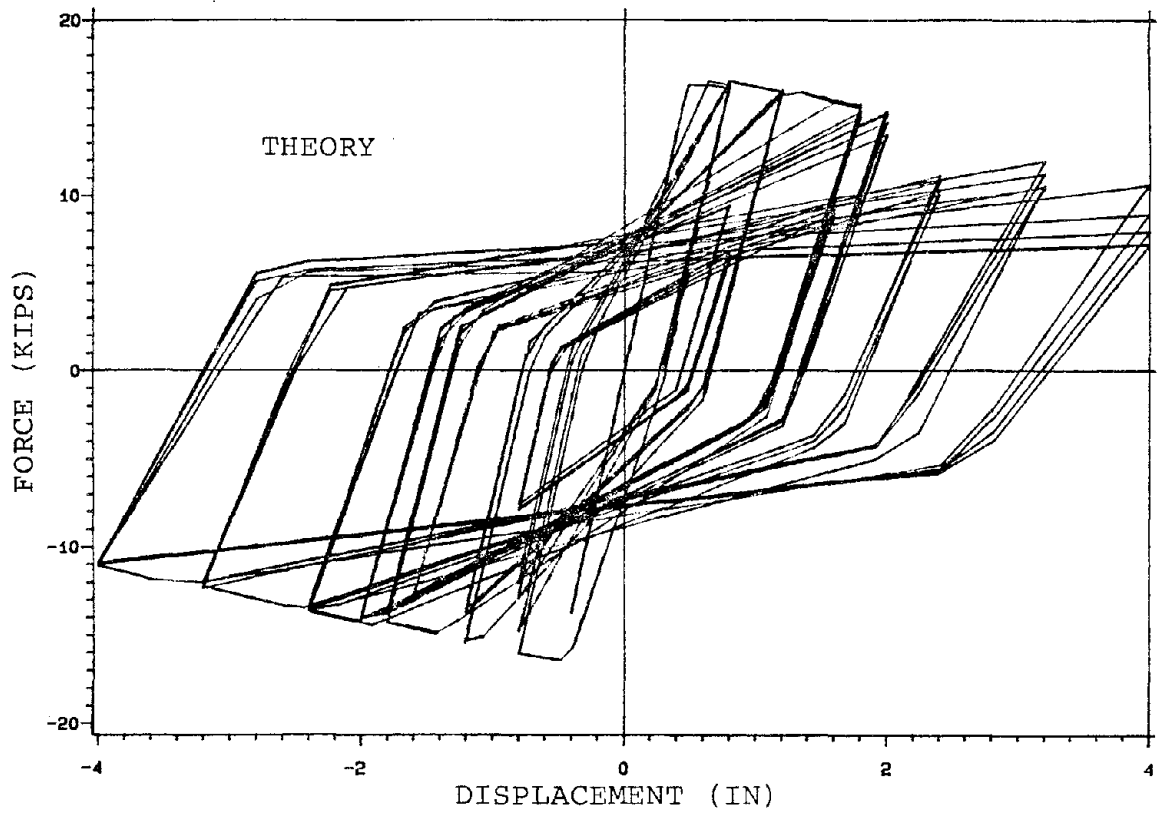
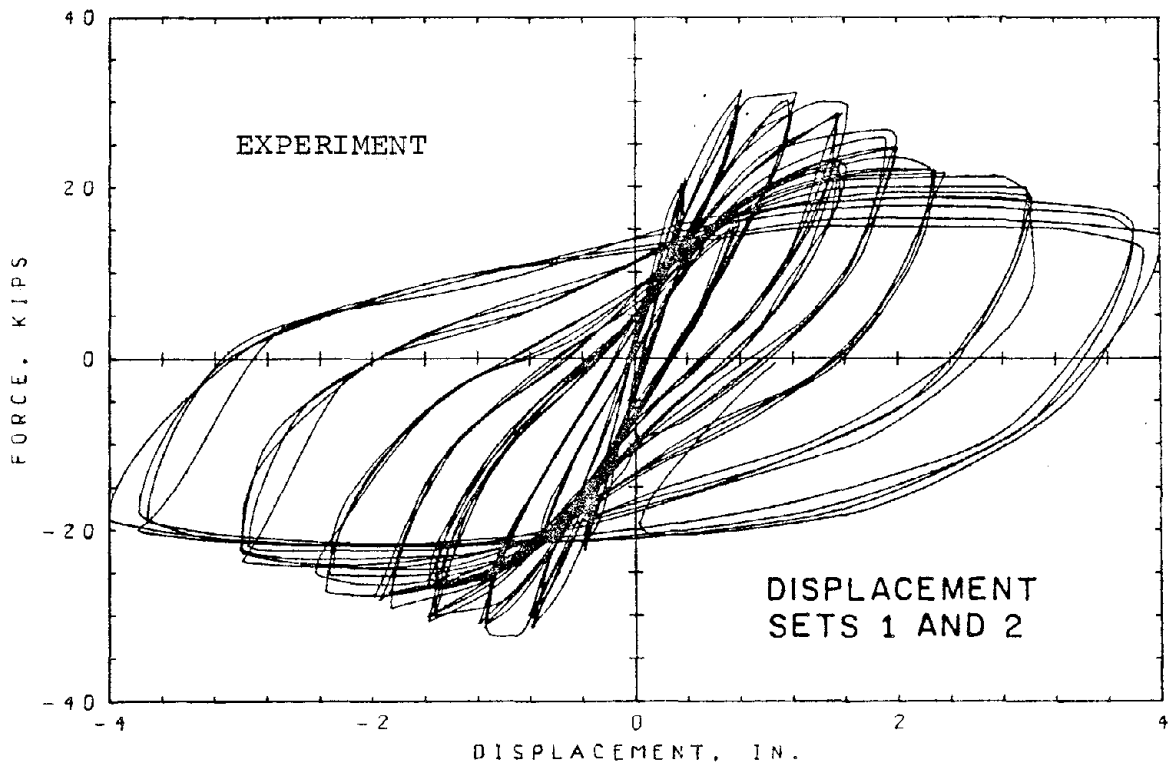


Fig. (3.6). Load-deflection curves for specimen S5 in the experiment by Atalay and Penzien⁽²⁹⁾

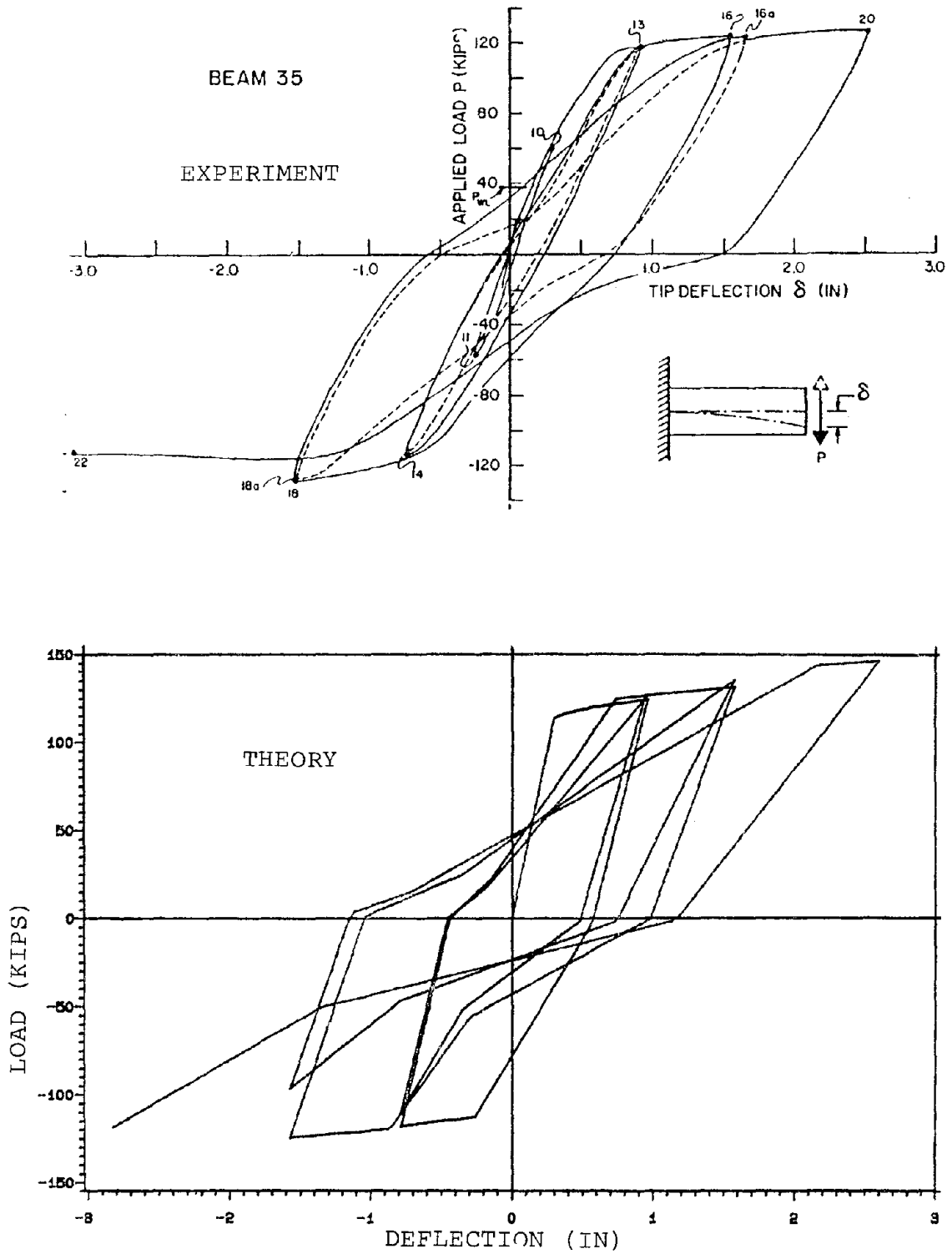


Fig.(3.7). Load-deflection curves for beam B35 in the experiment by Popov, Bertero and Krawinkler (48)

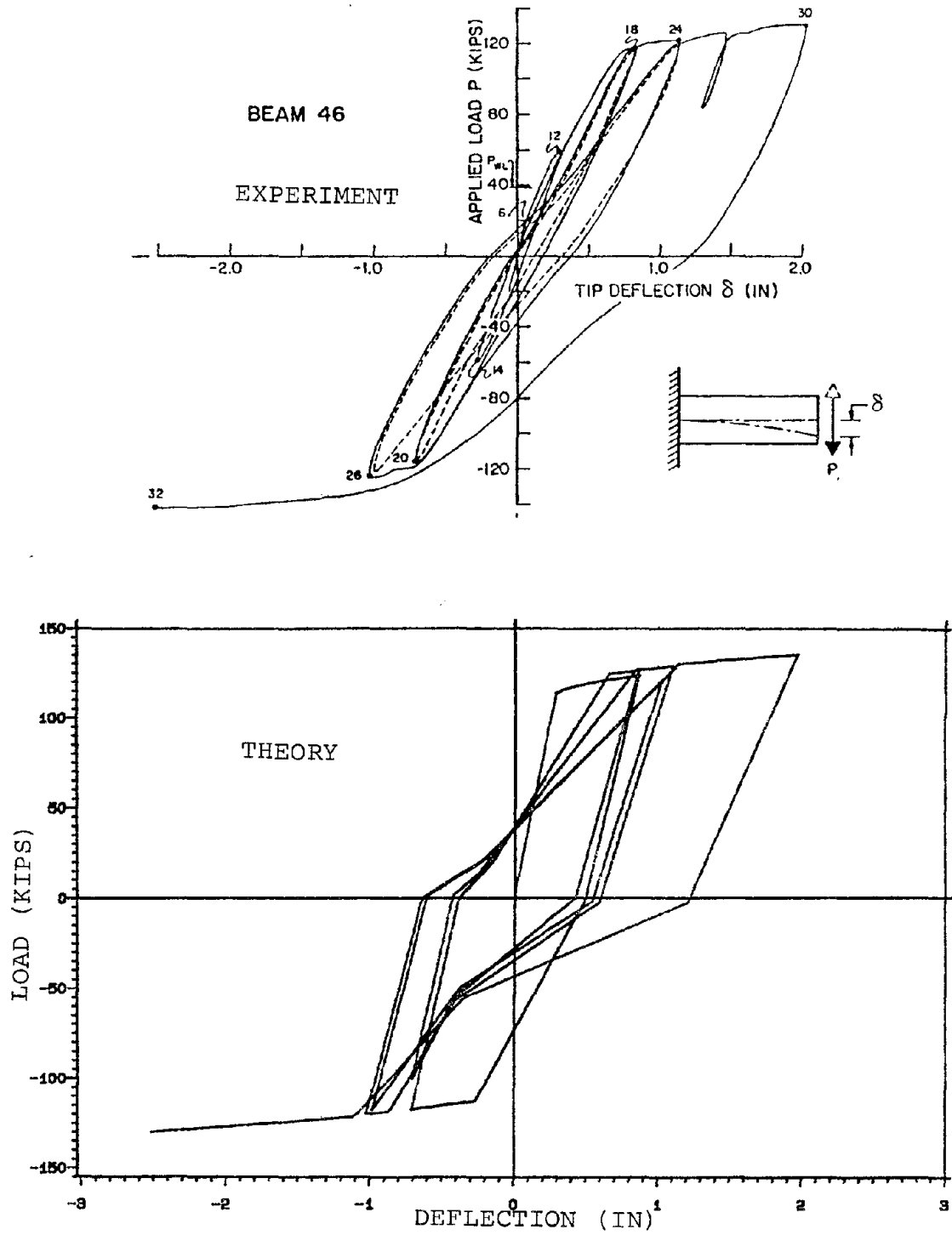


Fig.(3.8). Load-deflection curves for beam B46 in the experiment by Popov, Bertero and Krawinkler(48)

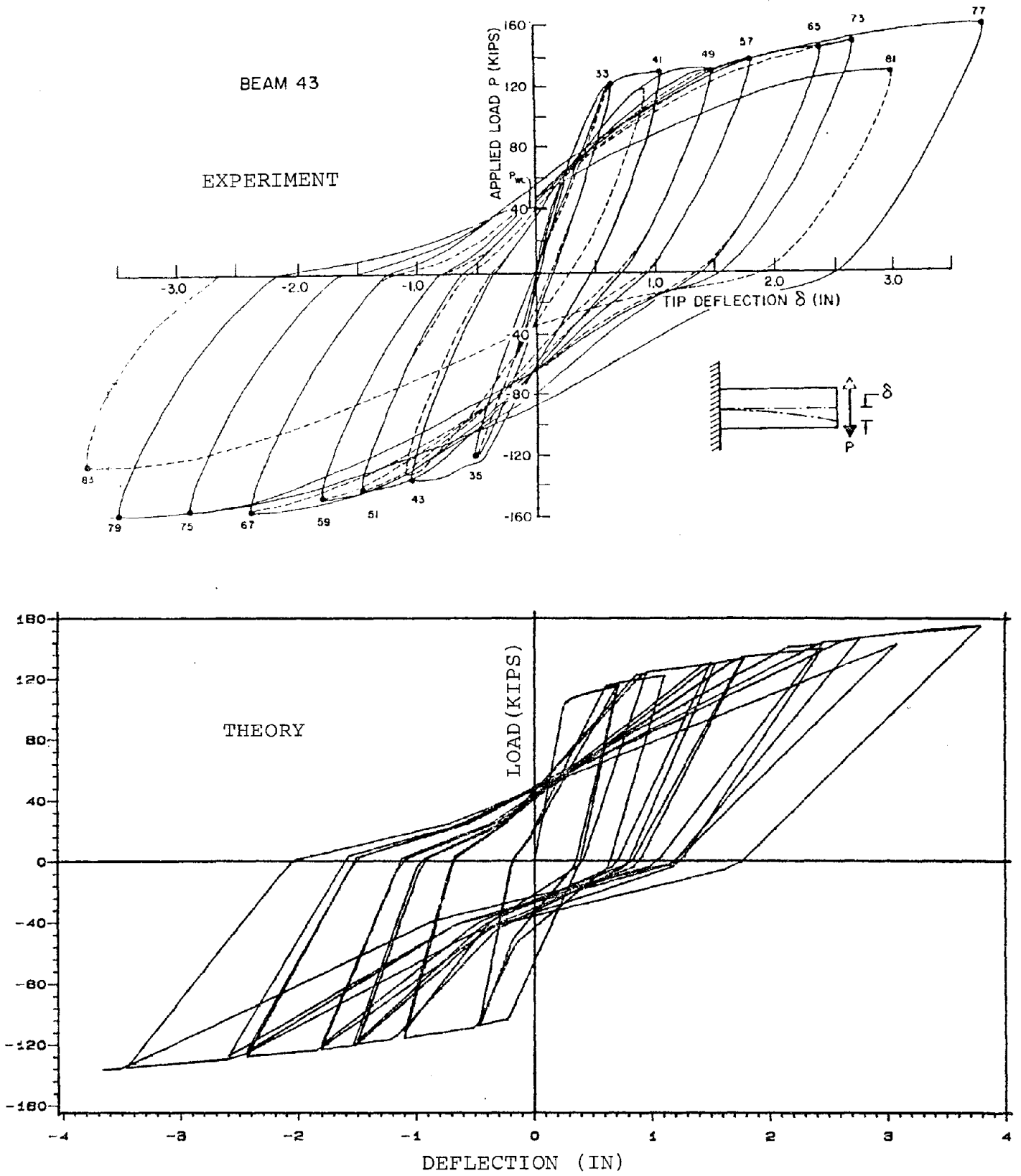


Fig.(3.9). Load-deflection curves for beam B43 in the experiment by Popov, Bertero and Krawinkler⁽⁴⁸⁾

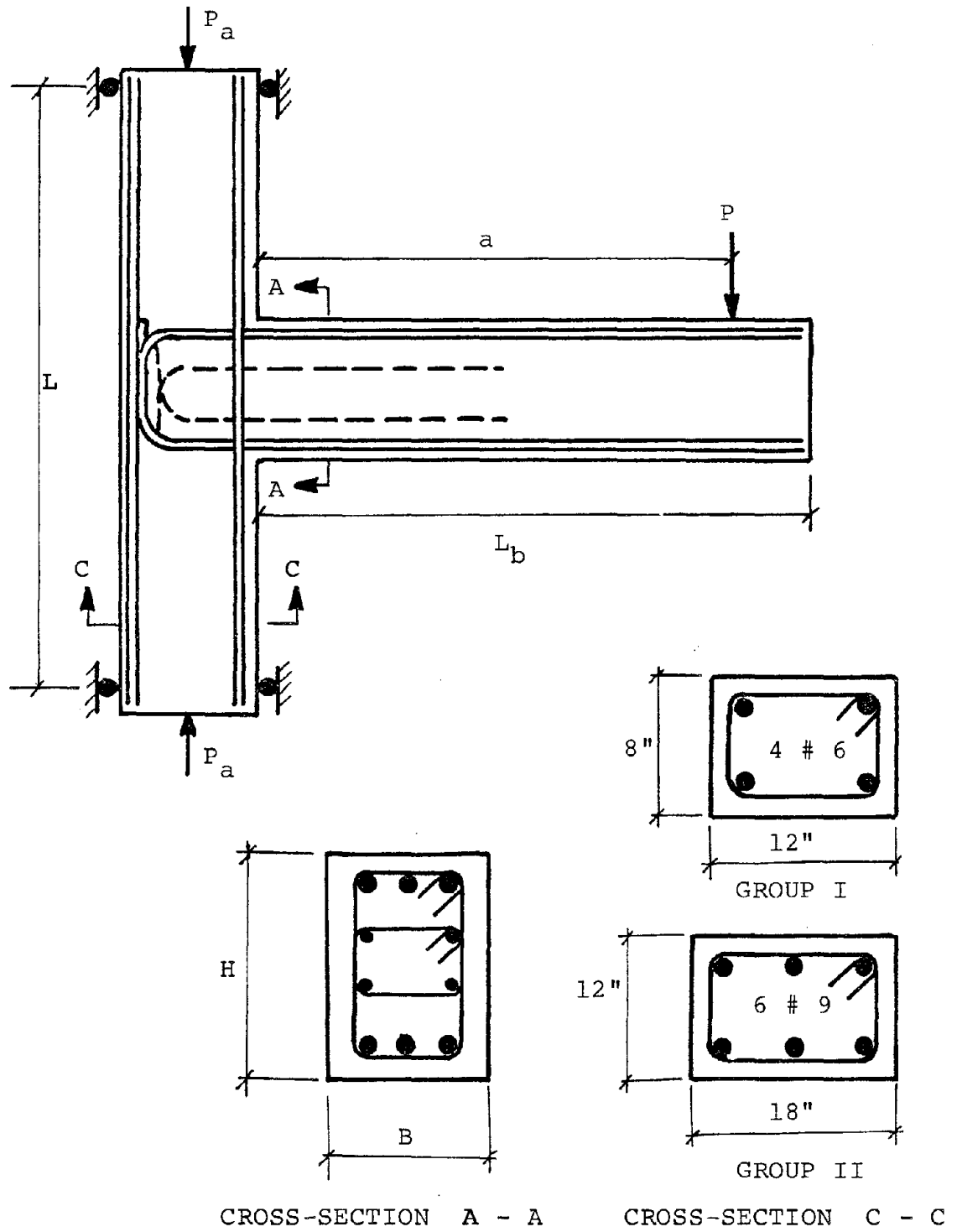


Fig.(3.10). Specimen configuration in the experiment by Scribner and Wight (49)

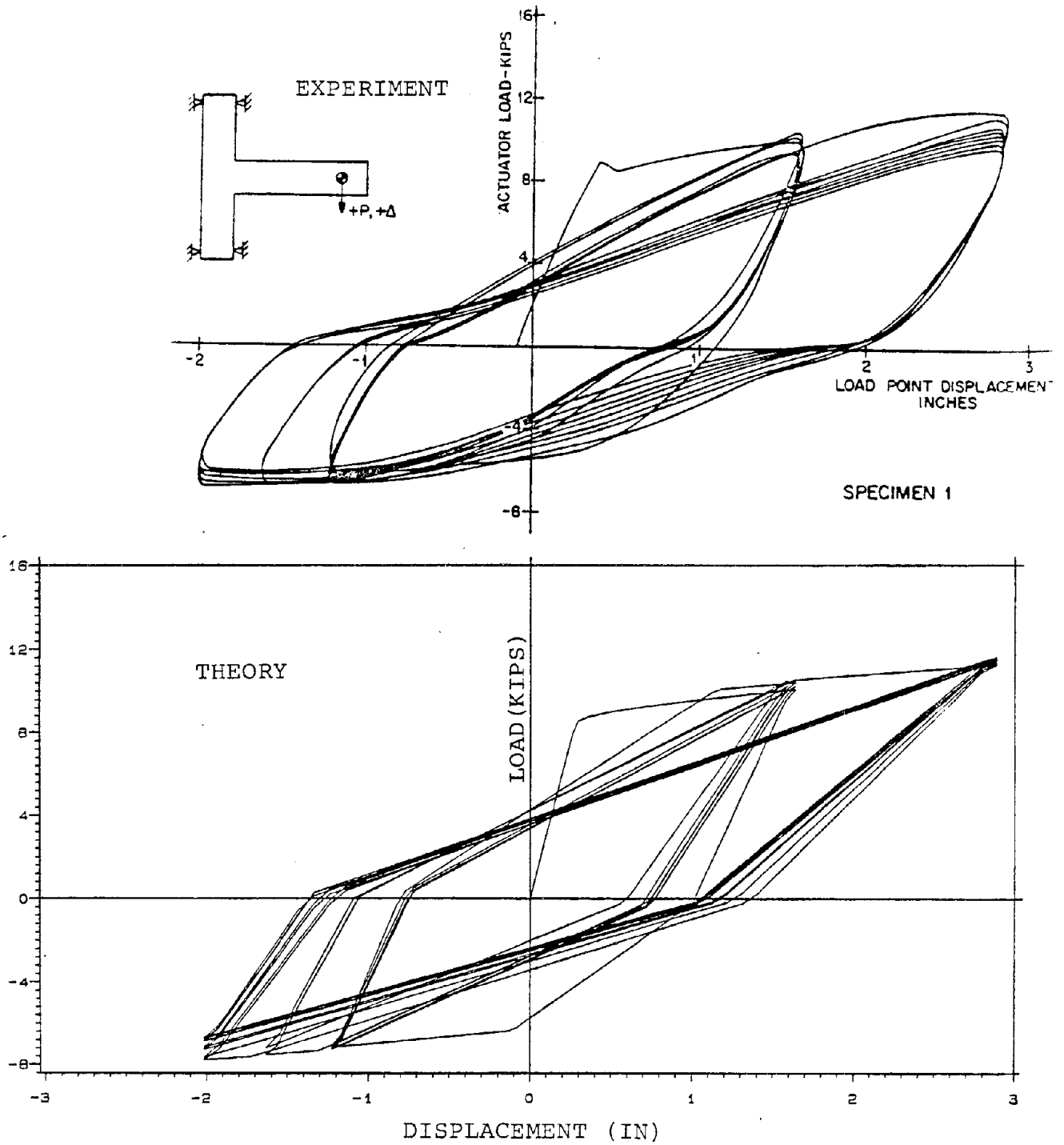


Fig.(3.11). Load-deflection curves for specimen 1 in the experiment by Scribner and Wight(49)

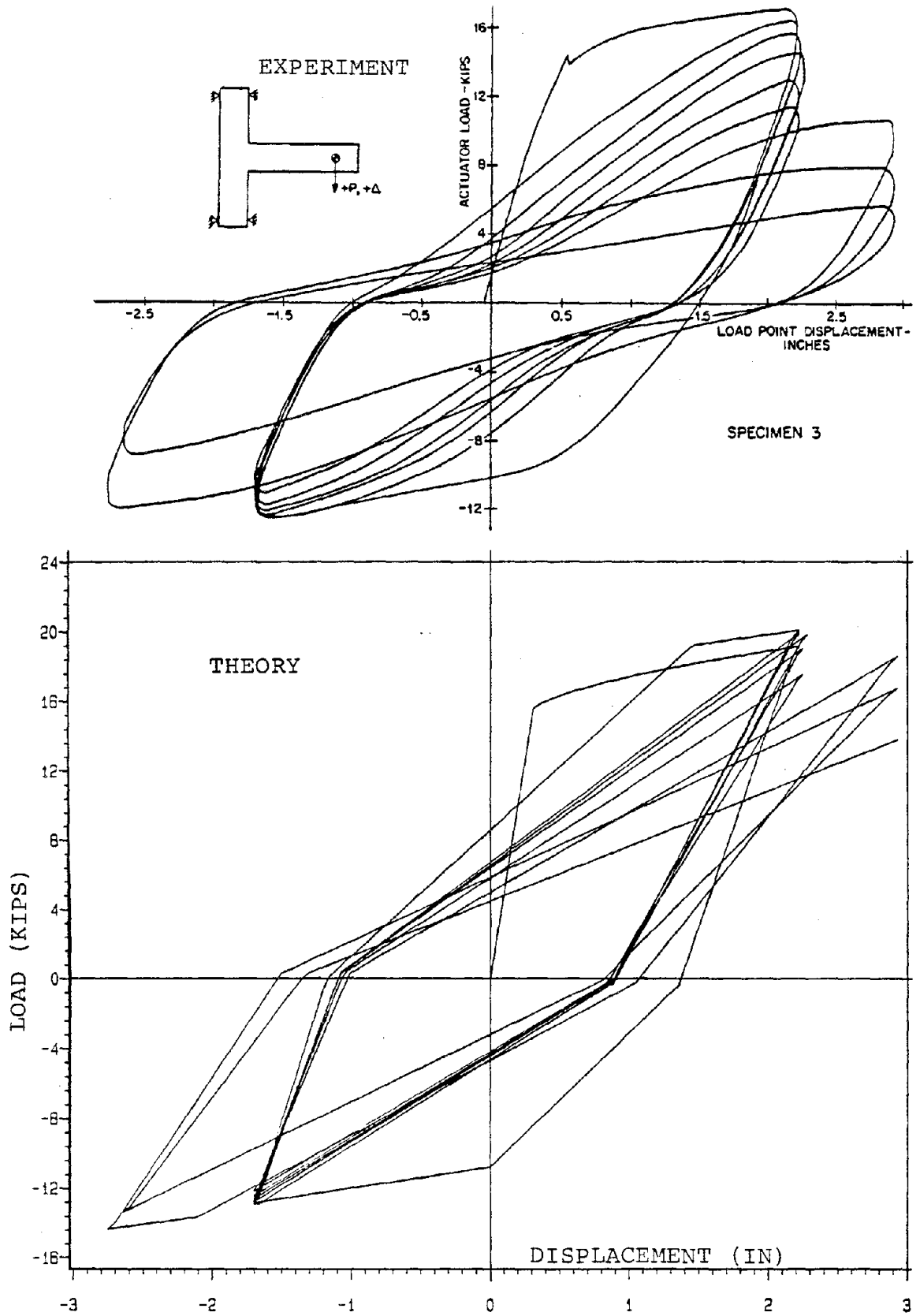


Fig. (3.12). Load-deflection curves for specimen 3 in the experiment by Scribner and Wight (49)

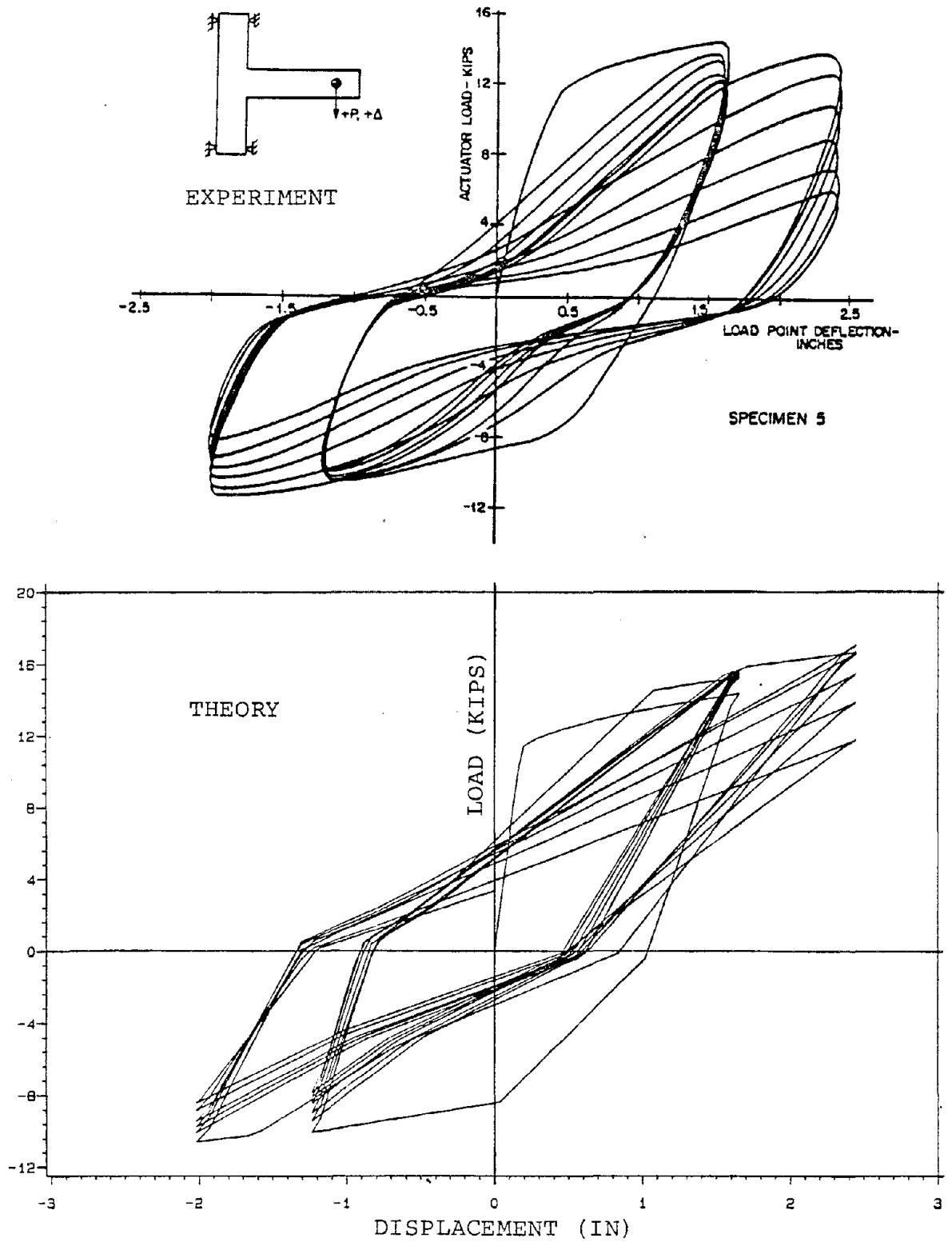


Fig.(3.13). Load-deflection curves for specimen 5 in the experiment by Scribner and Wight (49)

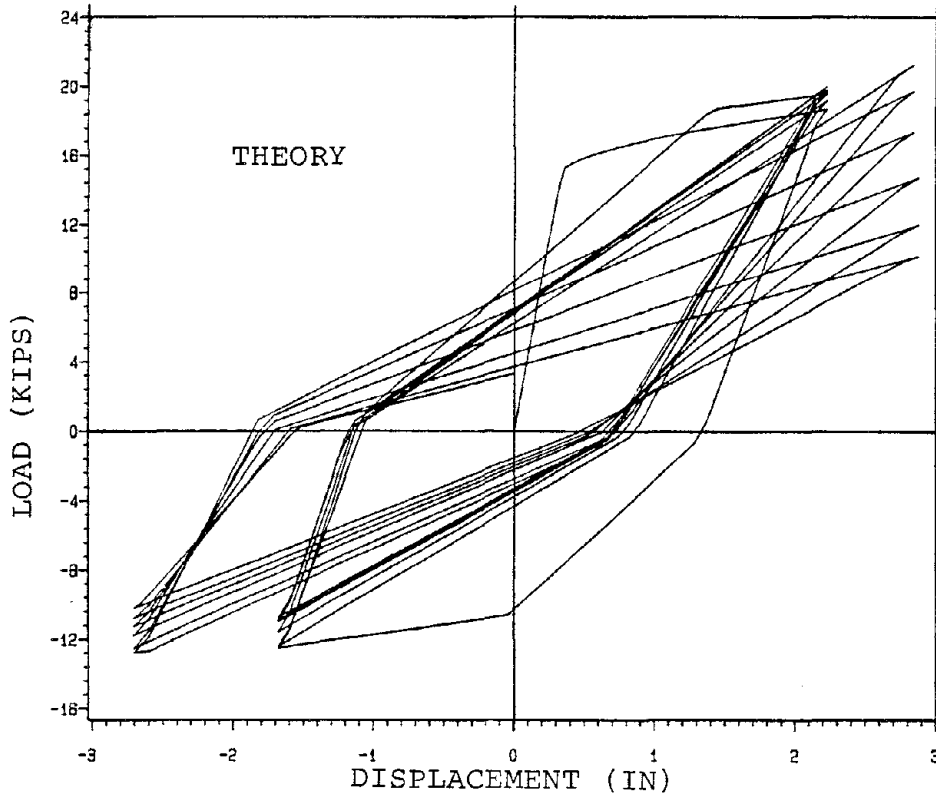
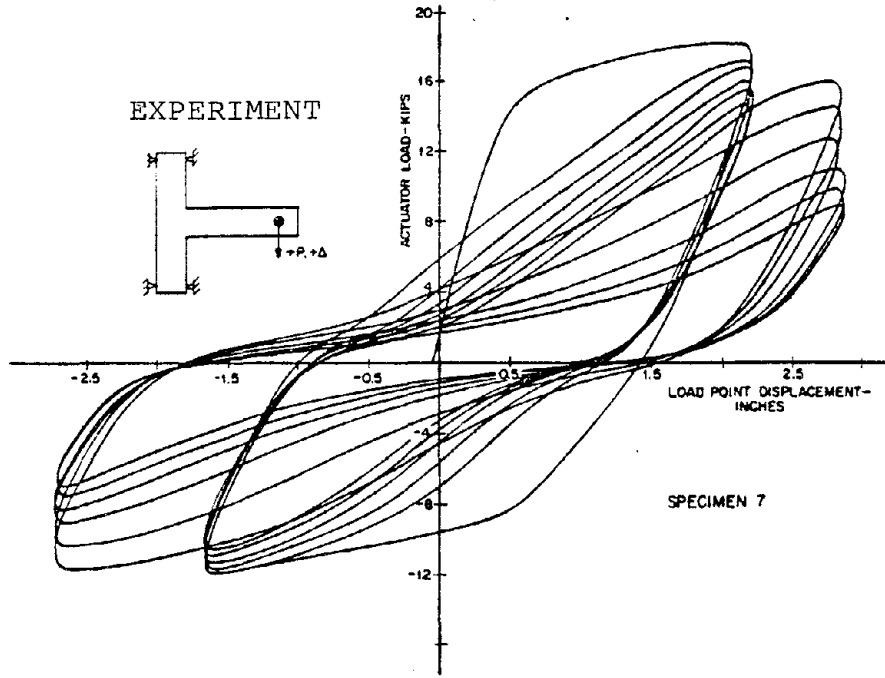


Fig.(3.14). Load-deflection curves for specimen 7 in the experiment by Scribner and Wight⁽⁴⁹⁾

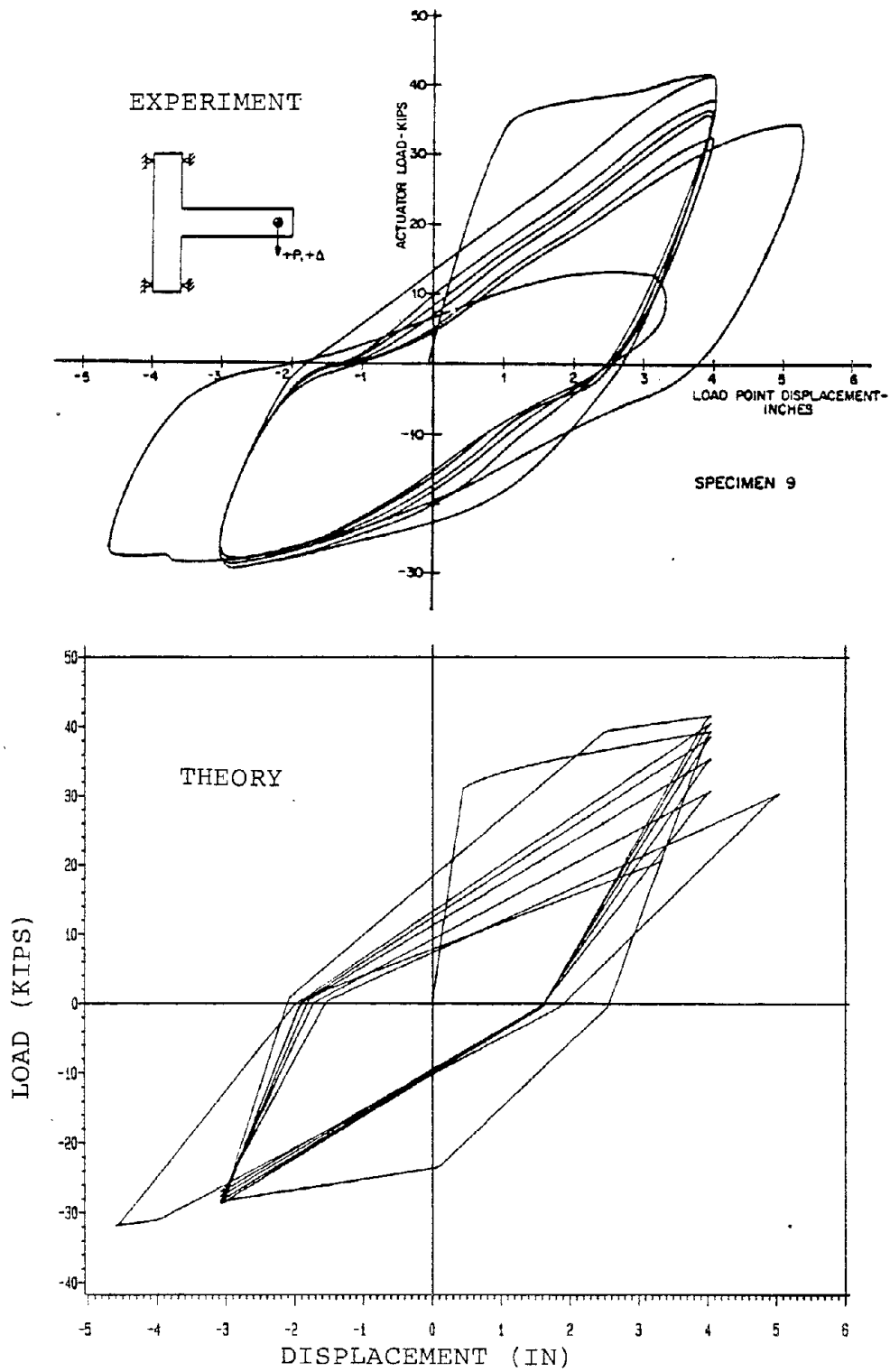


Fig.(3.15). Load-deflection curves for specimen 9 in the experiment by Scribner and Wight⁽⁴⁹⁾

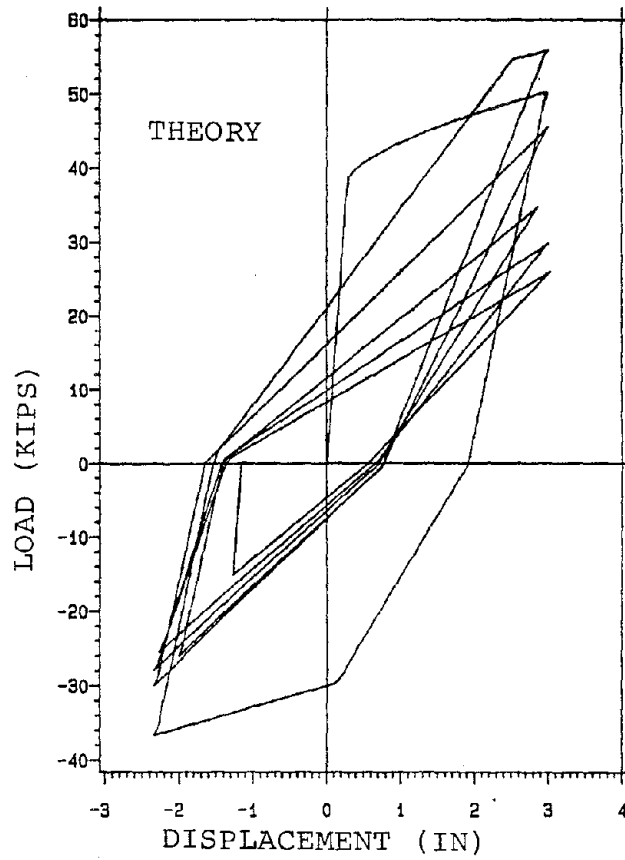
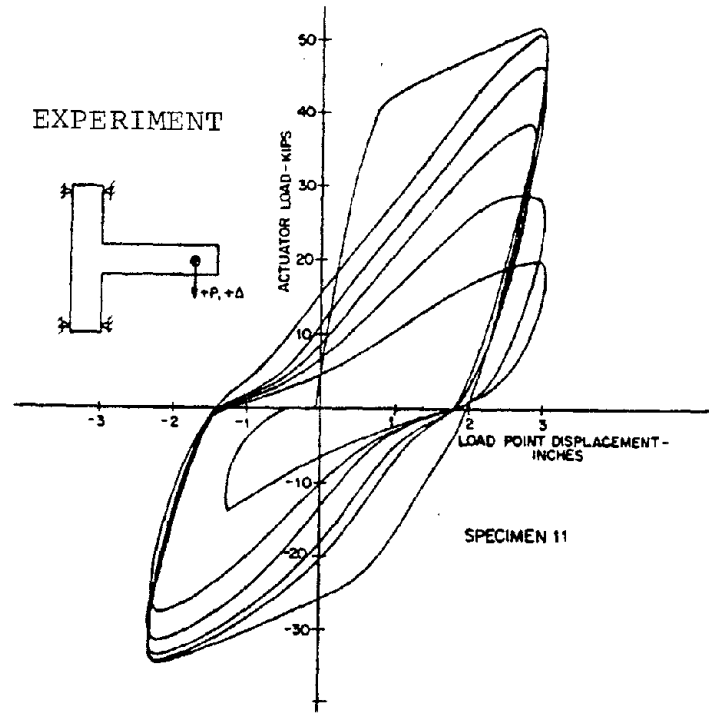
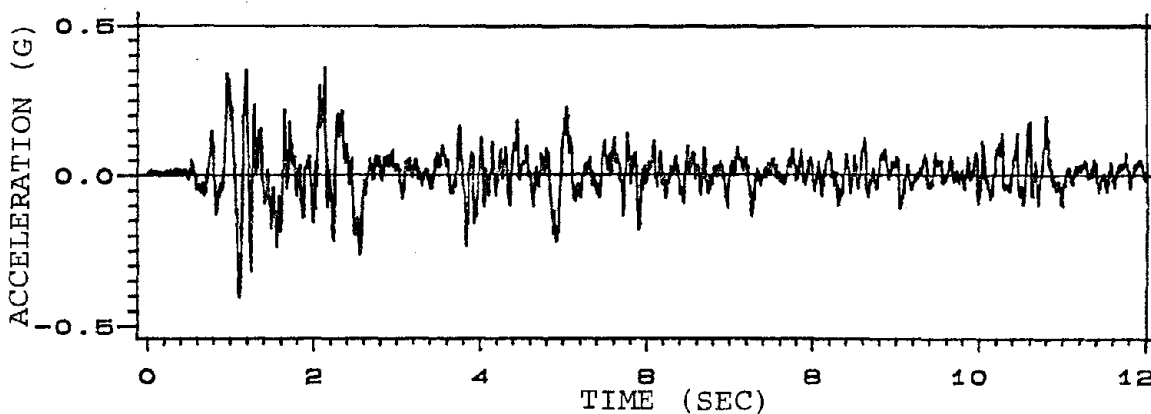
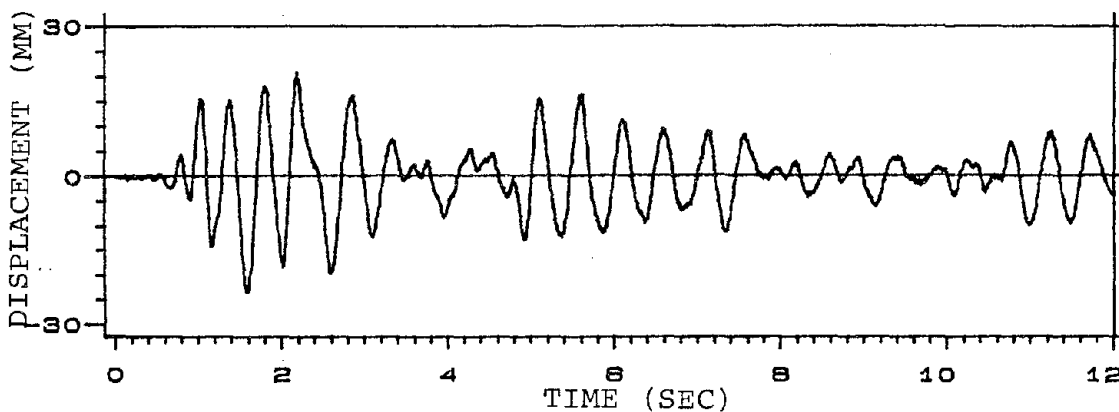


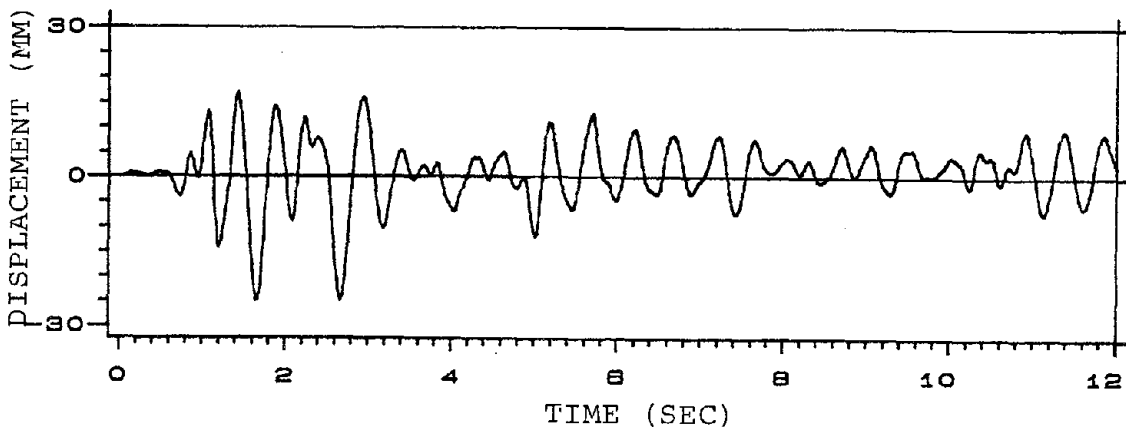
Fig.(3.16). Load-deflection curves for specimen 11 in the experiment by Scribner and Wight⁽⁴⁹⁾



a) GROUND ACCELERATION

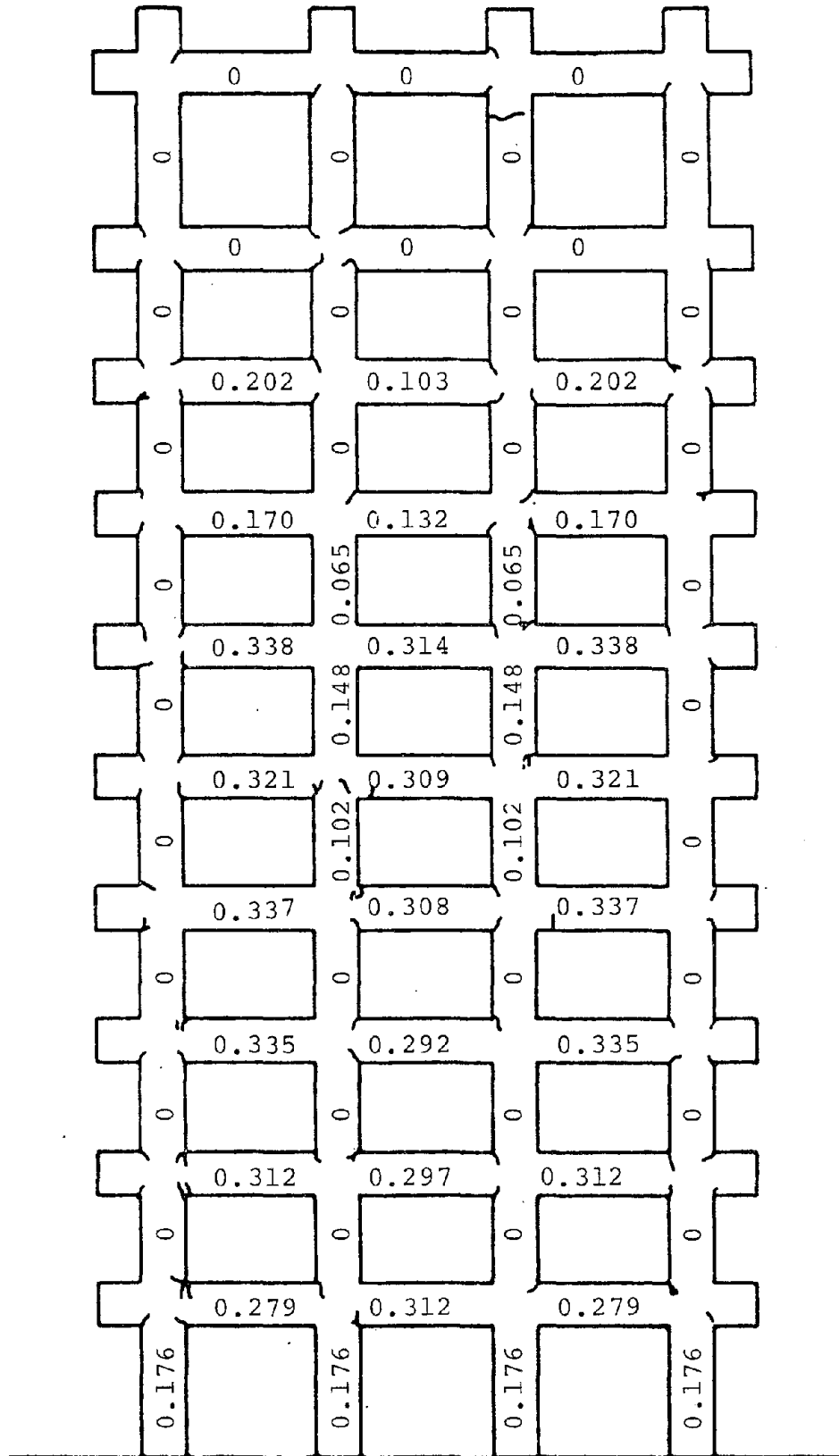


b) RECORDED RESPONSE

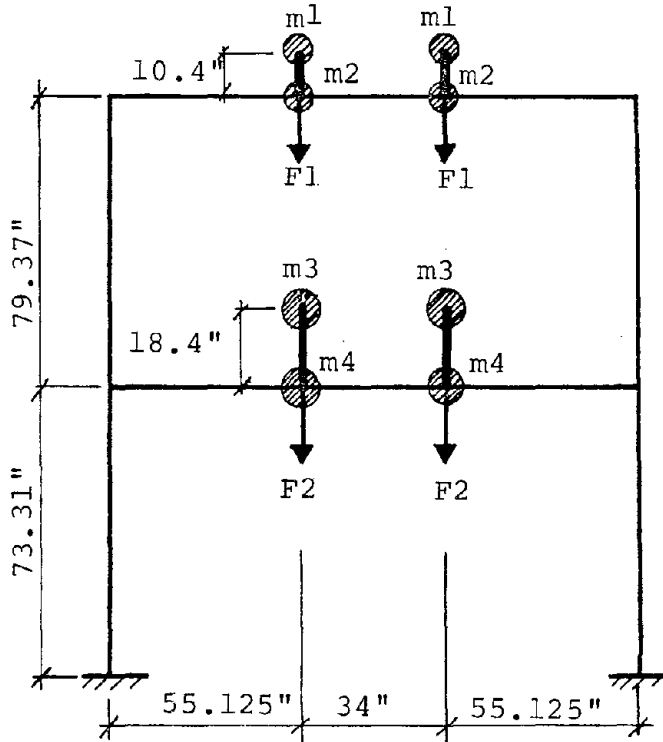


c) COMPUTED RESPONSE

Fig.(3.18). Response of the frame tested by Healey and Sozen⁽⁵⁰⁾ for Run One



(Not to Scale)
Fig. (3.19). Observed crack pattern and computed modified flexural damage ratios after test Run One in the experiment by Healey and Sozen (50)



$f'_c = 4.39 \text{ KSI}$

$\epsilon_o = 0.00335$

$P_s = 0.01$

LUMPED MASSES:

$m_1 = 0.00545 \text{ K-SEC}^2/\text{IN}$

$m_2 = 0.00335 \text{ K-SEC}^2/\text{IN}$

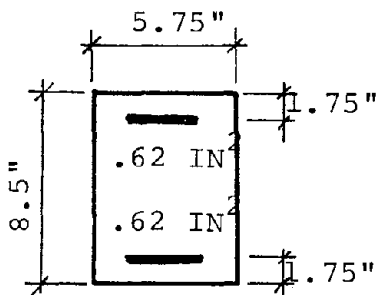
$m_3 = 0.01063 \text{ K-SEC}^2/\text{IN}$

$m_4 = 0.00368 \text{ K-SEC}^2/\text{IN}$

GRAVITY LOADS:

$F_1 = 3.07 \text{ K}$

$F_2 = 5.07 \text{ K}$



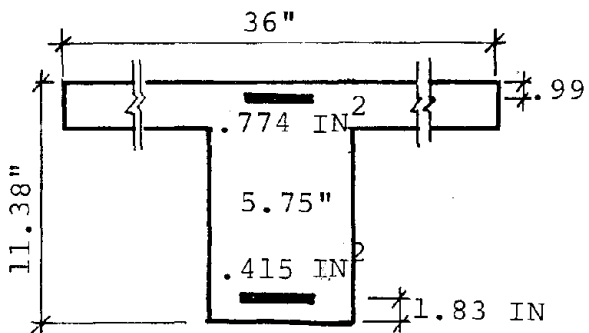
COLUMN CROSS-SECTION

	COLUMN	TOP GIRDER	BOTTOM GIRDER
--	--------	------------	---------------

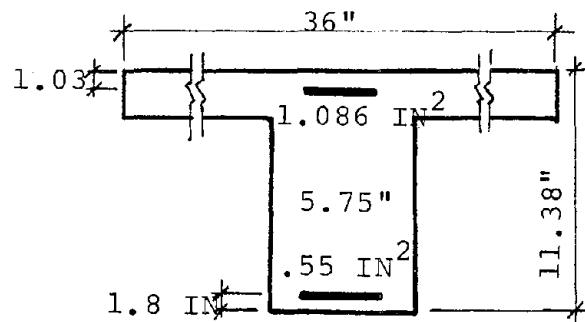
$E_s \text{ (KSI)}$ 29,800 28,200 29,100

$f_{sy} \text{ (KSI)}$ 41.5 54.05 46.75

$\rho \text{ (\%)}$ 3.07 2.05 2.05

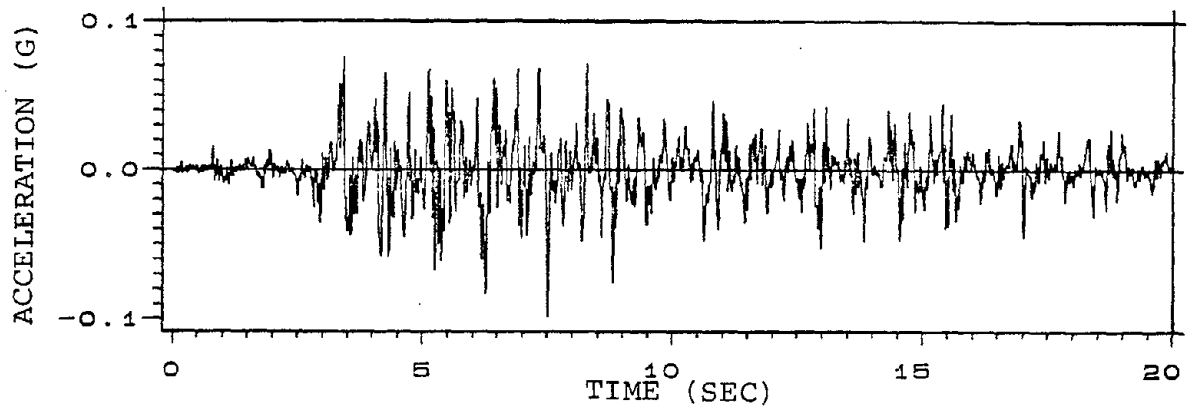


TOP STORY GIRDER

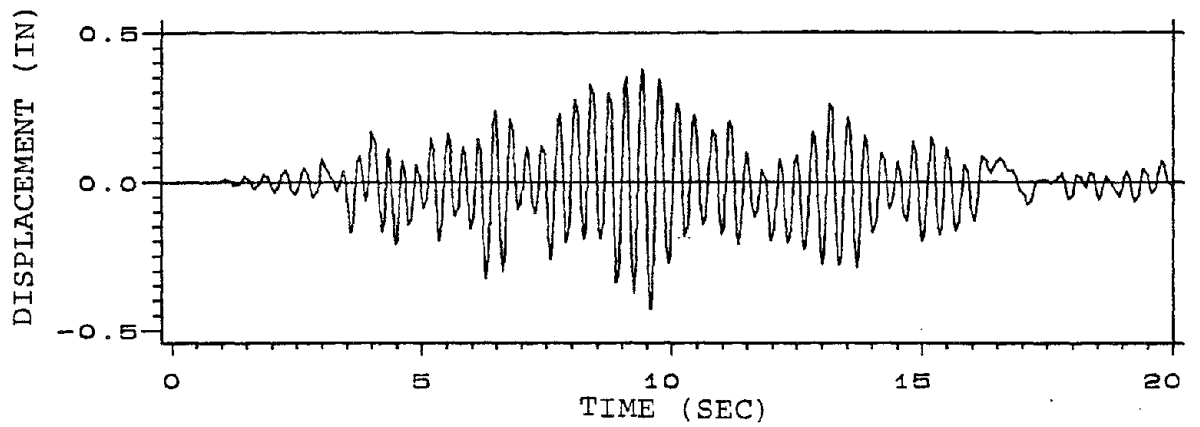


BOTTOM STORY GIRDER

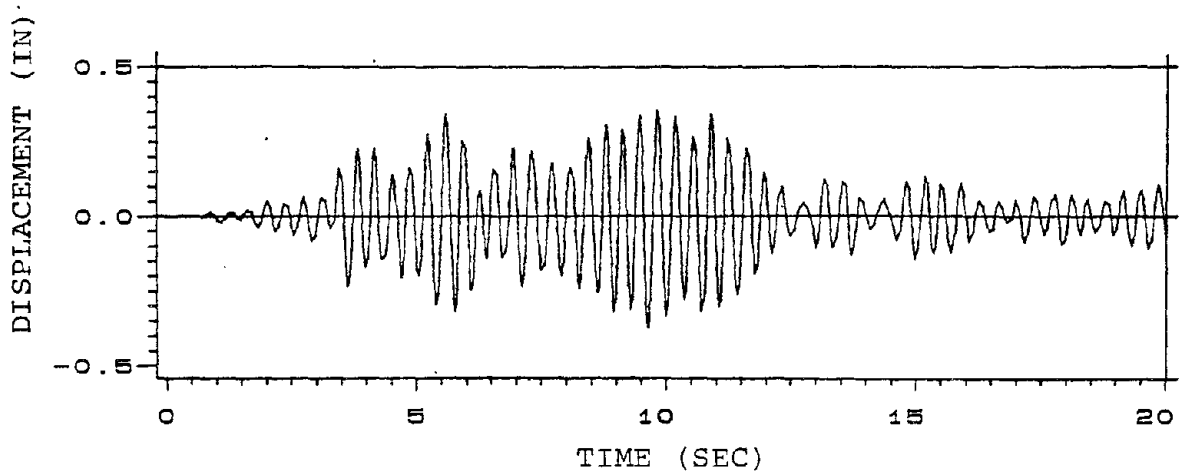
Fig.(3.21). Idealization of the frame model tested by Clough and Gidwani (51)



a) GROUND ACCELERATION

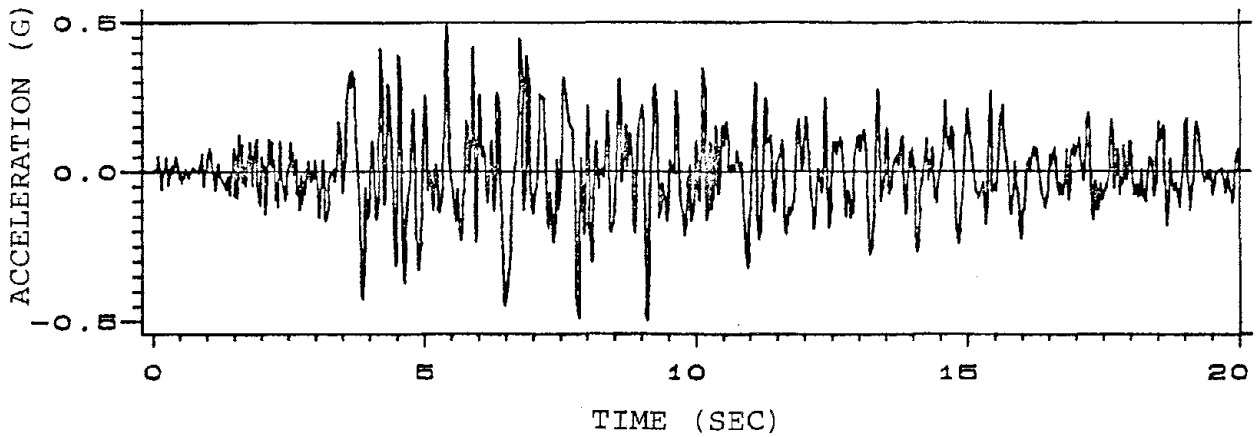


b) RECORDED RESPONSE

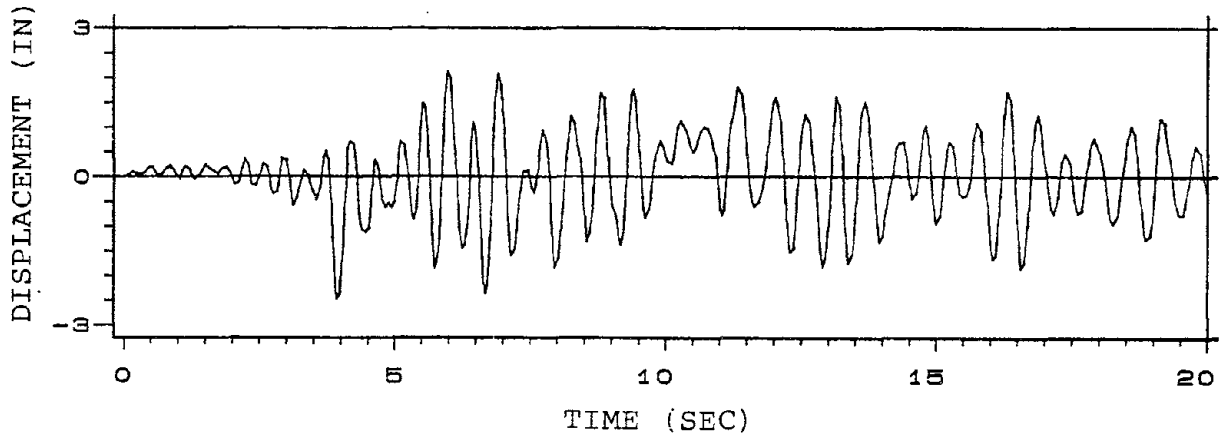


c) COMPUTED RESPONSE

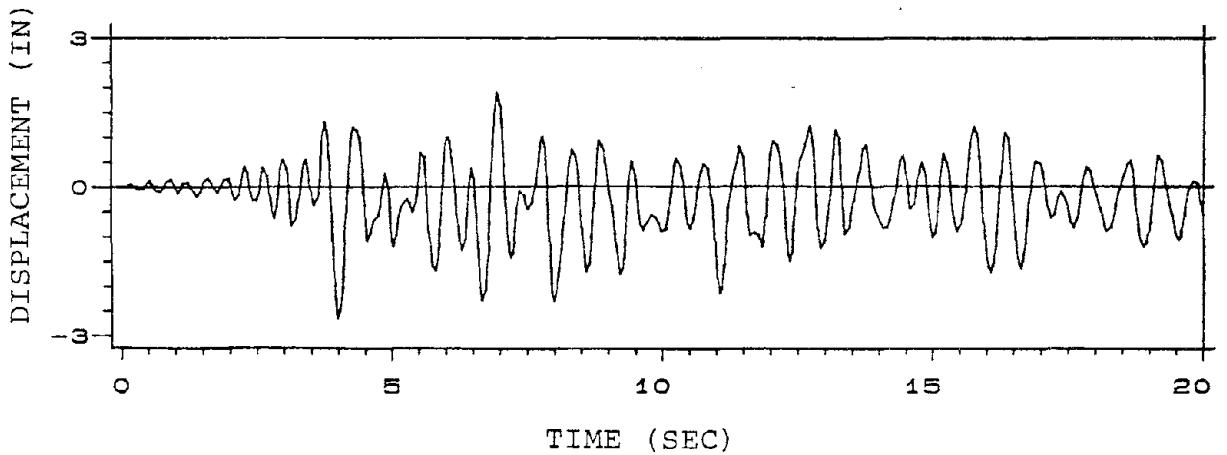
Fig. (3.22). Response of the frame tested by Clough and
Gidwani ⁽⁵¹⁾ for test W1.



a) GROUND ACCELERATION



b) RECORDED RESPONSE



c) COMPUTED RESPONSE

Fig. (3.23). Response of the frame tested by Clough and Gidwani⁽⁵¹⁾ for test W2

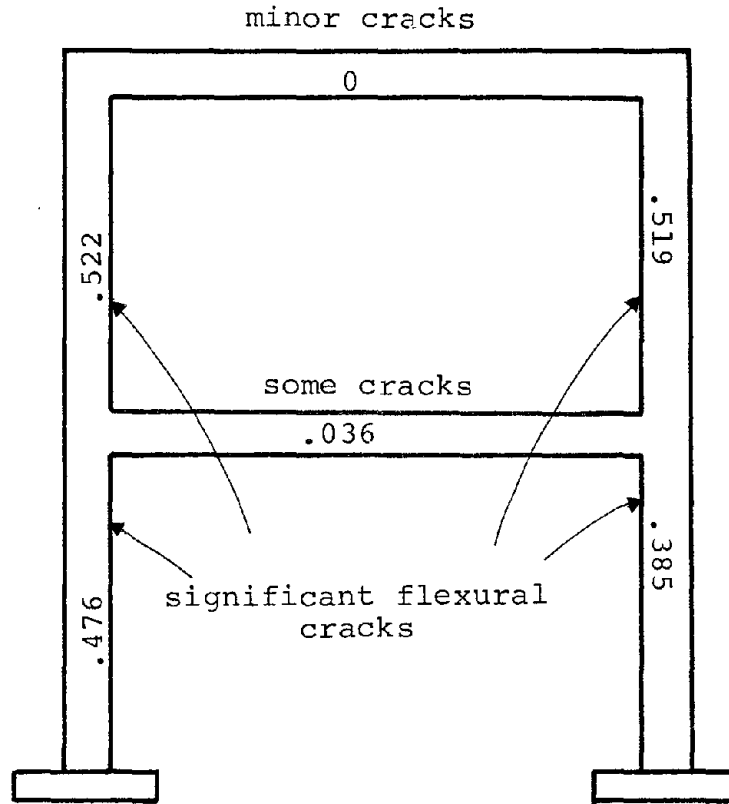


Fig. (3.24). Observed damage and computed modified flexural damage ratios after test W2 for the frame tested by Clough and Gidwani⁽⁵¹⁾.

CHAPTER 4

DYNAMIC ANALYSIS OF DAMAGED CONCRETE FRAMES

4.1 Introduction

The analysis of damaged reinforced concrete buildings has not received the attention it deserves. Current design philosophy accepts varying degrees of damage sustained by buildings exposed to increasing levels of ground shaking. But while considerable research has been performed on the analysis of (theoretically) undamaged buildings, the published literature on the analysis of damaged buildings is extremely scarce. In this chapter, a procedure is proposed for the analysis of the response of damaged reinforced concrete frames subjected to severe ground motions.

To the authors' knowledge there have been two attempts to analytically simulate the response of damaged frames to ground shaking. In the first attempt, by Otani and Sozen⁽¹⁰⁾, the damage sustained by the frame due to an earlier ground motion was ignored entirely when the frame was analyzed for a subsequent acceleration history. In other words, no attempt was made to account for the effect that the degraded stiffness might have on subsequent responses. As would be expected, this simplification can lead to substantial underestimation of the frame response.

In conjunction with the shaking table experiment of the two-story, one-bay frame mentioned in Chapter 3, Hidalgo and Clough⁽⁶⁾, and Clough and Gidwani⁽⁵¹⁾ also performed analytical response predictions for the initially undamaged

as well as the damaged frame. In order to assess the stiffness degrading effects of damage, they decreased the modulus of elasticity of concrete such that the reduced elastic frame stiffness would reproduce the two natural frequencies measured during the experiment. This method has a number of disadvantages:

- 1) The change in stiffness is proportional to the square of the change of the frequency. Therefore, errors in measuring the frequencies would result in correspondingly large errors in estimating the stiffness.
- 2) The experimental determination of the second and higher natural frequencies is subject to increasing uncertainties and therefore the cause of larger errors in any response analysis based on such values.
- 3) Natural frequencies are typically determined experimentally by means of small-amplitude vibration tests. The frequencies associated with more realistic large-amplitude vibrations may therefore be overestimated appreciably.
- 4) In their analytical simulation studies, Clough and Gidwani had found that the structure response is very sensitive to the factors used to modify the structure stiffness matrix. Small changes of these factors were found to cause large changes in the computed response.
- 5) When degrading the stiffness of each member equally (by reducing the concrete modulus of elasticity by a certain amount), this method disregards the fact that some

member stiffnesses might degrade considerably more than others, i.e., that the stiffness distribution in the structure might undergo appreciable changes.

4.2 Global Damage Parameter

A global damage parameter should be a clear measure of the degree of damage in a frame at any point in time. This applies specifically to the time prior and after the application of a particular ground motion history. In the following, four different damage parameters will be discussed, one of which will be chosen for subsequent analyses.

One definition of a global damage parameter is the modified flexural damage ratio (as defined in Section 2.10) for the most heavily stressed member in the structure. Although this parameter proved to be very useful in the analysis of initially undamaged frames, the same is not true when the objective is the analysis of damaged frames. There are two reasons for this. First, the MFDR value of any member, including the most heavily stressed one, is very difficult to determine in the field. It can be computed accurately only by actually performing an entire analysis of the frame for the ground acceleration history which caused the damage. The second reason is that in general poor correlation would be expected between a heavily damaged member and the overall state of damage of the entire frame. It is conceivable that in spite of the local failure or severe damage of individual girders, the overall load-

resisting capacity of a frame is effected only moderately.

A second definition of a global damage indicator is the residual roof displacement, as proposed in References 22 and 23. As was shown in this earlier study, however, the correlation between the degree of global damage and the residual roof displacement exhibited considerable statistical scatter and therefore was not entirely satisfactory.

The third global damage parameter is defined as the value of the fundamental natural frequency of the frame. This value can be a good measure for damage, because both the degree of damage and the amount of stiffness degradation have been found to correlate strongly with the value of this frequency. This parameter can be determined relatively quickly in the field using portable ambient vibration test equipment. In fact, the field measurement of frequencies of actual buildings is well established (53-57). But from the analysis point of view, this parameter is not an ideal one either, because the frequencies measured in ambient vibration tests usually overestimate the actual frequencies associated with large-amplitude motions (50). Also, the computed response has been shown to be rather sensitive to this parameter if used to degrade the entire frame stiffness uniformly (51).

The fourth definition which may be proposed for a global damage parameter is the maximum roof displacement, δ_R , attained during the entire past loading history of a building. Common engineering sense would expect a strong correlation between this maximum frame displacement

amplitude and the overall state of damage of a building. The only disadvantage of this damage definition is the fact that the maximum roof displacement cannot be measured in the field after an earthquake, unless the building was instrumented during the event. However, the evaluation of laboratory tests has confirmed the expected strong correlation between the maximum roof displacement experienced during a given loading history and the value of the fundamental natural frequency measured after termination of that particular loading. In Fig. (4.1) this correlation is clearly demonstrated for twenty tests, reported in References 10, 50 and 51. As ordinates, the maximum roof displacement, δ_R , is plotted normalized with respect to δ_Y , the first-mode amplitude (roof displacement) at which the first member in the frame reaches the yield moment,

$$\bar{\delta}_R = \frac{\delta_R}{\delta_Y} \quad (4.1)$$

On the abscissa, values of the frequency ratio

$$\bar{\omega} = \sqrt{\frac{\omega_e}{\omega}} \quad (4.2)$$

are entered, where ω_e is the initial fundamental frequency of the undamaged elastic frame, and ω is the corresponding frequency measured at the end of the test. Since the building stiffness can only decrease, we have $\omega_e > \omega$. The maximum roof displacement, δ_R , can be either smaller or

larger than δ_Y . However, if $\delta_R < \delta_Y$, no structural member in the frame has yet been strained beyond the yield capacity, therefore structural damage can be assumed to be nonexistent. For analysis purposes, we therefore can set $\delta_R > \delta_Y$.

The correlation coefficient exhibited by the data plotted in Fig. (4.1) was computed to be 0.825, which can be considered sufficiently adequate for practical purposes. A least-square fit of a straight line results in the functional relationship,

$$\bar{\delta}_R = 1 + 14.2(\bar{\omega} - 1) \quad \omega < \omega_e \quad (4.3)$$

This equation can be used to obtain an estimate for the maximum roof displacement, δ_R , once the fundamental frequency has been obtained through measurements in the field.

By basing the global damage definition only indirectly on the field-measured fundamental building frequency, some of the disadvantages of the earlier definitions are reduced. It is this definition, therefore, which will be used in the subsequent analyses.

Before applying the global damage parameter to analyses of damaged buildings, it will be useful to establish a scale ranging from zero for no damage to a value of one, which would correspond to a state of total failure or collapse of the frame.

It is possible to compute the critical displacement of

a single-degree-of-freedom oscillator at which the over-turning moment, including the P- Δ effect, exceeds the restoring moment of the spring element (58). For a multi-story frame, a comparable collapse analysis requires the incorporation of a general large-displacement formulation, which is available for elasto-plastic frames (59). Rather than attempting to actually compute such critical displacement amplitudes, it is proposed to simplify the analysis by observing that most of the test beams discussed in Chapter 3 failed at final displacements which would correspond to interstory drifts of approximately 6%. Until a more thorough analysis is available to refine this estimate, it will be assumed that a building frame subjected to an overall drift of 6% is most likely to be near or beyond the point of collapse and certainly in a state of damage which can be termed complete. Thus the roof displacement

$$\delta_F = .06 H \quad (4.4)$$

where H is the total building height, will be used to normalize the actual roof displacement, in order to define the global damage parameter

$$GDP = \frac{\delta_R - \delta_Y}{\delta_F - \delta_Y} > 0 \quad (4.5)$$

4.3 Damaged Frame Analysis Procedure

The analysis of a damaged reinforced concrete building is a difficult undertaking and subject to numerous uncertainties in addition to those associated with undamaged frame analysis. Each member is characterized by a number of strength and stiffness parameters which are functions of past loading histories, e.g., the maximum inelastic deformation. A complete deterministic analysis of a damaged frame would require the knowledge of all these parameters for each member of the frame. But this information is seldom available unless it has been stored during an analysis for the loading which caused the damage. The main difficulty in analyzing damaged frames is therefore the problem of estimating from the scant information available from a post-earthquake field inspection the restart parameters for all frame members.

The analysis procedure proposed herein can be summarized as follows:

- 1) If no better estimate is available for the maximum past roof displacements, δ_R , which the frame may have undergone during any one of the first (n-1) earthquakes, an approximate value can be obtained using Eq. (4.3). In this case, the frequency of the building is assumed to be known. Otherwise it will have to be determined in a field test.
- 2) The frame is statically loaded such that it maintains the first mode shape, until the roof displacement

reaches the value δ_y , defined as that value at which the first member reaches its yield capacity.

- 3) The static loading is continued into the inelastic range, still maintaining the first mode shape, until the roof displacement reaches the value $\delta_R^{(n-1)}$. For each load increment all member forces are computed and compared with the yield capacities, and the structure stiffness matrix is updated whenever a frame member changes its yield status. At the termination of this static analysis, all parameters for both ends of each member needed for restart analysis are known. These are primarily the maximum plastic region length, x_i , the maximum moment, M_x , and the maximum curvature, ϕ_x .
- 4) With the values of x_i , M_x and ϕ_x known, the stiffness of the plastic region is determined as shown in Fig. (4.2), and all other stiffness and strength parameters including the current member stiffness matrix can be initialized following the relationships given in Chapter 2.
- 5) With all initial conditions established in step 4, a nonlinear dynamic analysis can be performed for the n'th earthquake, and a new maximum roof displacement $\delta_R^{(n)} \geq \delta_R^{(n-1)}$, computed. By normalizing both $\delta_R^{(n-1)}$ and $\delta_R^{(n)}$ with regard to the failure displacement δ_F according to Eq. (4.5), the global damage before and after the n'th earthquake can be determined.

4.4 Analytical Study of a Damaged Frame

In order to evaluate the effect of damage on seismic response of reinforced concrete frames, extensive analyses have been carried out for the ten-story, three-bay frame⁽⁵⁰⁾ described in Chapter 3. Below, the results will be presented and evaluated under the following aspects:

1) accuracy of damaged frame response analysis; 2) global and local damage; 3) sensitivity of analysis results.

General observations about the effect of damage will conclude this chapter.

4.4.1. Accuracy of Damaged Frame Response Analysis

The ten-story, three-bay frame model, Fig. (3.17), has been subjected on the University of Illinois shaking table to three consecutive earthquake ground motions, all of which consisted of the El Centro recording scaled to three different peak accelerations. Before the frame responded to the base acceleration history of test Run One, it was undamaged. The results of the simulation of this experiment were discussed in Chapter 3, and the roof displacement history was shown in Fig. (3.18), with a maximum computed value of $\delta_R^{(1)} = 24.8$ mm.

The ground acceleration used in test Run Two was the same El Centro record scaled to a peak acceleration of 0.93g. Using the known value of the maximum past roof displacement $\delta_R^{(1)} = 24.8$ mm, the restart procedure outlined earlier was employed to initialize all member section

properties throughout the frame. With these initial properties the response of the frame was analyzed for the acceleration history of Run Two. In Fig. (4.3), the computed and recorded roof displacement histories can be compared directly. The maximum computed displacement was $\delta_R^{(2)} = 61$ mm, compared with the observed value of 51.2 mm. Considering the complexity of damaged frame behavior, this level of agreement is remarkable.

Using the same procedure, i.e., deriving from the known maximum past roof displacement, $\delta_R^{(2)} = 61$ mm, all necessary restart parameters, the frame was analyzed also for the ground accelerations of Run Three, consisting of the El Centro record scaled to a peak acceleration of 1.25g. The results are shown in Fig. (4.4) together with the base acceleration record. This time the maximum computed roof displacement was 83 mm, which exceeded the recorded peak displacement by about 18%.

The general agreement between experimental and analytical results is a measure of the accuracy with which the proposed analysis procedure can simulate the response of damaged concrete frames. However, it should be noted that general statements in this regard should await the outcome of similar studies of full-scale building frames, even though it will be difficult to secure reliable data from field measurements to compare against. Equally important is the restriction of this study to a single earthquake acceleration history, namely the El Centro recording. It is

essential that the applicability of the analytical procedure described herein be tested for widely different seismic ground motions, preferably employing random vibration models⁽⁶⁰⁾.

4.4.2 Global and Local Damage

The maximum roof displacements for the three tests of the ten-story frame were respectively, $\delta_R^{(1)} = 24.8$ mm, $\delta_R^{(2)} = 61$ mm, and $\delta_R^{(3)} = 83$ mm. The displacement at which the first member yielded was $\delta_Y = 9.4$ mm, whereas the failure displacement, corresponding to a 6% drift, was $\delta_F = 143$ mm. Substituting these values into Eq. (4.5), the global damage parameters for these cases become, respectively, 0.115, 0.386, and 0.551. These values illustrate that it is possible to characterize the overall state of damage in the load-carrying frame with a single number. This could very well have important application in practical situations. A more analytical application is the use of the global damage parameter in the reliability analysis of concrete frames employing damage probability matrices^(18,21,60).

In other situations it might be necessary to have more detailed knowledge of the distribution of local damage, which a single global damage parameter cannot provide. Such situations might arise out of damage investigations or during the determination of strengthening requirements. In such cases, the modified flexural damage ratio, MFDR, can

play a role to satisfy this requirement. For illustration, the MFDR values of all members are indicated in Figs. (3.19), (4.5) and (4.6) for Run One, Run Two, and Run Three, respectively, together with the observed crack patterns. According to Fig. (4.5) almost all members underwent inelastic deformations during test Run Two. In Run Three, not a single member remained elastic, Fig. (4.6). Generally, the beams suffered more damage than the columns, only the first story columns displayed comparable MFDR values.

In order to study the correlation between global and local damage, Table (4.1) summarizes 1) the global damage parameter, 2) the MFDR value for the first story columns, and 3) the maximum member MFDR value computed for each of the three test cases. It can be noticed that the global damage parameter, GDP, correlates well with the corresponding MFDR values for the first story columns, for each test. The maximum MFDR value, i.e., the damage ratio for the most heavily stressed member in the frame, has been contemplated earlier as a possible alternative for a global damage definition. In this example, it does not correlate nearly as well with the GDP as does the damage ratio for the first-story columns. However, it is impossible to derive from this single analysis a generally valid conclusion in this regard.

4.4.3 Sensitivity of Analysis Results

The restart analysis of the damaged frame, discussed in Section 4.4.1, was based on the knowledge of the maximum past roof displacement. If such displacement value is not available, it will have to be estimated from the fundamental natural frequency using Eq. (4.3). In our case, the fundamental frequencies prior to the three tests had been measured to be $\omega_e = 2.6$, $\omega^{(1)} = 2.1$, and $\omega^{(2)} = 1.7$ cps, respectively. With $\delta_Y = 9.4$ mm, Eq. (4.3) estimates the maximum roof displacement during Run one as $\delta_R^{(1)} = 24.4$ mm, as compared to the actually computed value of 24.8 mm. For Run Two the estimate is $\delta_R^{(2)} = 41$ mm as compared with the computed value of 61 mm. Using the estimated values for $\delta_R^{(1)}$ and $\delta_R^{(2)}$ rather than the actually computed ones, the analyses were repeated for Run Two and Run Three. The new maximum roof displacement of Run Two varied from the previously computed value by only 1.6% and the overall displacement histories were so similar that the second analysis results are not reproduced here. Likewise for Run Three, the response was very similar to the one obtained previously. The maximum roof displacement was different by only 4%, even though the restart parameter varied by about 33%.

These results clearly show that the response of this frame is rather insensitive to the precise amount of damage sustained during previous ground shaking. This conclusion, however, may not be generalized to other earthquake ground motions. The spectrum of the ground motion used here, Fig. (4.7), indicates a reduced response level for increased

fundamental periods in the domain of interest here. It should be expected that damaged frames exposed to more white-noise type ground motions will be less insensitive to the amount of damage sustained previously.

4.4.4 Effect of Damage on Subsequent Response

Let $GDP^{(n-1)}$ be the global damage after exposure to $n-1$ earthquakes. We shall now investigate the effect of $GDP^{(n-1)}$ on $GDP^{(n)}$, i.e., the amount of damage after exposure to an additional n 'th earthquake with prescribed peak acceleration. This study is again restricted to the ten-story frame studied earlier and the El Centro record. The analysis results are summarized in Fig. (4.8). The abscissa represents the previous damage value, $GDP^{(n-1)}$, while the damage after the n 'th earthquake, $GDP^{(n)}$, is plotted on the ordinate. Each curve represents the damage increments due to an El Centro earthquake with peak acceleration as indicated. The following observations can be made in reference to Fig. (4.8).

- 1) Values plotted for $GDP^{(n-1)} = 0$ represent the expected damage in a previously undamaged frame. It can be noticed that these values are normally the lowest for any given level of peak acceleration. This means that ignoring previously incurred damage in the analysis will underestimate the expected response by varying degrees. The errors are proportional to the state of previous damage as well as the peak acceleration.
- 2) For a given ground acceleration intensity, there exists

a certain amount of previous damage beyond which the particular earthquake will not increase the degree of damage any further. This point is found as the intersection of the curve for a given earthquake intensity with the 45° straight line through the origin. Points on this line represent the cases where $GDP^{(n)} = GDP^{(n-1)}$, i.e., the n'th earthquake does not increase damage.

- 3) Figure (4.8) can help to answer the following important question: What peak acceleration must the earthquake have in order to increase the degree of damage in the frame, if previous damage is given? The data that can be used to answer this question are contained in Fig. (4.8), but are plotted for clarity separately in Fig. (4.9). For a given level of expected ground shaking, Fig. (4.9) indicates whether or not a given amount of previous damage will be increased. This kind of information should be rather useful when evaluating the reliability of a concrete frame damaged during a strong earthquake and about to be subjected to a series of aftershocks. As can be seen in Fig. (4.9), Run Two and Run Three exceeded their respective critical acceleration levels by large margins.

It should be stressed again that because of the restriction of these analyses to one building and one ground motion history, the above conclusions are preliminary and cannot be generalized without further study.

Table (4.1) Comparison between global and local damage

Test	GDP (1)	MFDR (2)	max (MFDR) (3)
Run One	.115	.176	.338
Run Two	.386	.453	.539
Run Three	.551	.622	.622

- (1) Global damage parameter, Eq. (4.5)
- (2) Modified flexural damage ratio for lower level columns
- (3) Maximum value of the modified flexural damage ratio

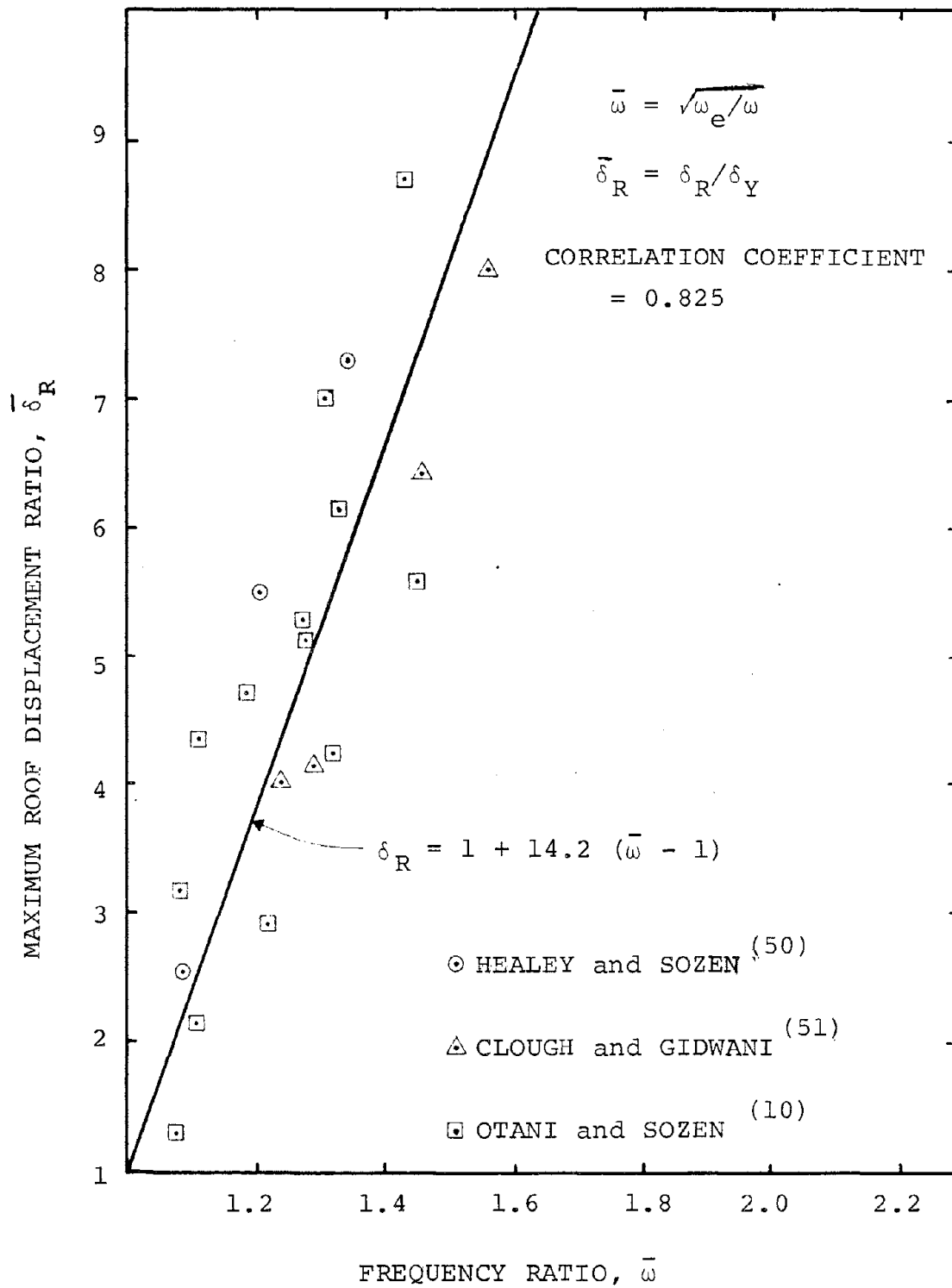


Fig. (4.1). Experimental relationship between maximum roof displacement and fundamental frequency.

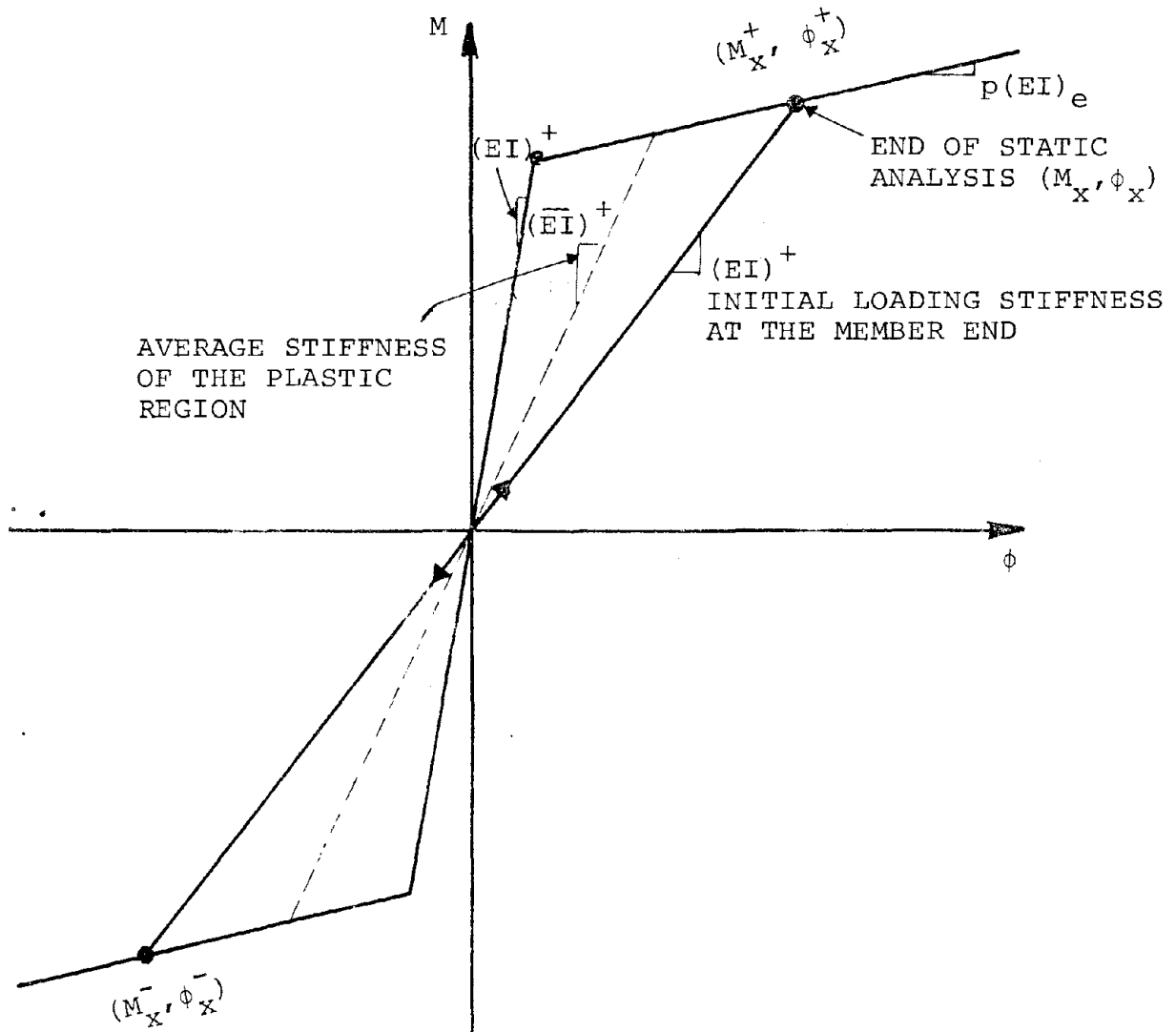
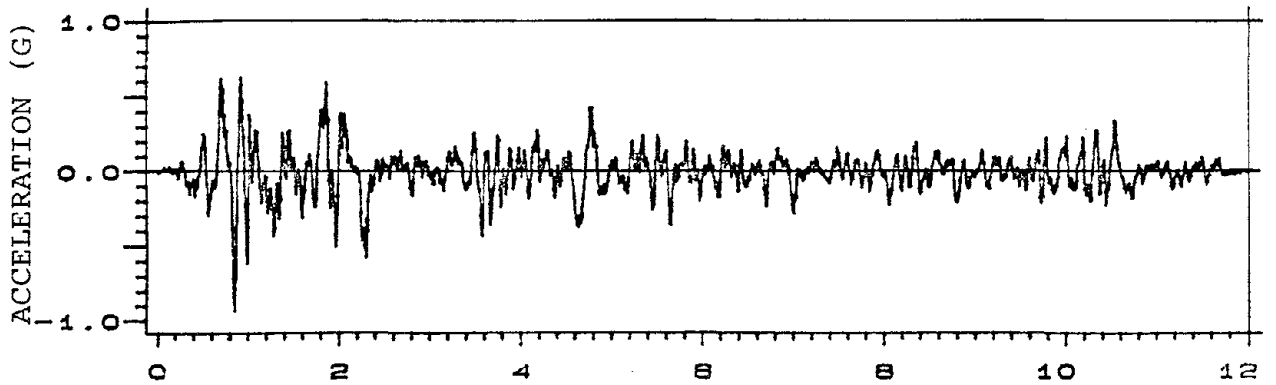
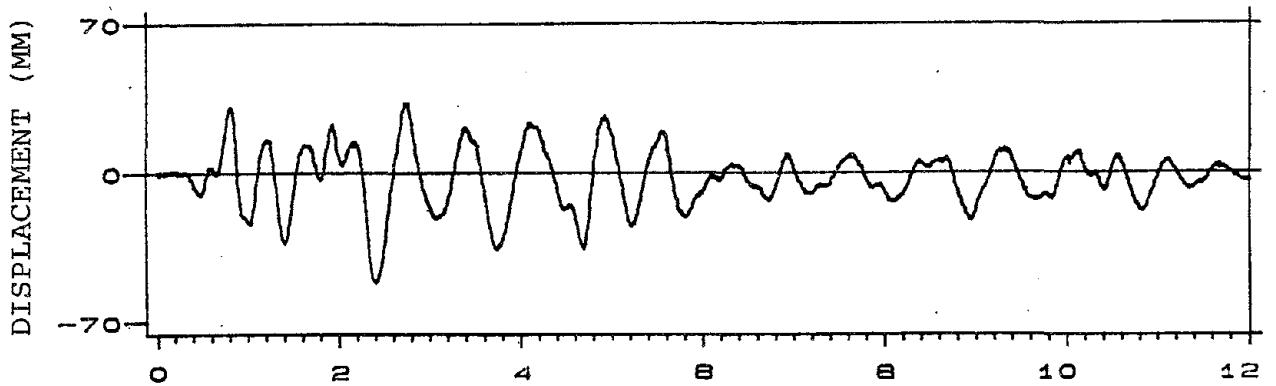


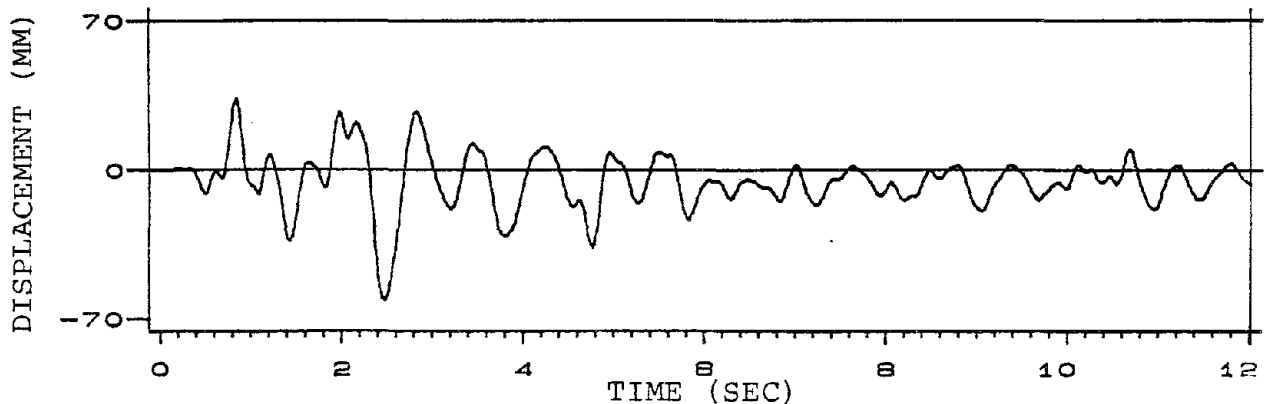
Fig. (4.2). Initial conditions for restart analysis.



TIME (SEC)
a) GROUND ACCELERATION

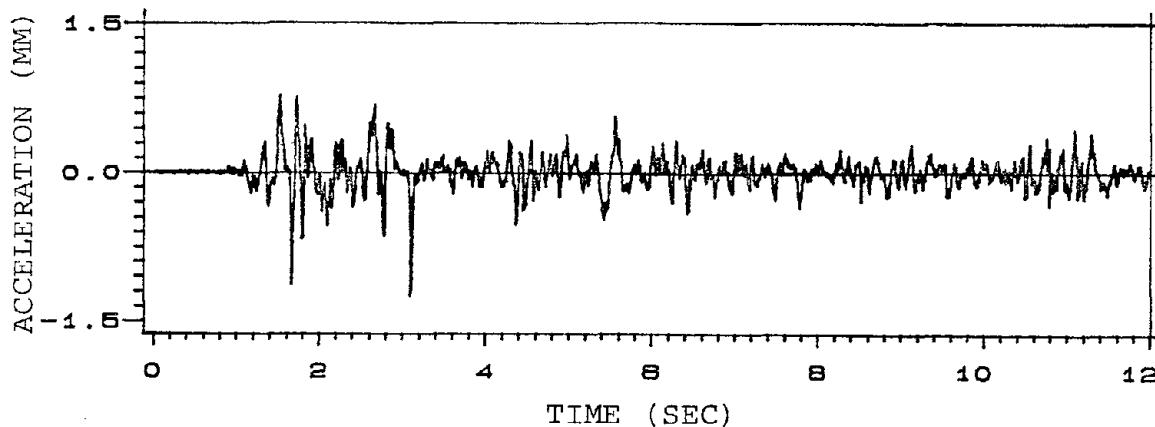


TIME (SEC)
b) RECORDED RESPONSE

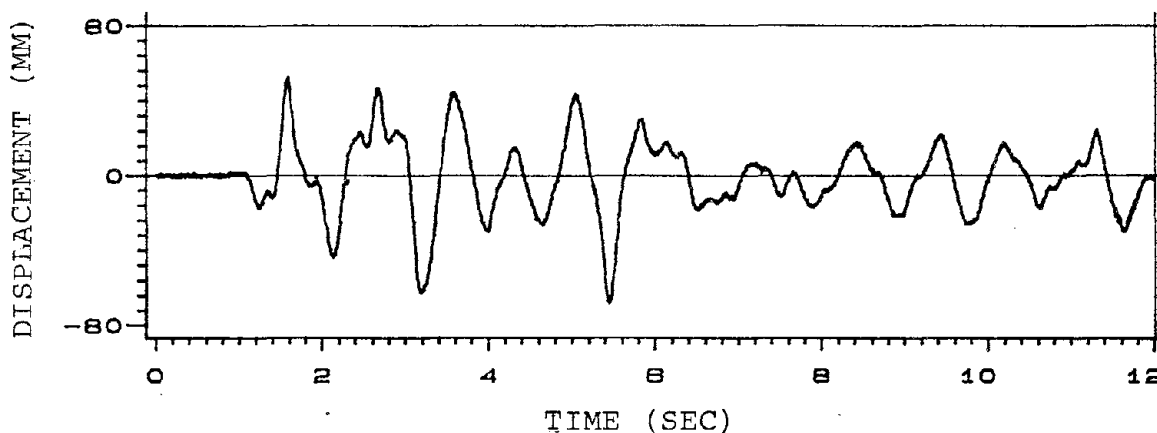


TIME (SEC)
c) COMPUTED RESPONSE

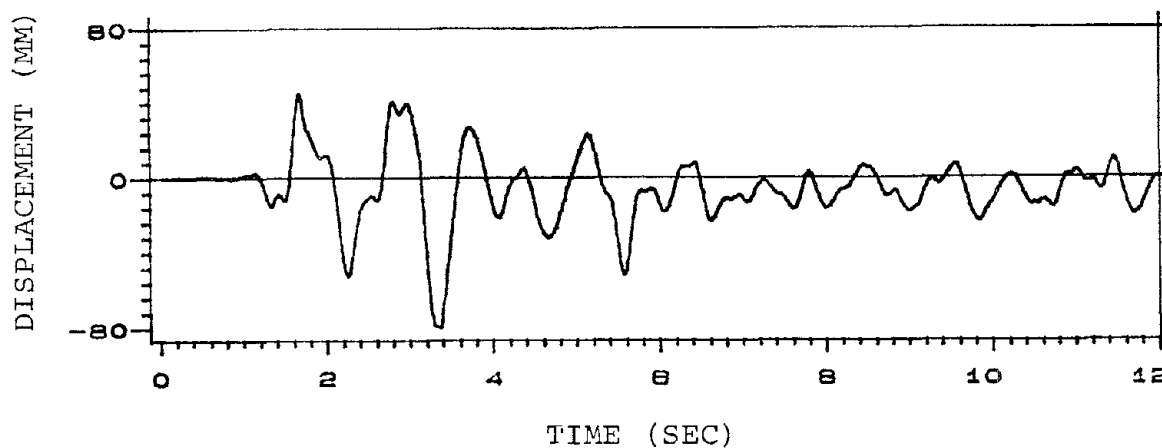
Fig.(4.3). Response of the frame tested by Healey and Sozen⁽⁵⁰⁾ for Run Two



a) GROUND ACCELERATION



b) RECORDED RESPONSE



c) COMPUTED RESPONSE

Fig. (4.4). Response of the frame tested by Healey and Sozen (50)
for Run Three.

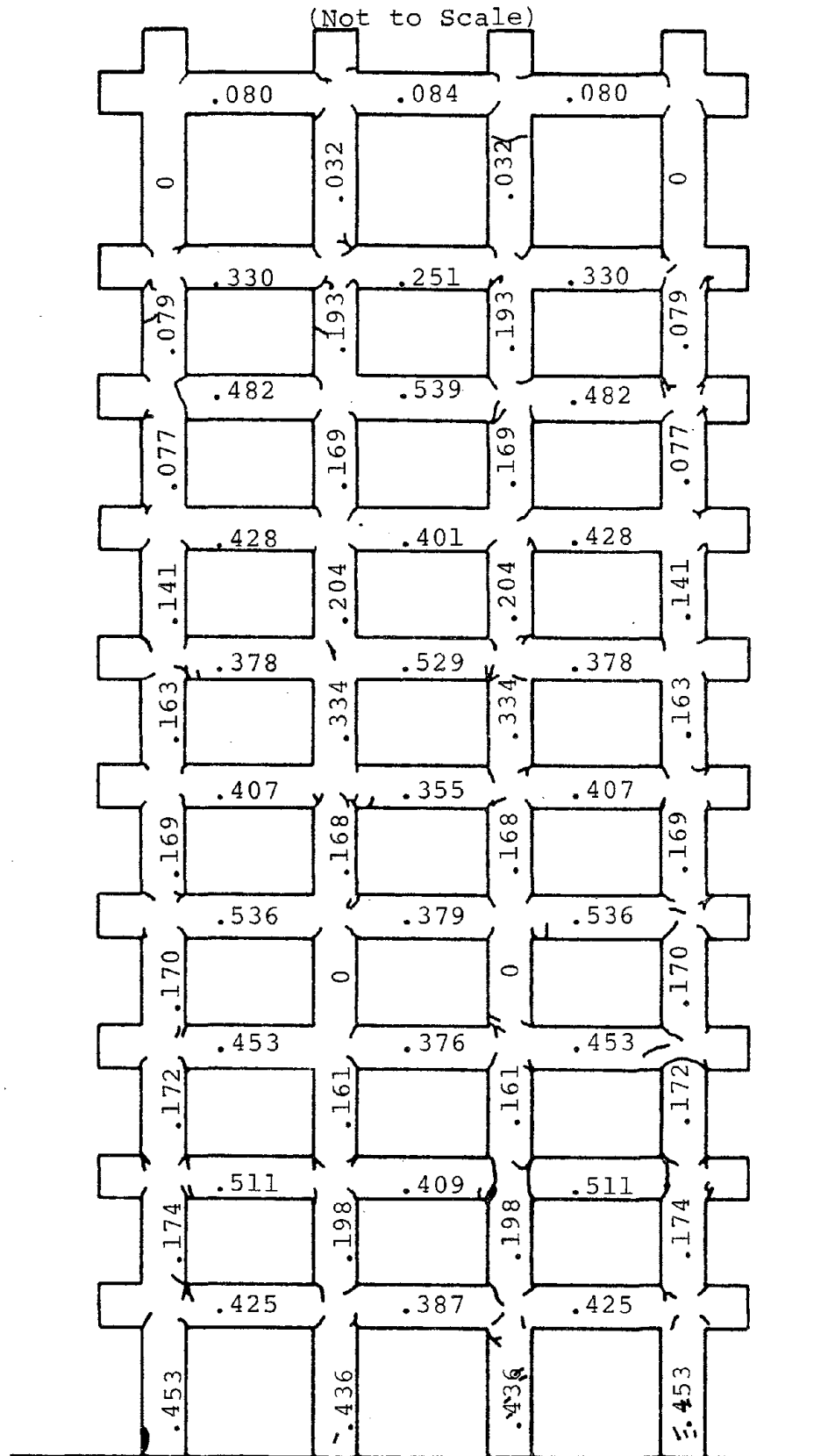


Fig.(4.5). Observed Crack pattern and computed modified flexural damage ratios after test Run Two in the experiment by Healey and Sozen (50)

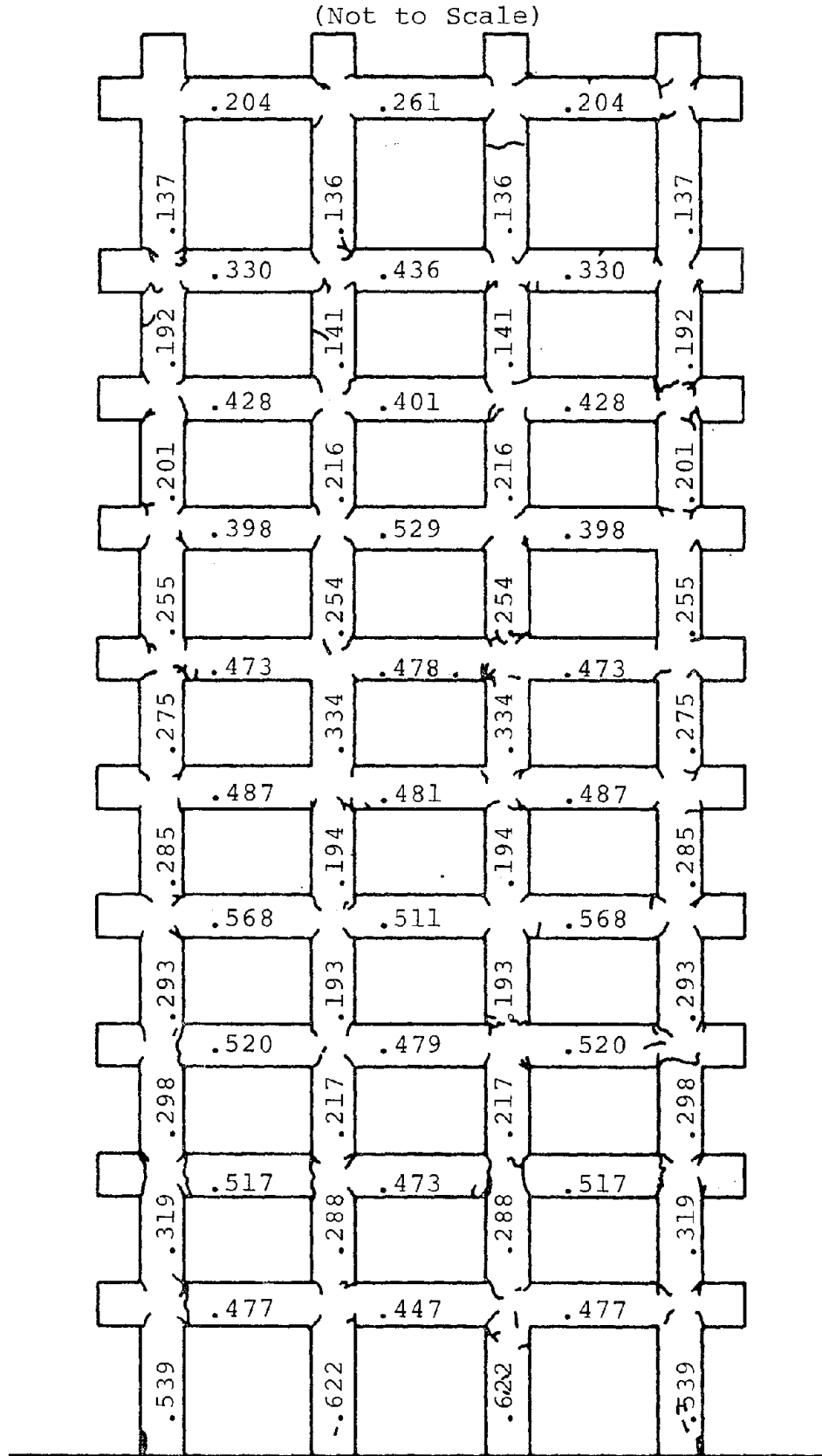


Fig. (4.6). Observed crack pattern and computed modified flexural damage ratios after test Run Three in the experiment by Healey and Sozen(50)

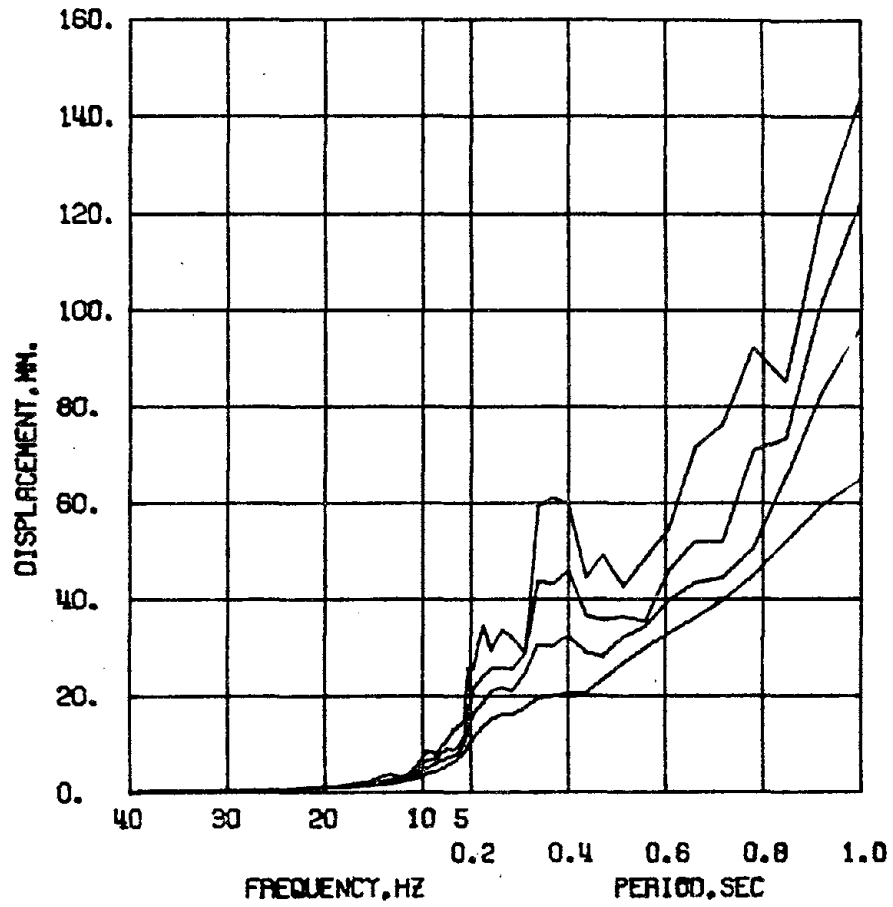


Fig. (4.7). Linear response spectrum of acceleration record Run Two

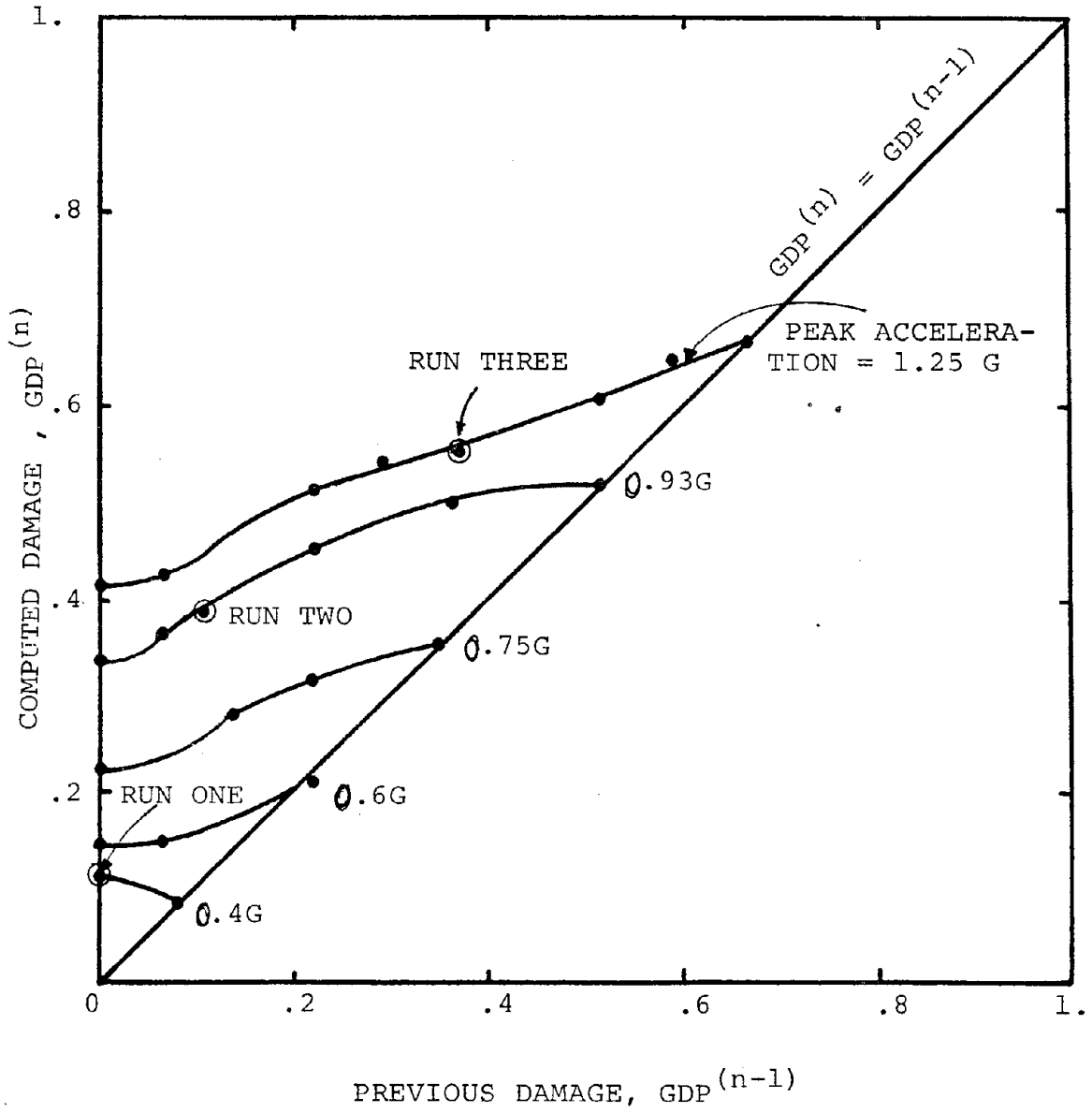


Fig. (4.8). Effect of previous damage on the response

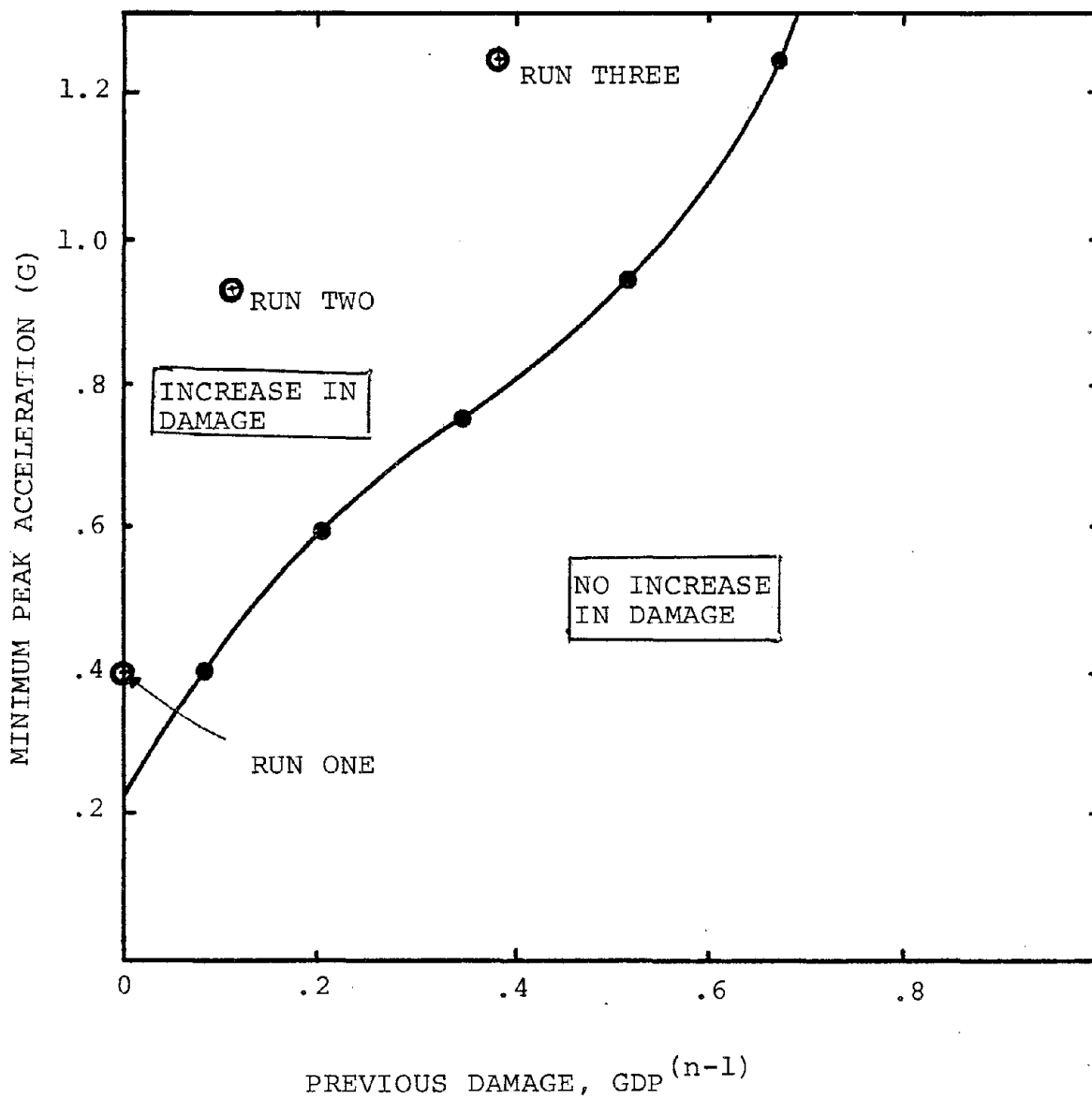


Fig. (49). Minimum peak acceleration required to increase previous given degree of damage

CHAPTER 5

SUMMARY AND CONCLUSIONS

5.1 Summary

The behavior of damaged concrete buildings during earthquakes is extraordinarily complex and influenced by a variety of material and structural parameters, in addition to the ground motion characteristics. A few laboratory experiments have been conducted, which have helped to improve considerably our understanding of such behavior. It has been the objective of this study to develop a general analysis procedure for simulating the response of reinforced concrete frame buildings, which may or may not have been damaged during previous exposures to strong earthquake ground motions. Such an analysis capability will be a useful tool for the post-earthquake evaluation and, more generally, for the reliability assessment of buildings. The establishment of this analysis procedure required the completion of the following tasks:

1. The accurate modeling of the response of general reinforced concrete frame members to strong cyclic loads;
2. The definition of a damage parameter which correlates well with the structure's residual strength and stiffness, and which is suitable for subsequent reliability analyses;

3. The establishment of a procedure for the dynamic analysis of damaged concrete frames subjected to strong earthquake ground motions.

To complete task 1, the theory for a new mathematical model was presented in Chapter 2, the most important aspects of which are as follows:

1. The model considers explicitly the finite size of the plastic regions, unlike most other models proposed previously in the literature, which have in common the assumption of fictitious plastic hinges of zero dimensions. By dropping this commonly made assumption it was possible to derive a straightforward theory and to avoid some of the inconsistencies and difficulties inherent in some of the other models. Although the required computational effort is increased slightly, it is felt that the theoretical advantages are worth this extra effort.
2. There is no need for a priori test data with which the free parameters of some other models have to be adjusted to fit given experimental load-deformation curves. Only elementary material data and geometric section properties are required for the proposed model, making it independent of data which in practical situations may not be available.
3. The model is capable of reproducing the response of frame members to strong cyclic loads even under the presence of high shear and axial forces.

4. The strength degradation, which has been observed in laboratory tests to accompany successive excursions into the inelastic range has been accounted for.

The model has been thoroughly tested and evaluated by simulating virtually all comprehensive tests for which data were available in the open literature. Comparisons between analytical and experimental results, reported in Chapter 3, were very satisfactory and adequate for practical purposes.

To complete task 2 of the overall objective, member and global damage parameters have been defined. The modified flexural damage ratio, MFDR, has been proposed as a measure of local damage in an individual member, which is also indicative of the amount of stiffness and strength degradation. The value MFDR = 0 indicates that the yield capacity of the member has never been exceeded, therefore damage and concrete cracking can be expected to be negligible. A value of MFDR = 1 corresponds to the onset of failure, i.e., a level of deformation beyond which members exhibit a rapid deterioration of strength and a significant amount of cracking. For practical purposes it is appropriate to consider this damage level as synonymous with failure.

In order to introduce a measure for the overall or global state of damage in a frame, a global damage parameter, GDP, was defined. Again, a value of GDP = 0

indicates that not a single member in the frame has been stressed beyond the yield capacity, therefore damage can be considered to be zero. The value $GDP = 1$ is defined as virtual failure and is taken to correspond to a maximum roof displacement of 6% of the building height. Thus, the GDP is a measure of the maximum roof displacement of the frame during any previous earthquake, relative to the 6% failure displacement δ_F and δ_Y , the roof displacement at which the first member in the structure yields, Eq. (4.5). The maximum roof displacement has been shown to strongly correlate with the fundamental natural frequency of a frame, Fig. 4.1. Therefore, if the past maximum roof displacement is not known, it can be estimated from the fundamental frequency which in turn can be determined in the field with relative ease, using portable ambient vibration equipment.

For task 3, finally, an analysis procedure has been proposed which permits the prediction of damaged concrete frame response to future earthquakes of given intensity. This procedure can be summarized as follows:

1. Given the value of the global damage parameter prior to the n'th earthquake, $GDP^{(n-1)}$, the value $\delta_R^{(n-1)}$ can be determined by using Eq. (4.5). This value is an estimate for the largest roof displacement that the frame has experienced in its lifetime.
2. The frame is statically loaded such that it maintains the first mode shape until the roof displacement reaches the value $\delta_R^{(n-1)}$.

3. The level of strain reached for the loading of step 2 permits an estimate of the stiffness degradation and possibly strength deterioration of each member in the frame. Thus it is possible to estimate all initial member properties needed for a subsequent response analysis.
4. With all initial conditions established in step 3, a nonlinear dynamic analysis can be performed for the n'th earthquake and a new maximum roof displacement $\delta_R^{(n)} \geq \delta_R^{(n-1)}$ computed. By normalizing the value of $\delta_R^{(n)}$, an updated value for the global damage parameter $GDP^{(n)}$ is obtained.

This analysis procedure has been tested by simulating the response of the scale model of a ten-story frame to three consecutive earthquakes, for which shaking table test results were available. Agreement between theory and experiment was excellent, and a number of additional studies were carried out, which led to some preliminary conclusions about the behavior of damaged frames.

5.2 Conclusions

Based on the comparison between theoretical and experimental results, both on the element and structure level, it was possible to draw the following conclusions with regard to the proposed analysis procedure.

1. Judging the new reinforced concrete frame model by the accuracy of the load-deflection curves obtained

for those cyclic static loadings, for which experimental data were available, it can be concluded that the accuracy is excellent for practical purposes.

2. The proposed modified flexural damage ratio, MFDR, has been found to be a useful and reliable measure of local member damage.
3. The proposed global damage parameter, GDP, seems to satisfy the need for an objective measure of the global state of damage in the structure which is indicative of the overall stiffness and strength deterioration.

A number of additional conclusions can be drawn from the studies reported herein. But since these are based on only one frame subjected to a single earthquake scaled to different peak accelerations, they should be considered only preliminary, pending the outcome of additional studies involving different frames and random ground acceleration histories.

1. The agreement between experimental recordings and theoretical response predictions for the damaged frame is remarkable.
2. The global damage parameter is a suitable indicator of the overall state of damage. The usefulness of this indicator will become even more apparent, when it is used in the reliability analysis of concrete frames employing damage probability matrices.

3. In some situations it might be necessary to obtain detailed knowledge of the distribution of local damage. Such situations might arise during post-earthquake damage investigations or determination of strengthening requirements. In such cases, the modified flexural damage ratio, MFDR, can play a role.
4. The limited studies indicate a correlation between the global damage parameter, GDP, and the MFDR value for the most heavily stressed member in the structure.
5. Ignoring previously incurred damage when analyzing a frame will underestimate the expected response and damage by varying degrees. The errors are proportional to the state of previous damage as well as to the earthquake intensity.
6. For a given ground acceleration intensity, there exists a certain amount of previous damage beyond which an earthquake of given peak acceleration will not increase the degree of damage any further, assuming the failure displacement δ_F has not been exceeded.

5.3 Recommendations for Further Studies

The studies reported herein provide some insight into the behavior of damaged frames. However, because of the limited scope of this investigation, some challenging questions could not be pursued further. These can be the subject of future studies.

1. The most immediate application of this analysis procedure is the reliability study of damaged concrete frames. It is this objective for which the present study was carried out.
2. In view of the large uncertainties associated with structural behavior as well as ground motions, a thorough statistical evaluation of the sensitivity of structural response to key input parameters is called for.
3. In the present analysis, the member axial forces were considered to remain constant throughout the response, leading to a constant geometric stiffness matrix to approximate the P- Δ effect. A more realistic analysis will have to consider the effects of variable axial forces both due to overturning moments and vertical accelerations. Also, the effect on changing yield capacities should be investigated. Such effects could conceivably be of significance with regard to very tall buildings.
4. Although it is well known that the displacement response of tall elastic frames is controlled mostly by the first mode, it is appropriate to verify this assumption for the analysis of nonlinear (damaged) frames.
5. For the failure roof displacement, an empirical value of $\delta_F = 0.06 H$ was chosen. If the analysis

were to incorporate an accurate large-displacement formulation, then such an arbitrary value would be superfluous, because actual instability, i.e., collapse, due to overturning could be simulated directly.

6. Many realistic buildings contain shear walls in addition to a ductile moment frame. It is not appropriate to model such structural walls using the mathematical model presented herein. Therefore it would be very useful if another member-size model were to be developed, which could accurately simulate the cyclic response of shear wall elements.

REFERENCES

1. Meyer, C., "Dynamic Finite Element Analysis of Reinforced Concrete Structures," Advanced Mechanics of Reinforced Concrete, IABSE Colloquium, Delft, 1981.
2. Task Committee on Finite Element Analysis of Reinforced Concrete Structures, "State-of-the-Art Report on Finite Element Analysis of Reinforced Concrete," ASCE Special Publication, 1982.
3. Park, R., Kent, D.C. and Sampson, R.A., "Reinforced Concrete Members with Cyclic Loading," Journal of the Structural Division, ASCE, Vol. 98, ST7, 1972, pp. 1341-1360.
4. Ma, S.M., Bertero, V.V. and Popov, E.P., "Experimental and Analytical Studies on the Hysteric Behavior of Reinforced Concrete Rectangular and T-Beams," Earthquake Engineering Research Center, Report No. EERC 76-2, University of California, Berkeley, May 1976.
5. Clough, R.W. and Johnston, S.B., "Effect of Stiffness Degradation on Earthquake Ductility Requirements," Proceedings of Japan Earthquake Engineering Symposium, October 1966.
6. Hidalgo, P. and Clough, R.W., "Earthquake Simulator Study of a Reinforced Concrete Frame," Earthquake Engineering Research Center Report No. EERC 74-13, University of California, Berkeley, 1974.
7. Giberson, M.F., "Two Nonlinear Beams with Definitions of Ductility," Journal of the Structural Division, ASCE, Vol. 95, ST2, February 1969, pp. 137-157.
8. Litton, R.W., "A Contribution to the Analysis of Concrete Structures Under Cyclic Loading," Ph.D. Thesis, Department of Civil Engineering, University of California at Berkeley, 1975.
9. Suko, M. and Adams, P.F., "Dynamic Analysis of Multibay Multistory Frames," Journal of the Structural Division, ASCE, Vol. 97, ST10, October 1971, pp. 2519-2533.
10. Otani, S. and Sozen, M., "Behavior of Multistory Reinforced Concrete Frames During Earthquakes," Structural Research Series No. 392, Report No. UILU-ENG-72-2018, University of Illinois, November, 1972.

11. Meyer, C., Lee, J.L. and Roufaiel, M.S.L., "Discussion of Paper-Seismic Damage in Reinforced Concrete Frames," *Journal of Structural Engineering, ASCE*, Vol. 109, January 1983, pp. 286-288.
12. Wiggins, J.H., Jr. and Moran, D.F., "Earthquake Safety in the City of Long Beach Based on the Concept of Balanced Risk," J.H. Wiggins Company, Redondo Beach, California, September 1971.
13. Culver, C.G., Lew, H.S., Hart, G.C. and Pinkham, C.W., "Natural Hazards Evaluation of Existing Buildings," National Bureau of Standards, Building Science Series No. 61, January 1975.
14. Bertero, V.V. and Bresler, B., "Design and Engineering Decisions: Failure Criteria (Limit States)," Developing Methodologies for Evaluating the Earthquake Safety of Existing Buildings, Earthquake Engineering Research Center Report No. UCB/EERC 77-6, University of California, Berkeley, 1977.
15. Ting, E.C., Hong Chen, S.J. and Yao, J.T.P., "System Identification, Damage Assessment and Reliability Evaluation of Structures," Purdue University, Structural Engineering Report No. CE-STR-78-1, February 1978.
16. Liu, S.C. and Yao, J.T.P., "Structural Identification Concept," *Journal of the Structural Division, ASCE*, Vol. 104, ST12, December 1978, pp. 1845-1858.
17. Shibata, A. and Sozen, M.A., "Substitute-Structure Method for Seismic Design in Reinforced Concrete," *Journal of the Structural Division, ASCE*, Vol. 102, ST1, January 1976, pp. 1-18.
18. Meyer, C. and Shinozuka, M., "Earthquake Damage Assessment of Reinforced Concrete Buildings," ACI, 1979 Fall Convention, Washington, DC, October 1979.
19. Shinozuka, M. and Meyer, C., "Building Response under Random Earthquake Ground Motions," Proceeding of the Research Conference on Earthquake Engineering, Skopje, Yugoslavia, June 30-July 3, 1980.
20. Arzoumanidis, S.G. and Meyer, C., "Modelling Reinforced Concrete Beams Subjected to Cyclic Loads," Report No. NSF-PFR-7924695-CU-1, Department of Civil Engineering and Engineering Mechanics, Columbia University, May 1981.

21. Shinozuka, M. and Tan, R.Y., "Seismic Reliability of Damaged Reinforced Concrete Beams," Report No. NSF-PFR-7924695-CU-2, Department of Civil Engineering and Engineering Mechanics, Columbia University, May 1981.
22. Roufaiel, M.S.L. and Meyer, C., "Nonlinear Analysis of Reinforced Concrete Frames For Dynamic Loading," Report No. NSF-7924695-CU-3, Department of Civil Engineering and Engineering Mechanics, Columbia University, December 1981.
23. Meyer, C., Roufaiel, M.S.L. and Arzoumanidis, S.G., "Analysis of Damaged Concrete Frames for Cyclic Loads," Journal of Earthquake Engineering and Structural Dynamics, Vol 11, pp. 207-228, April 1983.
24. Bertero, V.V. and Felippa, C., Discussion of "Ductility of Concrete" by Roy, H.E.H. and Sozen, M.A., Proceedings of the International Symposium on Flexural Mechanics of Reinforced Concrete, ASCE-ACI, Miami, November 1964, pp. 227-234.
25. Chan, W.W.L., "The Ultimate Strength and Deformation of Plastic Hinges in Reinforced Concrete Frameworks," Magazine of Concrete Research, Vol. 7, No. 21, November 1955, pp. 121-132.
26. Soliman, M.T.M. and Yu, C.W., "The Flexural Stress-Strain Relationship of Concrete Confined by Rectangular Transverse Reinforcement," Magazine of Concrete Research, Vol. 19, No. 61, December 1967, pp. 223-238.
27. Roy, H.E.H. and Sozen, M.A., "Ductility of Concrete," Proceedings of the International Symposium on Flexural Mechanics of Reinforced Concrete, ASCE-ACI, Miami, November 1964, pp. 213-224.
28. Kent, D.C. and Park, R., "Flexural Members with Confined Concrete," Journal of the Structural Division, ASCE, Vol. 97, ST7, July 1971, pp. 1969-1990.
29. Atalay, M.B. and Penzien, J., "The Seismic Behavior of Critical Regions of Reinforced Concrete Components as Influenced by Moment, Shear and Axial Force," Earthquake Engineering Research Center Report No. EERC 75-19, University of California, Berkeley, December 1975.
30. Veletsos, A. and Newmark, N., "Effect of Inelastic Behavior on the Response of Simple Systems to Earthquake Motions," Second World Conference on Earthquake Engineering, Vol. II, Session II, Japan, 1960, p. 895.

31. Aoyama, H., "Moment Curvature Characteristics of Reinforced Concrete Members Subjected to Axial Load and Reversal of Bending," Proceedings of the International Symposium on Flexural Mechanics of Reinforced Concrete, Miami, Florida, 1964.
32. Takeda, T., Sozen, M.A. and Nielsen, N.N., "Reinforced Concrete Response to Simulated Earthquakes," Journal of the Structural Division, ASCE, Vol. 96, No. ST12, December 1970, pp. 2557-2573.
33. Goto, H., Kasai, T. and Imanishi, N., "Inelastic Earthquake Response of Tall R.C. Bridge Piers with Emphasis on Ultimate States," Proceedings of the Seventh World Conference on Earthquake Engineering, Istanbul, September 1980.
34. Takayanagi, T. and Schnobrich, W.C., "Non-Linear Analysis of Coupled Wall Systems," Earthquake Engineering and Structural Dynamics, Vol. 7, No. 1, 1979, pp. 1-22.
35. Iwan, W.D., "A Model for the Dynamic Analysis of Deteriorating Structures," Proceedings of the Fifth World Conference on Earthquake Engineering, Rome, June 1973.
36. Baber, T.T. and Wen, Y.K., "Stochastic Equivalent Linearization for Hysteretic Degrading Multistory Structures," Civil Engineering Studies, SRS No. 471, University of Illinois, Urbana-Champaign, Illinois, 1979.
37. Celebi, M. and Penzien, J., "Experimental Investigation into the Seismic Behavior of Critical Regions of Reinforced Components as Influenced by Moment and Shear," Earthquake Engineering Research Center Report No. EERC 73-4, University of California, Berkeley, 1973.
38. Bertero, V.V., Popov, E.P. and Wang, T.V., "Hysteretic Behavior of Reinforced Concrete Flexural Members with Special Web Reinforcement," Earthquake Engineering Research Center Report No. EERC 74-9, University of California, Berkeley, 1974.
39. Tani, S., Nagasaka, T., Nomura, S. and Hiramatsu, A., "Study on Restoring Force Characteristics of Reinforced Concrete Structures," Proceedings of Third Japan Earthquake Engineering Symposium, Paper V8, pp. 699-706, 1970.

40. MacGregor, J.G. and Hage, S.E., "Stability Analysis and Design of Concrete Frames," *Journal of the Structural Division, ASCE*, Vol. 103, ST10, October 1977, pp. 1953-1970.
41. Johnston, B.C., ed., The Column Research Council Guide to Design Criteria for Metal Compression Members, 2nd ed., John Wiley and Sons, Inc., New York, 1966, p. 217.
42. Rosenblueth, E., "Slenderness Effects in Buildings," *Journal of the Structural Division, ASCE*, Vol. 91, No. ST1, January 1965, pp. 229-252.
43. Wood, B.R., Beaulieu, D. and Adams, P.F., "Column Design by P Delta Method," *Journal of the Structural Division, ASCE*, Vol. 102, ST2, February 1976, pp. 411-427.
44. Hage, S.E., "The Second-Order Analysis of Reinforced Concrete Frames," University of Alberta, Canada, M.Sc. Thesis, 1974.
45. Bolotin, V.V., The Dynamic Stability of Elastic Systems, Holden-Day, San Francisco, 1964.
46. Mirza, S.A. and MacGregor, J.G., "Variations in Dimensions of Reinforced Concrete Members," *Journal of the Structural Division, ASCE*, Vol. 105, ST4, April 1979, pp. 751-766.
47. Kanaan, A.E. and Powell, G.H., "DRAIN-2D, A General Purpose Computer Program for Dynamic Analysis of Inelastic Plane Structures," Report No. EERC 73-6 and EERC 73-22, University of California, Berkeley, April 1973, Revised September 1973 and August 1975.
48. Popov, E.P., Bertero, V.V. and Krawinkler, H., "Cyclic Behavior of Three R.C. Flexural Members with High Shear," Earthquake Engineering Research Center, Report No. EERC 72-5, University of California, Berkeley, October 1972.
49. Scribner, C.F. and Wight, J-K. "Delaying Shear Strength Decay in Reinforced Concrete Flexural Members under Large Load Reversals," Report UMEE 78R2, Department of Civil Engineering, The University of Michigan, May 1978.
50. Healey, T.J. and Sozen, M.A., "Experimental Study of the Dynamic Response of a Ten-Story Reinforced Concrete Frame with a Tall First Story," Structural Research Series No. 450, Report No. UILU-ENG-78-2012, University of Illinois, August 1978.

51. Clough, R.W. and Gidwani, J., "Reinforced Concrete Frame 2: Seismic Testing and Analytical Correlation," Earthquake Engineering Research Center Report No. EERC 76-15, University of California, Berkeley, June 1976.
52. Banon, H., Biggs, J. and Irvine, H.M., "Prediction of Seismic Damage in Reinforced Concrete Frames," Publication No. R80-16, Department of Civil Engineering, MIT, May 1980.
53. Kawasumi, K. and Kamai, K., "Small Amplitude Vibrations of Actual Buildings," Proceedings, World Conference on Earthquake Engineering, Berkeley, California, 1974.
54. Hisada, T. and Nakagawa, K., "Vibration Tests on Various Types of Building Structures up to Failure," Proceedings, World Conference on Earthquake Engineering, Berkeley, California, June 1956, Paper No. 7.
55. Hudson, D.E., "Synchronized Vibration Generators for Dynamic Tests of Full-Scale Structures," Earthquake Engineering Research Laboratory, California Institute of Technology, Pasadena, California, 1962.
56. Nielsen, N.N., "Dynamic Response of Multistory Buildings," Earthquake Engineering Research Laboratory, California Institute of Technology, Pasadena, 1964.
57. Bouwkamp, J.G. and Blohm, J.K., "Dynamic Response of Two-Story Steel Frame Structure," Bulletin of the Seismological Society of America, Vol. 56, No. 6, December 1966, pp. 1289-1303.
58. Jennings, P.C. and Husid, R., "Collapse of Yielding Structures During Earthquakes," Journal of the Engineering Mechanics Division, ASCE, Vol. 94, EM5, October 1968, pp. 1045-1065.
59. Chan, Ka-Kin, "Buckling and Post-Buckling Behavior of Elasto-Plastic Structures," Department of Civil Engineering and Engineering Mechanics, Columbia University, Ph.D. thesis, 1979.
60. Shinozuka, M. and Tan, R.Y., "Seismic Reliability of Damaged Concrete Beams," Journal of Structural Engineering, ASCE, to be published.

APPENDIX A

PRIMARY MOMENT-CURVATURE RELATIONSHIP

The primary moment-curvature curve of a reinforced concrete section is defined to be the moment curvature relationship for a moment increasing monotonically from zero up to failure. The failure moment is defined herein as the moment corresponding to the curvature at which the compressive strain in the extreme fiber reaches the characteristic value ϵ_m which was defined in Section 2.2.2.

It is the purpose of this Appendix to summarize the method of computing the bending moment, M , and curvature, ϕ , corresponding to a prescribed concrete strain, ϵ_c . The complete M - ϕ curve can be obtained by repeating this computation for different values of ϵ_c between zero and ϵ_m .

This analysis is based on the following assumptions:

- 1) The stress strain curves of reinforcing steel and concrete are idealized as shown in Figs. (2.1) and (2.4), respectively;
- 2) The tensile strength of concrete is ignored;
- 3) Plane sections remain plane after deformation;
- 4) The axial force (if any) is acting at the plastic centroid of the section.

Equilibrium of all axial forces acting on the cross section shown in Fig. (A.1) requires that

$$C_c + C_s - T - P = 0 \quad (A.1)$$

This can be written in the form

$$\alpha \bar{y}^2 + \beta \bar{y} - \gamma = 0 \quad (\text{A.2})$$

and solved for \bar{y} , the distance of the neutral axis from the compression face

$$\bar{y} = \frac{-\beta + \sqrt{\beta^2 + 4\alpha\gamma}}{2\alpha} \quad (\text{A.3})$$

where

$$\begin{aligned} \alpha &= \alpha_c + \alpha_s + \alpha_t + \alpha_p \\ \beta &= \beta_c + \beta_s + \beta_t + \beta_p \\ \gamma &= \gamma_c + \gamma_s + \gamma_t + \gamma_p \end{aligned} \quad (\text{A.4})$$

The individual terms in Eq. (A.4) are given in Tables (A.1-A.4) as functions of ϵ_c . The variables with subscripts s and t depend on the yield condition of the compression and tension steel, respectively; therefore an iterative procedure is required to find the correct location of the neutral axis. Once the neutral axis has been computed according to Eq. (A.3), the curvature of the section can be determined as

$$\phi = \epsilon_c / \bar{y} \quad (\text{A.5})$$

and the steel strains follow as

$$\epsilon_s = \phi (d - \bar{y}) \quad (A.6)$$

$$\epsilon'_s = \phi (\bar{y} - d')$$
(A.7)

If both steel strains, ϵ_s and ϵ'_s , are compatible with their assumed yield condition, then the computed value of \bar{y} is correct. Otherwise, the constants in Eq. (A.4) have to be updated and \bar{y} recalculated.

Once both steel strains are compatible with their yield condition, we may then proceed to establish moment equilibrium of all forces acting on the cross section, about the plastic centroid, Fig. (A.1),

$$M = M_c + M_s + M_t \quad (A.8)$$

The contribution of concrete compression force is

$$\begin{aligned} M_c &= M_{c1} && \text{for } \epsilon_c < \epsilon_{cy} \\ &= M_{c1} - M_{c2} && \text{for } \epsilon_{cy} < \epsilon_c < \epsilon_{cu} \\ &= M_{c1} - M_{c2} - M_{c3} && \text{for } \epsilon_c > \epsilon_{cu} \end{aligned} \quad (A.9)$$

where

$$M_{c1} = E_c \phi \frac{b}{2} \bar{y}^2 (d'' - \frac{\bar{y}}{3}) \quad (A.10)$$

$$M_{c2} = \frac{E_c b(1 - p_c)(\epsilon_c - \epsilon_{cy})^2}{2\phi} (d'' - \frac{\epsilon_c - \epsilon_{cy}}{3\phi}) \quad (A.11)$$

$$M_{c3} = \frac{E_c b(p_c + \bar{p}_c) (\epsilon_c - \epsilon_{cu})^2}{2\phi} \left(d'' - \frac{\epsilon_c - \epsilon_{cu}}{3\phi} \right) \quad (A.12)$$

The moment contribution of the tensile steel is

$$M_t = T(d - d'') \quad (A.13)$$

where

$$\begin{aligned} T &= E_s A_s \epsilon_s && \text{for } \epsilon_s < \epsilon_{sy} \\ &= E_s A_s [(1-p_s)\epsilon_{sy} + p_s\epsilon_s] && \text{for } \epsilon_s > \epsilon_{sy} \end{aligned} \quad (A.14)$$

Finally, the compression steel contributes the following moment:

$$M_s = C_s(d'' - d') \quad (A.15)$$

where

$$\begin{aligned} C_s &= (n-1) E_c A'_s \epsilon'_s && \text{for } \epsilon'_s < \epsilon_{sy} \\ &= (n-1) E_c A'_s [(1-p_s)\epsilon_{sy} + p_s\epsilon'_s] && \text{for } \epsilon'_s > \epsilon_{sy} \end{aligned} \quad (A.16)$$

The above procedure has been used to compute primary moment-curvature curves for a cross section with different magnitudes of axial force, and the results are shown in Fig. (2.13).

Table (A.1) Coefficients of equilibrium equation
(concrete)

ϵ_c	α_c	β_c	γ_c
$\leq \epsilon_{cy}$	b	0	0
$> \epsilon_{cy}$ $\leq \epsilon_{cu}$	$b[p_c + 2(1-p_c) \frac{\epsilon_{cy}}{\epsilon_c} - (1-p_c) (\frac{\epsilon_{cy}}{\epsilon_c})^2]$	0	0
$> \epsilon_{cu}$	$b\{-\bar{p}_c + (1-p_c) [2 \frac{\epsilon_{cy}}{\epsilon_c} - (\frac{\epsilon_{cy}}{\epsilon_c})^2]$ $+ (p_c + \bar{p}_c) [2 \frac{\epsilon_{cu}}{\epsilon_c} - (\frac{\epsilon_{cu}}{\epsilon_c})^2]\}$	0	0

Table (A.2) Coefficients of equilibrium equation
(axial force)

α_p	β_p	γ_p
0	$-\frac{P}{E_c \epsilon_c}$	0

Table (A.3) Coefficients of equilibrium equation
(tension steel)

ϵ_s	α_t	β_t	γ_t
$\leq \epsilon_{sy}$	0	nA_s	$nA_s d$
$> \epsilon_{sy}$	0	$nA_s [p_s - (1-p_s) \frac{\epsilon_{sy}}{\epsilon_c}]$	$nA_a p_s d$

Table (A.4) Coefficients of equilibrium equation
(Compression steel)

ϵ'_s	α_s	β_s	γ_s
$\leq \epsilon_{sy}$	0	$(n-1)A'_s$	$(n-1)A'_s d'$
$> \epsilon_{sy}$	0	$(n-1)A'_s [p_s + (1-p_s) \frac{\epsilon_{sy}}{\epsilon_c}]$	$(n-1) A'_s p_s d'$

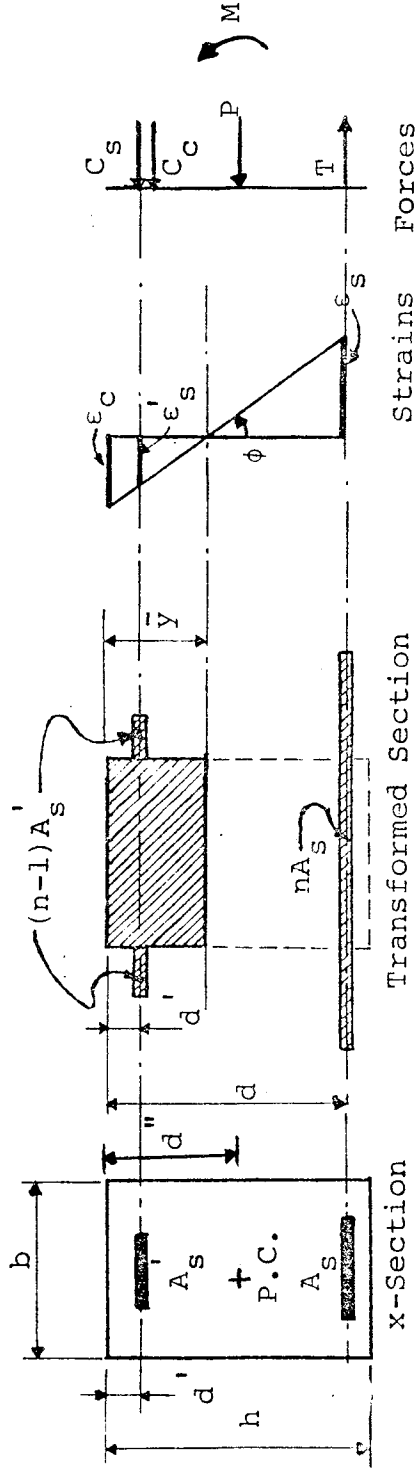


Fig. (A.1). Moment-curvature relationship